THE ABRASIVE WEAR RESISTANCE

OF

AUSTEMPERED SPHEROIDAL GRAPHITE IRONS

by

S.V. SHEPPERSON

A thesis submitted to the Faculty of
Engineering, University of Cape Town
for the degree of Master of Science
in Applied Science

Department of Materials Engineering,
University of Cape Town, April 1987.

ABSTRACT

A study has been made of the structure and abrasive wear resistance of two austempered commercial spheroidal cast irons. Heat treatments have been carried out for different times between 2 and 120 minutes for a range of austenitising temperatures between 850°C and 950°C and austempering temperatures between 250°C and 450°C. The morphology and constitution of the resulting dual phase ferrite/austenite structure has been examined using optical and scanning electron microscopy and x-ray analysis.

The maximum quantity of retained austenite in the structure has been shown to vary up to 50% and to be strongly dependent on heat treatment parameters and the composition of the iron.

Laboratory abrasive wear testing has been carried out on these austempered irons and compared with the results of similar tests on a range of abrasion resistant carbon steels. All the austempered irons were found to have better abrasion resistance than proprietary abrasion resistant steels.

These austempered irons derive their outstanding properties from the morphology of the dual phase ferritic/austenitic matrix coupled to the high work hardening characteristics brought about by the stress induced austenite to martensite transformation during abrasion. The influence of microstructure and mechanically induced transformation has been studied as a function of austempering temperature and time.

ACKNOWLEDGEMENTS

I would like to thank the following people who assisted me in producing this thesis.

Professor C. Allen, my supervisor, for his patience, support and guidance.

Mr. B. Greeves for his photographic work.

Miss C. Lang for the many hours spent typing this manuscript.

Mrs. H. Böhm and Mrs. S. Betz for their help in the preparation of the manuscript.

Mr. N. Dreze and Mr. G. Newins for their technical assistance.

Miss L. Hankey and fellow students for their support and encouragement.

The CSIR for financial support.

CONTENTS

CHAPTER 1

INTRODUCTION

1.1 AIMS AND OBJECTIVES

In recent years considerable interest has been shown in the development of, and applications for, austempered spheroidal cast irons. This interest has stemmed from the realisation that strength levels of spheroidal cast irons can be doubled without incurring the penalty of a reduction in ductility or toughness values. Tensile strengths between 800 and 1600 Nmm^{-2} can be achieved with elongation values ranging from 14 to 1% respectively. These mechanical properties allied to the relative cheapness and ease of manufacture of these cast irons woud appear to make them potential candidates for many diverse applications in engineering, mining, transportation and agricultural industries, involving wear such as in chutes, digger teeth, gears and tracks.

However, little quantitative information is presently available on the wear behaviour of these austempered spheroidal cast irons. This work is an attempt to assess the wear behaviour of two austempered commercial spheroidal cast irons.

The specific aims and objectives of the work were to:

a) establish the heat treatment parameters relevant to the control of structure and mechanical behaviour of these irons,
b) determine the relative abrasive wear resistance of these irons,
c) compare the abrasive wear behaviour of austempered irons with proprietary abrasion resistant alloys,
d) elucidate the mechanisms of abrasive wear in these alloys and their relation to the structural parameters.

1.2 AN HISTORICAL BACKGROUND TO CAST IRON

There are three basic commercial categories of iron namely wrought iron, cast iron and steel. Wrought iron is now effectively extinct but cast iron and steel are extensively used in thousands of applications daily.

Cast iron can be simply defined as an alloy of iron and other elements, chiefly carbon, phosphorus, silicon and manganese. These can be present to a total of about 10%. Carbon is the primary alloying element.

Cast iron is a crystalline metal, easily melted and capable of being cast but not wrought. Traditionally it is poor in tension but good in compression, being able to withstand heavy crushing loads. It cannot be forged, rolled or shaped in any way, either hot or cold and although it can be welded this requires special techniques. In recent years, by special treatment, cast iron can be made to acquire one or more of several special properties not otherwise present in traditional cast iron. These 'high duty' cast irons have improved ductility, tensile strengths, fatigue and corrosion resistance.

The Chinese first perfected the art of making cast iron in the fifth century B.C. This achievement was possible because they had well developed kilns, used coal as fuel, had better ores and possessed the necessary refractory clays to line the kilns. The Greeks, by the middle of the fifth century B.C., were also able to melt iron successfully and run it into moulds as 'cast iron'.

With the advent of the Dark Ages in Western Europe cast iron production came to a halt. It was only after the thirteenth century that cast iron was again produced.

The invention of gunpowder made cast iron favourable once again. The earliest cannon were made from wrought iron staves bound with loops like a barrel. As the increase in capacity of furnaces and the skill of the ironmakers improved cannon began to be cast. As early as 1543 the first cast iron cannon to be made in Britain were cast in Buxted, Sussex. The early guns burst almost as frequently as the built up wrought iron ones, but they were much cheaper. Cast iron, being weak and unreliable in tension, was an unsuitable material for a pressure vessel like a gun barrel. It was however, up to the 1860's, the only economic cannon available, brass and bronze being extremely expensive.

Between the fifteenth and seventeenth centuries cast iron was used mainly in such applications as garden rollers, grave slabs and firebacks. All castings were of simple shape and with the exception of cannon, they were all solid. During this period large castings of up to seventy feet were available in England. The inherent weakness in tension however limited the iron's use to situations where the stresses were predominantly compressive. This limitation also prevented the use of cast iron as a mass production material.

An obvious use for cast iron was bridge building. The early iron bridges were made from cast voussoirs in the form of open lattice frameworks which fitted together like a stone bridge.

As time went on iron castings found many more uses; the development of the steam engine and the countless types of machinery which steampower brought into common use extended the demand enormously.

In 1722 the French scientist Reaumer discovered a method of treating iron castings to make them more malleable. He treated the castings for several days at red heat in contact with powdered iron ore, and so altered the metallurgical structure that the castings emerged tough and ductile. It was not until 1804 that this process was used in Britain and even then the material had a rather doubtful reputation.

In 1826 Boyden, an American, developed another process for producing malleable castings, and this, though producing a similar result as far as toughness and ductility went, was different metallurgically. Boyden's castings, when broken, had a dark fracture, in contrast to those made by the older process which had a bright and steely appearance. Boyden's product thus became known as Blackheart cast iron while the older one got the name Whiteheart cast iron. Both processes are still in use today.

In 1885 Thomas Turner published research that was to become a landmark in the metallurgy of cast irons. Turner showed that the amount of silicon present in the iron determines the condition of the cast iron. With only 1% silicon the iron tends to be white i.e. the fracture surface is bright and shiny, while with about 3% silicon, even rapidly cooled irons are grey i.e the fracture surface is dark and dull. Later it was found that the presence of other alloying elements also had an effect on the structure of cast iron e.g. the addition of chromium produces white iron whilst nickel produces grey iron.

In more recent years remarkable new alloy cast irons have been produced. These high quality irons which include Meehanite and spheroidal cast iron are produced by treating the cast iron while it is still molten. Spheroidal graphite cast iron, first produced in the 1940's, was made by adding magnesium to the melt. This modifies the structure by causing the carbon to form small nodules when the iron cools instead of graphite flakes, which are a source of weakness in ordinary cast iron.

Several varieties of cast iron can be produced by the selection of different pig irons, by variations of melting conditions and by special alloying conditions, but in general three main classifications exist viz. white cast irons, grey cast irons and malleable iron. The classification of cast iron can be seen in Figure 1.1 (1).

Modern cast irons are used in motor-car cylinder blocks, in many hot water radiators, in machine parts such as lathes and other machines- tool beds, pillar, columns and gearboxes.

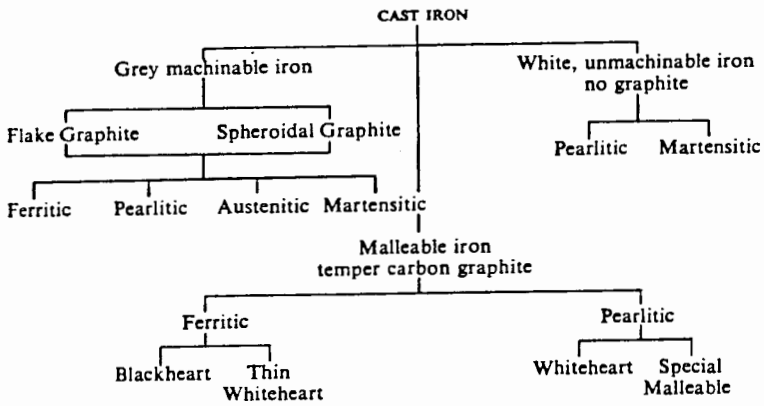

Figure 1.1 : Classification of cast iron (1)

The latest addition to the cast iron family is the recently developed austempered ductile iron (ADI). Initially developed in the early seventies, it has since become increasingly popular due to a variety of properties that were previously not attainable in traditional cast irons. These include greater toughness, and high strength. This iron will be discussed extensively in Chapter 2.

CHAPTER 2

A REVIEW OF AUSTEMPERED DUCTILE IRON METALLURGY

2.1 SPHEROIDAL CAST IRON - THE PARENT MATERIAL

2.1.1 Introduction

The emergence of spheroidal cast iron (SCI) as an engineering material in the late forties and early fifties is regarded as a major advance in cast iron technology. Controlling the form in which the graphite phase precipitates during solidification produces dramatic improvements in strength, toughness and ductility.

This has led to SCI becoming established as the material in the cast iron family with the most advanced range of properties for exacting engineering standards.

2.1.2 Description of Spheroidal Cast Iron

SCI is defined as a high carbon containing, iron-base alloy in which the graphite is present in compact, spherical shapes rather than in the shape of flakes, the latter being typical of grey cast iron.It always contains carbon in excess of 1.5% - normally in excess of 3%. It also contains silicon between 1 and 4%.

Cast iron differs from steel in that it always contains carbon in excess of its solubility in solid iron. This excess carbon precipitates during freezing in the form of pure, crystalline graphite. Ordinarily, the graphite assumes the shape of flakes (Figure 2.1) but through controlled treatment the graphite will crystallise in the form of spheroids or nodules (Figure 2.2).

Unpolarised

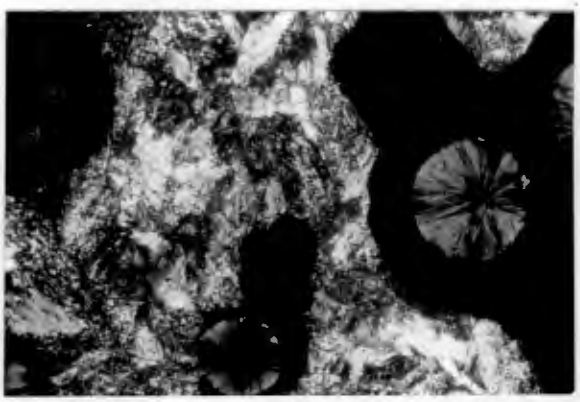

Polarised

Figures 2.1 and 2.2 : Microscopic structures of a flake cast iron and a spheroidal graphite cast iron (22) (x 100)

The formation of this spheroidal graphite is affected by adding small amounts of cerium or magnesium to the molten iron just before casting. Since both these elements have strong carbide forming tendencies, the silicon content of the iron must be high enough (at least 2.5%) in order to prevent formation, by chilling, of white iron in thin sections.

2.1.3 Microstructure

2.1.3.1 Composition

Spheroidal cast iron is essentially a ternary alloy of iron, carbon and silicon of near-eutectic composition. The two most important alloying elements are thus carbon and silicon.

Carbon: Carbon exists in two forms in all cast irons, namely as free graphite or combined with some of the iron to form iron carbide (cementite). These two varieties are usually referred to as graphitic carbon and combined carbon respectively, and the total amount of both types in the specimen of iron as total carbon.

Silicon: Silicon dissolves in the ferrite of the cast iron and is the element which has the predominant effect on the relative amounts of free graphite and cementite which are present. Silicon tends to increase the instability of cementite so that it decomposes, producing free graphite. The higher the silicon content the greater the degree of decomposition of the cementite, and the coarser the graphite produced. Thus, whilst silicon strengthens the ferrite by dissolving in it, at the same time it produces softness by causing the cementite to break down to graphite. The addition of silicon therefore modifies the simple iron-carbon phase diagram as can be seen in Figure 2.3

The effects of other alloying elements such as nickel, chromium, copper etc, on the microstructure of spheroidal cast iron is generally the same as in steels, e.g. alloys such as chromium and nickel improve hardenability; graphitization is facilitated by additions of silicon and carbide formation is enhanced by tungsten.

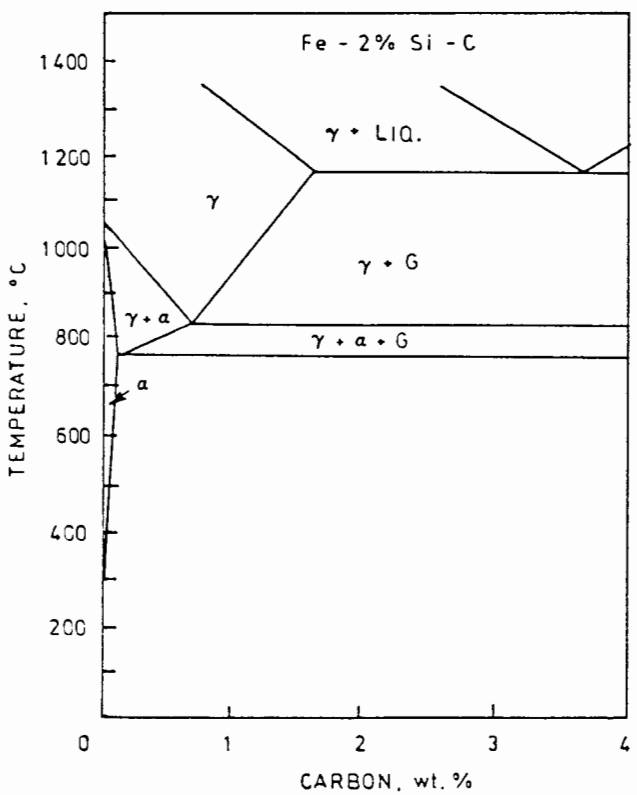

Figure 2.3 : Equilibrium diagram of iron, 2% silicon and carbon (2)

2.1.3.2 Graphite Spheroids

The graphite, in spheroidal form, does not significantly influence properties but the qualities of the metallic matrix in which the graphite spheroids are embedded do alter properties within wide limits. The spherical shape of the graphite removes the 'crack' effect i.e. the graphite flakes act as stress raisers and under stress promote crack propogation (Figure 2.4). The graphite spheroids act as 'crack arrestors' i.e. crack propogation is stopped (Figure 2.5). Properties such as strength and toughness are remarkably improved (Figure 2.6), e.g. grey cast irons have ultimate tensile strengths (UTS) of 150-400 MPa and practically no elongation while spheroidal cast irons have UTS of 400-1500 Mpa and elongation values of up to 14%.

Figure 2.4 : Effect of flake graphite in promoting crack propogation (3)

Figure 2.5 : Effect of of spheroidal graphite in resisting crack propogation (3)

The nodule count i.e. the number of graphite spheroids per square millimetre, is a critically important factor in the microstructure (1). It is the most sensitive indicator of ductile iron quality. A high nodule count above 100 minimises segregation and carbides in the intercellular regions. Nodule counts that are high also tend to improve tensile strength and tensile elongation. Toughness and fatigue properties are also dependent on nodule count (1).

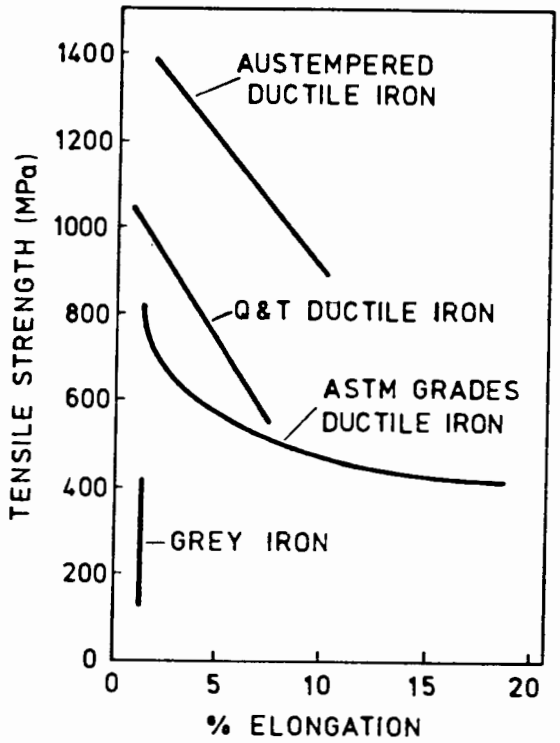

Figure 2.6 : Properties of cast irons (2)

2.1.3.3 Matrices

The matrices obtainable in spheroidal cast iron are much the same as those attainable in carbon steels. Ferrite matrices will have high ductility while pearlite matrices will be characterised by high strength.

The variety of matrix structures is wide and often two or more components are simultaneously present. In Table 2.1 examples of some of the matrix structures with their mechanical properties are shown.

TABLE 2.1 : Effect of Matrix on Mechanical Properties in SG Irons

MATRIX STRUCTURE	HARDNESS H_b	TENSILE STRENGTH Nmm^{-2}	% ELONGATION
Ferrite	175	370	17
Ferrite	200	420	12
Ferrite and Pearlite	230	600	3
Pearlite	265	700	2
Pearlite, or a heat treated structure	300	800	2

2.2 AUSTEMPERED SPHEROIDAL CAST IRON

2.2.1 Introduction

After the development of SCI in the early fifties, metallurgists felt that the properties of SCI could not be further improved by modifying the spherical nature of the graphite. The modification of the matrix became increasingly desirable and as early as 1952 International Harvester managed to produce high-strength, high-toughness ductile iron in cast track shoes through the process of austempering.(2)

This new technology remained dormant until the early 1970's when China, America and Finland began commercial production of ADI castings (5). Kymi Kymene in Finland and General Motors in the USA demonstrated the new material and its advantages by manufacturing gears that replaced their forged steel counterparts (6).

Since then the ADI industry has grown steadily. ADI components have replaced many of their forged steel counterparts ranging from crankshafts to agricultural components (Figure 2.7).

Automobile	Crankshafts Camshafts Steering Knuckles Suspension Components
Pumps & Compressors	Bodies Crankshafts Drive Shafts
Railway	Couplings
Agriculture	Undercarriage Parts Constructional Equipment

Figure 2.7 : Engineering Applications for Austempered Ductile Iron (5)

2.2.2 Heat treatment of Austempered Ductile Iron

Austempered ductile iron is obtained from the parent material, SCI, by undergoing a carefully controlled heat treatment process which involves austenitisation followed by austempering. This two stage process is discussed below.

2.2.2.1 Austenitising of Spheroidal Cast Iron

Austenitising is performed in the range 840-950°C (i.e. above the Ac_3). The austenitising temperature will strongly influence the amount of carbon dissolved in the austenite matrix which in turn affects the transformation during the subsequent austempering process.

Harris and Maitland (8) found that by increasing the austenitising temperature the amount of carbon dissolved in the austenite matrix increased. The greater the amount of dissolved carbon in the austenite, the greater the amount of stabilzed austenite that remains after a set austempering time (9).

At higher austenitising temperatures, the transformation kinetics of the subsequent bainitic reaction are also affected. As well as carbon content increasing, the austenite grain size also increases with increasing austenitising temperatures. These two factors increase the hardenability and upon austempering the beginning and the end of the bainitic reaction is delayed. Rundman and Klug (9) found that ductile iron austenitised at 1066°C developed a matrix containing about 1.2% C while iron austenitized at 900°C had a matrix content of approximately 0.83%.

Harris and Maitland (8) concluded that for a fixed austenitising temperature the transformation time increased with austenitising time, while for a fixed austenitising time the transformation was retarded by an increase in austenitising temperature (Figure 2.8).

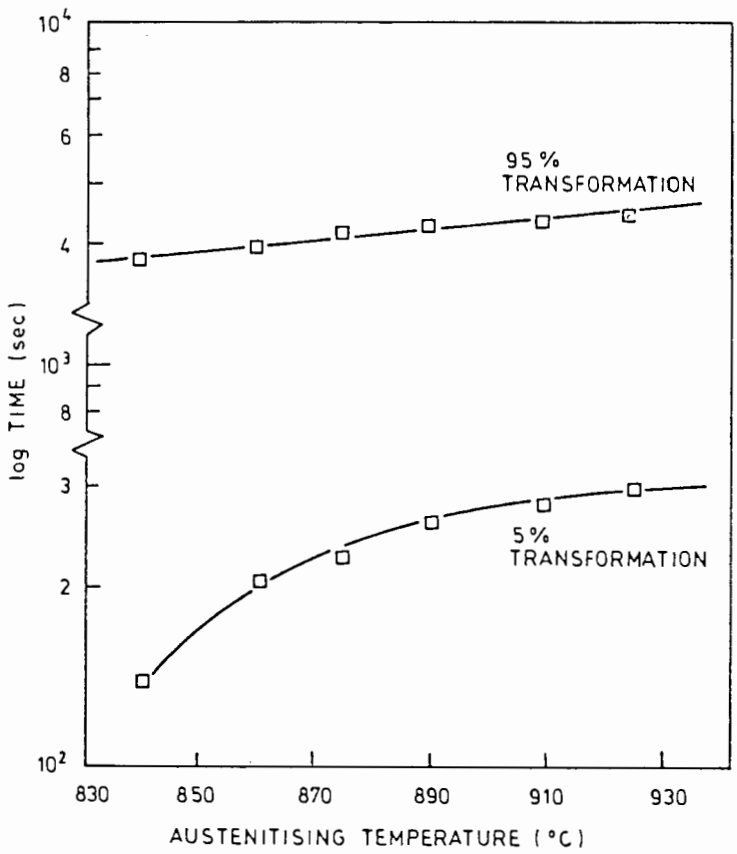

Figure 2.8 : Variation in transformation times with austenitising temperature (8)

Depending on the initial matrix of the parent material the austenitising time will vary. A finely pearlitic iron which already contains carbon in the form of cementite will, if austenitised at 900°C, develop a uniform carbon content in less than 30 minutes soaking time. A fully ferritic iron austenitised at 900°C may require more than one hour to acquire a uniform carbon content in the austenite matrix (2).

2.2.2.2 Austempering of Spheroidal Cast Iron

There is a distinct difference between the resulting structures in the austempering process used for steels and SCI. In steels a complete bainitic microstructure is produced whereas in SCI varying quantities of acicular ferrite and retained austenite are present (10).

Austempering of SCI occurs between the temperature range 205°C-450°C, i.e. above the M_S and below the pearlite/ferrite formation curve (Figure 2.9). The metal is quenched and held isothermally for a predetermined time. The quench must be sufficiently fast so that ferrite and pearlite are avoided and also it must occur above the Ms so that no brittle martensite is formed.

The actual temperature in the salt bath and the holding time are functions of the desired amount of retained austenite (Figure 2.10).

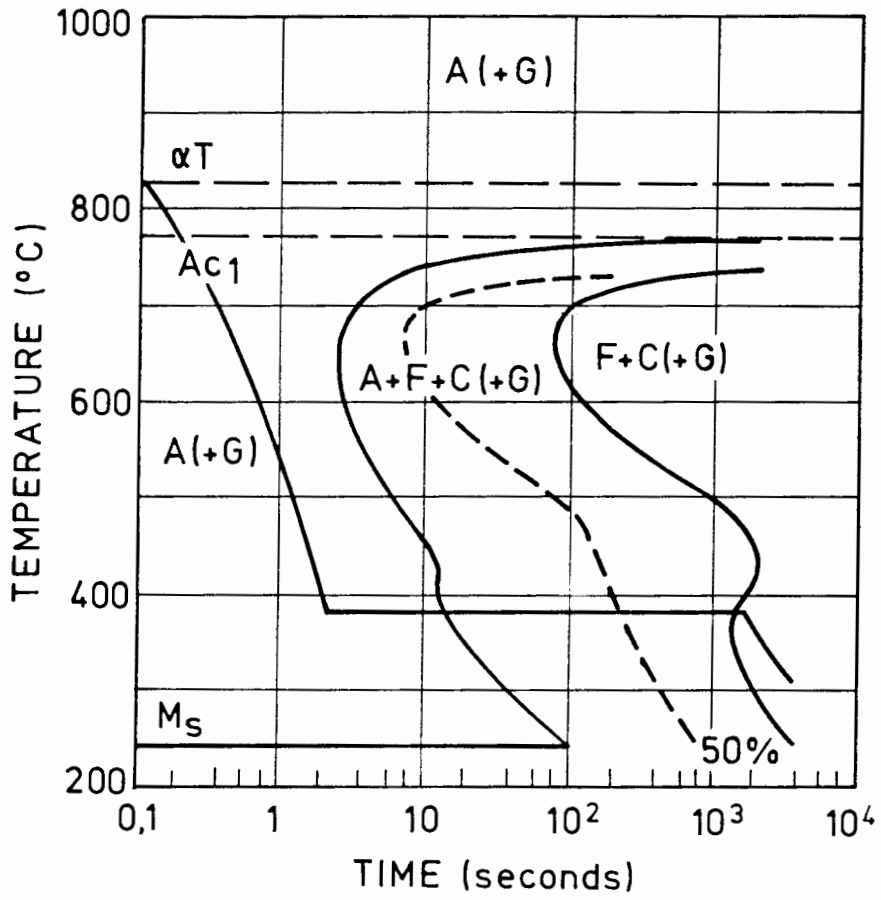

Figure 2.9 : Illustrating typical austempering heat treatment for ductile iron (11)

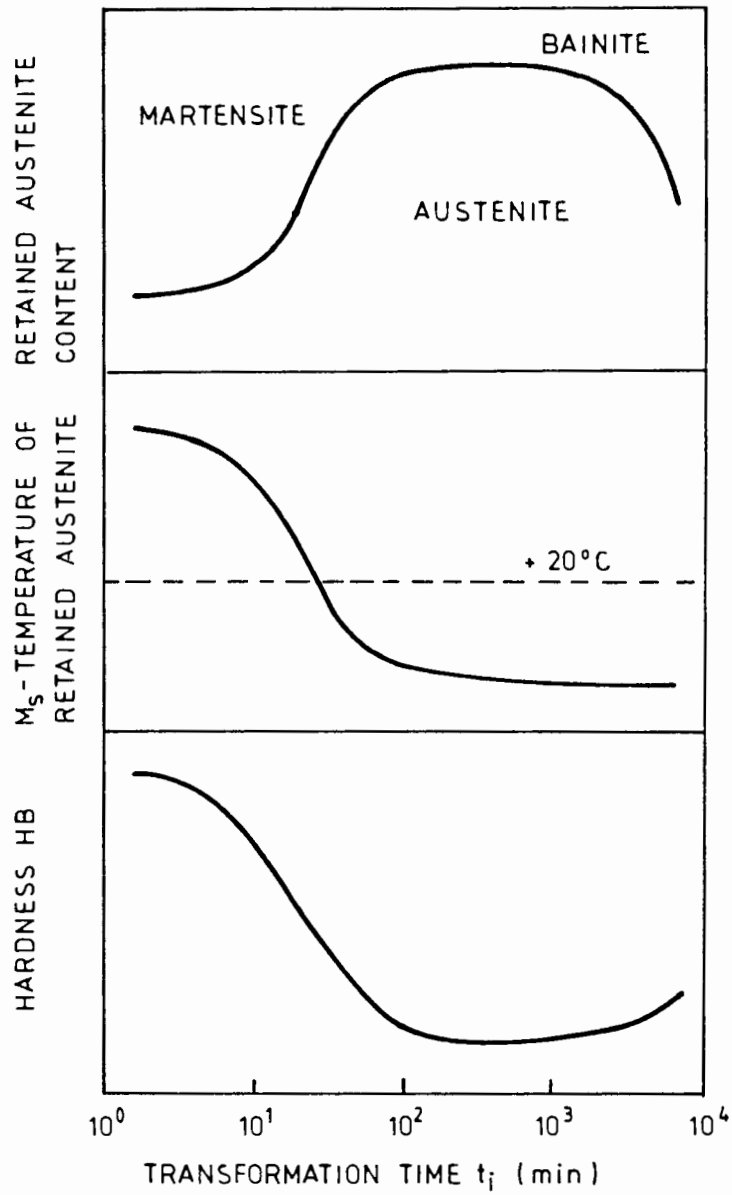

Figure 2.10 : A schematic representation of the dependance of retained austenite, its M_s temperature and hardness, on the isothermal holding time (12)

2.2.2.3 Austempering Reactions

The matrix of ADI consists of a two phase mixture of austenite and acicular ferrite.

During the austempering process, acicular ferrite precipitates and grows into the austenite matrix. This growth is unaccompanied by the formation of cementite (Figure 2.11). The carbon that is rejected from the growing acicular ferrite plates enriches the surrounding austenite. The austenite is able to continue absorbing this carbon due to the high silicon content of the ductile iron. The silicon suppresses the cementite phase associated with bainitic transformation. (2)

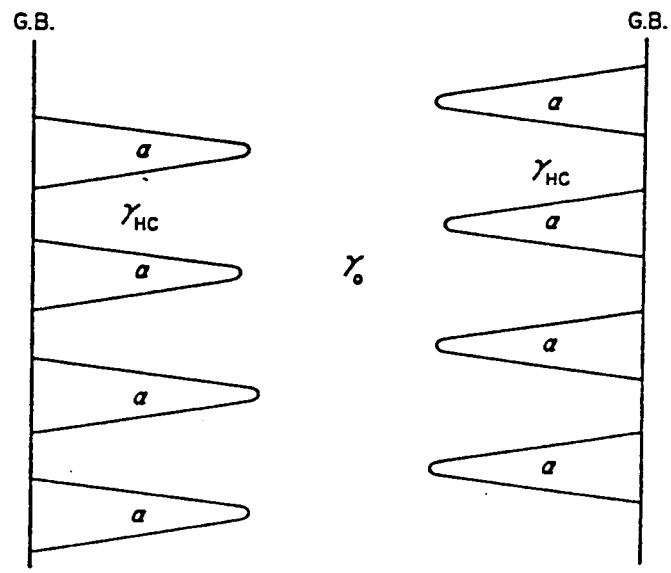

Figure 2.11 : Schematic illustration of acicular ferrite platelets (α) growing from a grain boundary (GB) into the original austenite (γ_o) and creating zones of high carbon austenite (γ_{HC}) (10)

The richer the austenite becomes in carbon the more inhibited the ferrite reaction becomes until it stops altogether. Johanneson has shown that the carbon content of the austenite can be as high as 2.0% and that the austenite is stable to below -120°C (8).

However, this austenite, at sufficiently long austempering time breaks down into ferrite and carbides.

The austempering can therefore be broken down into two main reactions:

1. The decomposition of austenite to acicular ferrite and carbon enriched austenite. This reaction is sometimes called the toughening reaction due to the high toughness attributed to the austenite/ferrite structure produced.

   Heheman reported that the bainitic reaction in high silicon steels is notably different to that of normal steels in that the ferrite plates are unaccompanied by iron carbide, hence in future the term acicular ferite will be used rather than bainitic ferrite or bainite (13).

2. The decomposition of carbon-enriched austenite to ferrite and carbides. This is an undesirable reaction due to the embrittlement caused by the carbides (Figure 2.12) (10).

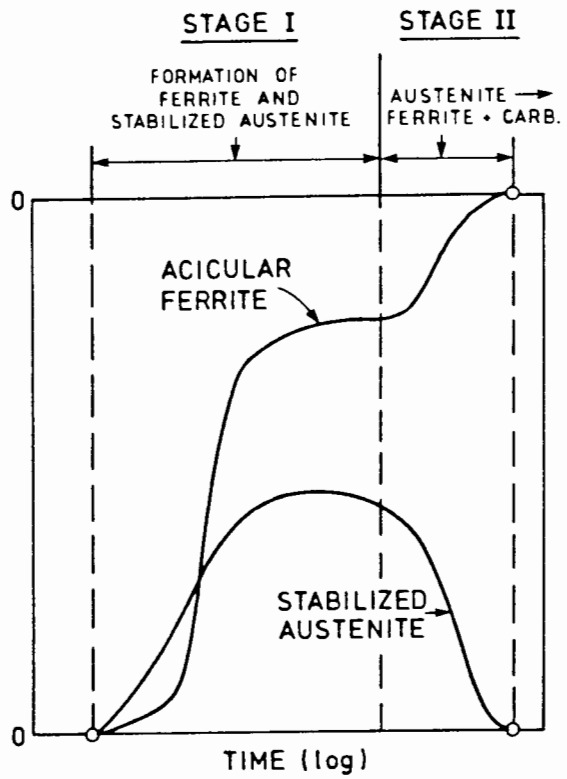

Figure 2.12 : Schematic illustration of the formation of ferrite, austenite and carbide during austempering (14, 15)

It is important to remember that if the austempering temperature is too high or the austempering time is too long then the start of the second reaction will be speeded up. Carbides will therefore precipitate and deleteriously effect the properties of the material. Rundman and Klug (9) have shown that for an austempering time of 60 minutes the change in austempering temperature significantly decreased the amount of carbon in the retained austenite due to carbide precipitation, e.g. 317°C - 1.60% C
371°C - 1.58% C

Reaction 1

Toughening: $\gamma_o \rightarrow \alpha + \gamma_{HC}$

The austempering time and temperature largely determine the morphology of the matrix and the relative amounts of acicular ferrite and austenite present.

The higher range of austempering temperature, i.e. 350-450°C produces coarse acicular ferrite needles in the austenite matrix. These acicular ferrite needles are produced during the first reaction. If the first reaction is interrupted, i.e. before the retained austenite is sufficiently stabilized by the rejected carbon (M_S below room temperature), then there will be martensite present in the matrix upon cooling. The martensite affects the properties of the iron by increasing hardness but decreasing toughness and ductility.

The lower range of austempering temperatures, i.e. 205-350°C produces much finer matrix structures. The acicular ferrite needles are finer and closer together - the ferrite/austenite spacing decreases. Again any interruption of this process will lead to a certain percentage of the final matrix being martensitic (10).

Isothermal transformation diagrams show that often two 'bainitic' noses are present (Figure 2.13), one occurring around 425°C and the other around 300°C.

These two noses probably correspond to the two different types of matrix morphology that are found (10).

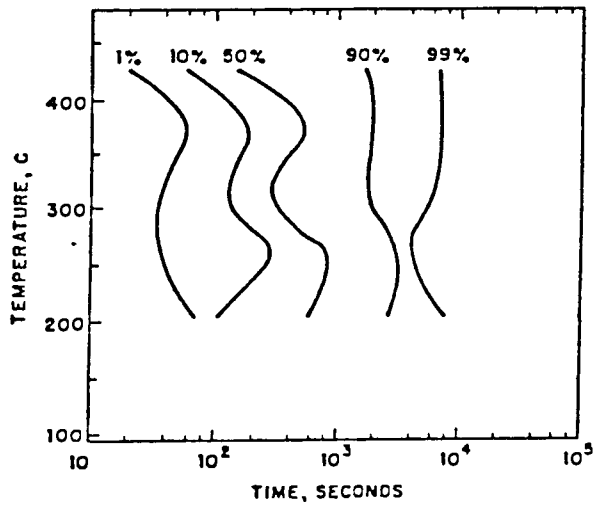

Figure 2.13 : Isothermal transformation diagram for alloyed ductile iron austenitised at 843°C (16)

The kinetics and mechanisms of the austenite to acicular ferrite transformation have not been comprehensively studied but a qualitative understanding has been achieved. Harding (17) has summarised the possible kinetics and mechanisms.

The austempering range 205-450°C allows transformation to start by the nucleation of the acicular ferrite at interfaces and grain boundaries. The high silicon content of the iron suppresses the reaction to a degree, unlike the reaction in steels. At isothermal treatments below 350°C, the ferritic needles have a high growth rate, but the rate of carbon diffusion is relatively low. The result is high carbon contents in the acicular ferrite which can initially have a distorted tetragonal crystal structure. During the initial stages of the austempering process this carbon is rejected from the acicular ferrite and precipitates as epsilon carbide ($Fe_{2.4}C$) in the ferritic needles (Figure 2.14). Little carbon is therefore rejected into the austenite and hence only small quantities of retained austenite are present after cooling.

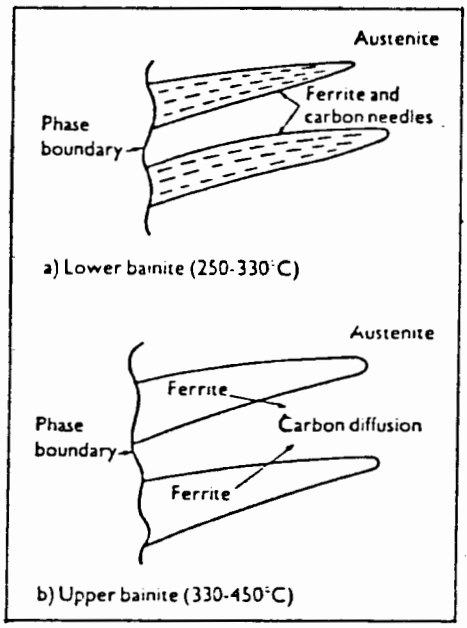

Figure 2.14 : Illustrating the mechanism of formation of lower and upper acicular ferrite (17)

Above 350°C the mechanism of transformation changes. Carbon diffusion is more rapid and carbon is therefore able to diffuse out of the growing bainitic ferritic plates thereby enriching the austenite, especially between the growing ferritic plates. The level of the carbon in the retained austenite will gradually increase and can reach levels of up to 2.0% (12). At this level of carbon the ferritic reaction stops. The increase in carbon content in the austenite will serve to stabilise the austenite i.e. lower the Ms temperature to a point below room temperature such that martensite will not form in the stabilised austenite upon quenching. It has been shown that a fully austempered specimen can be quenched to -260°C without the austenite transforming to martensite (9). Retained austenite levels of up to 50% can be attained.

Reaction 2

Embrittlement: $\gamma_{HC} \longrightarrow \alpha + \text{CARBIDE}$

The second reaction is undesirable because it results in embrittlement.

The carbide precipitation takes place in the carbon-enriched austenite phase. As the austenite carbon content is thus lowered, further transformation to acicular ferrite occurs (17). The final microstructure at room temperature will be ferrite plates, carbides and a small percentage of retained austenite.

The precipitation of several different carbides has been reported. Sandvik (18) described the carbide in the second reaction as having a triclinic crystal structure whose lattice parameters closely resemble cementite. The shape of these carbides was lenticular plates approximately 0.1 μm in thickness and parallel to the acicular ferrite platelets (Figure 2.15).

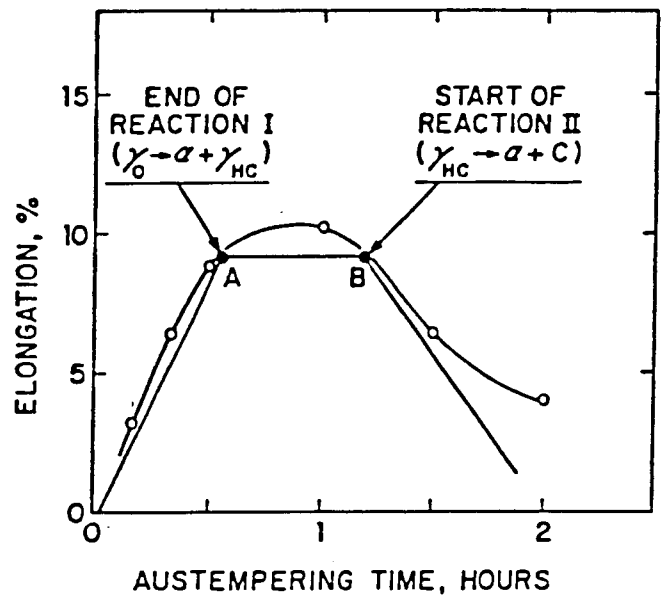

Figure 2.15 : Idealised characterisation of the influence of the two acicular reactions on toughness during austempering (10)

More recently, Franetovic, Sachdev and Ryntz (19) concluded one of the first studies in transmission electron microscopy on austempered ductile iron. They studied ADI that had been austenitized at 915°C for 2 hours and austempered at 240°C for 2 hours.

The transmission electron microscope study confirmed the presence of orthorhombic cementite (Fe_3C) in the ferrite of both low and high silicon ADI in the lower bainitic region.

The presence of epsilon-carbide as reported by Sandvik (18) and Hwang and Thomas (20) for high silicon steels of a composition similar to the matrix of the ductile iron was not observed.

The orthorhombic iron carbide (Fe_3C) appeared to have two morphological distributions in the ADI. One consisted of fine particles and the other of thin, wavy lamellae. The precipitation of carbides within the ferrite but not in the cementite appears to be similar to precipitation of carbides in lower bainitic steels. The lower acicular ferrite was considered to form initially as a carbon supersaturated ferrite from the austenite (21). Subsequent cementite precipitation occurred to relieve the inherited supersaturation in the acicular ferrite.

It was suggested in the study that as the time dependence of carbide precipitation was not studied, the possibility did exist that the epsilon-carbide may have precipitated earlier and was subsequently replaced by cementite.

2.2.3 Microstructure

The morphology of the acicular ferrite and the relative amounts of the ferrite and austenite formed during reaction 1 are largely determined by the temperature and duration of austempering time.

Austempering at temperatures above approximately 350°C will produce a structure that consists of relatively coarse acicular ferrite platelets (needles) in the austenite (Figure 2.16). As discussed above, if the reaction is prematurely interrupted, some martensite will form on cooling. When austempering at temperatures below 350°C,the structure that is produced will consist of much finer acicular ferrite platelets (Figure 2.17).

As previously discussed there is evidence to suggest that at the lower austempering temperatures epsilon-carbide precipitation occurs within the acicular ferrite platelets (2).

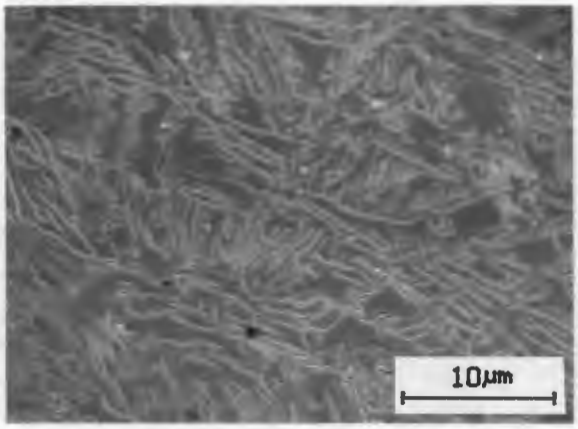

Figure 2.16 : Showing coarse structure of ferrite plates and retained austenite after austempering at 400°C (22)

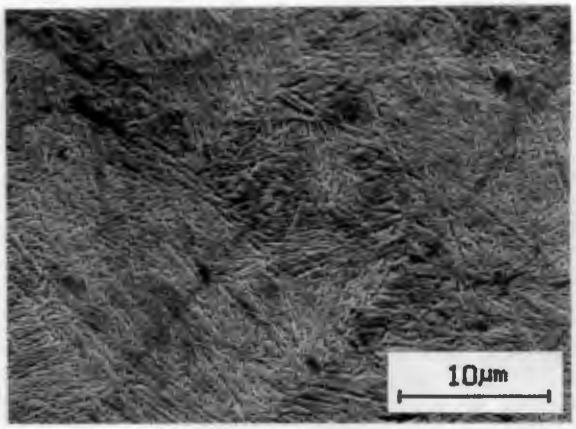

Figure 2.17 : Showing fine structure of acicular ferrite in retained austenite after austempering at 250°C (22)

2.2.3.1 Retained Austenite

One of the most important aspects of the microstructure of ADI is the uniformity of the retained austenitic phase. This can be described by defining three distinct austenite volumes within conventional austempered matrices.

Type 1 - Slivers of recarburised austenite between adjacent ferrite plates. This austenite would be relatively uniform in carbon composition and hence desirable from a microstructural point of view.

Type 2 - Larger and more blocky volumes of retained austenite between bundles or bunches of ferrite plates. These austenite volumes would be relatively non-uniform in carbon content due to their larger size and hence would be undesirable from a stability point of view.

Type 3 - Very large interdendritic volumes of retained austenite which possibly contain high concentrations of alloying elements. This type of microstructure would again have non-uniform carbon concentrations which could transform to martensite on cooling after austempering (23).

It is obvious that types 2 and 3 reduce the uniformity of the ferrite-austenite matrix and promote possible formation of martensite which would be detrimental to the overall properties of the material.

2.2.3.2 Optimum Austenite Content

There is evidence that ductility and toughness in ductile irons are maximised when the amount of retained austenite is optimised. According to Dorazil (24) the optimum amount is achieved by employing a different austenitising temperature for each austempering temperature. From Figure 2.18 it is seen that as the austempering temperature is decreased both the ferrite and austenite phases dissolve increasing amounts of carbon. Therefore, for a given initial carbon content (austenitising temperature) as the transformation temperature decreases, more acicular ferrite forms and less austenite remains at the end of the first reaction. Thus to maintain a constant proportion of austenite to acicular ferrite, it is necessary to increase the austenitising temperature when decreasing the austempering temperature. For ADI's there is a limiting factor however; increasing the carbon content by increasing the austenitising temperature eventually leads to the occurrence of untransformed intercellular austenite, i.e: alloy segregations occur more easily at higher austenitising temperatures. This form of austenite is not as thermally or mechanically stable as the carbon enriched austenite produced by the formation of acicular ferrite. Some martensite may form on cooling and this is deleterious to ductility and toughness. The optimum amount of austenite should therefore be the maximum amount obtainable without resulting in intercellular austenite.

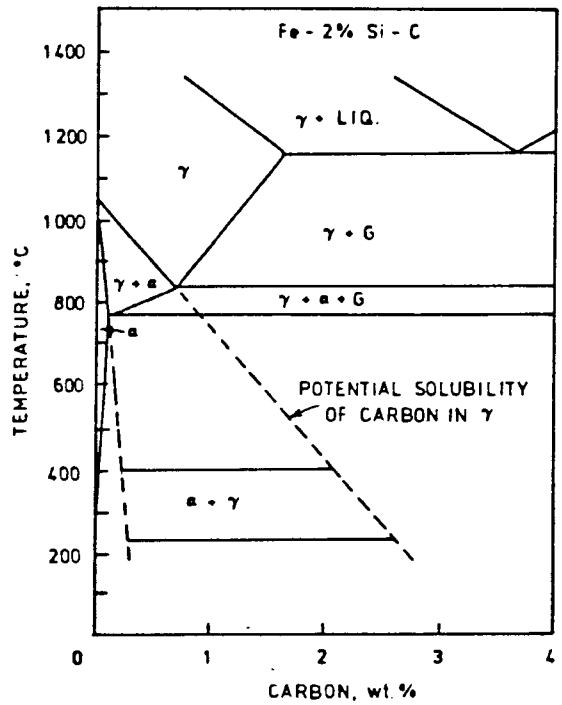

Figure 2.18 : Section of the Fe-C-2%Si equilibrium phase diagram illustrating a metastable projection of the $\alpha+\gamma$ two-phase field into the acicular transformation temperature range (2)

2.2.4 Composition

Composition is an important factor in the processing of ADI. Some alloy additions are usually required to increase the hardenability. This will ensure freedom from pearlite, polygonal ferrite and Widmanstatten ferrite during cooling to the austempering temperature.

The effects of metal composition can be divided into two parts:

- the effects due to elements regarded as variables in the production of the iron such as silicon and carbon; and

- the effects due to elements that may be added deliberately to alter the hardenability of the iron.

As previously discussed in Section 2.2.2.1 the carbon content of the matrix is determined by the initial carbon content of the parent material, the matrix before heat treatment and the austenitising time and temperature. The effect of more carbon in the austenite is to stabilize greater amounts of retained austenite after a set austempering time. Matrix carbon content is therefore a variable that can be altered by altering treatment conditions. Silicon is primarily responsible for delaying the second reaction, i.e. it appears to promote a carbide-free acicular ferrite/austenite structure (2).

Recently results obtained by Franetovic, Sachdev and Ryntz (19) showed that in the range 1.8 - 3.1% wt % Si there was very little effect on the decomposition rate of the austenite in the lower bainitic region. The time dependence of carbide precipitation was not studied in this investigation however, and an austempering time of 2 hours was used with an austempering temperature of 250°C.

2.2.4.1 Hardenability

Hardenability in unalloyed spheroidal cast irons can be problematic, especially irons that have low matrix concentrations of carbon before heat treatment, i.e. ferrite matrices.

Dorazil (25) has shown that in unalloyed SCI the maximum critical size section for through-hardening by austempering is approximately 10mm. Various alloy additions can be made to improve the hardenability but these additions can have a deleterious effect on the toughness of the austempered iron. An example of the effects of nickel and molybdenum on the critical cooling rate is shown in Figure 2.19 (2).

Certain alloy elements such as nickel, copper and molybdenum appear to delay the second reaction thereby creating a wider range of processing time to achieve the austempered iron (Figure 2.20).

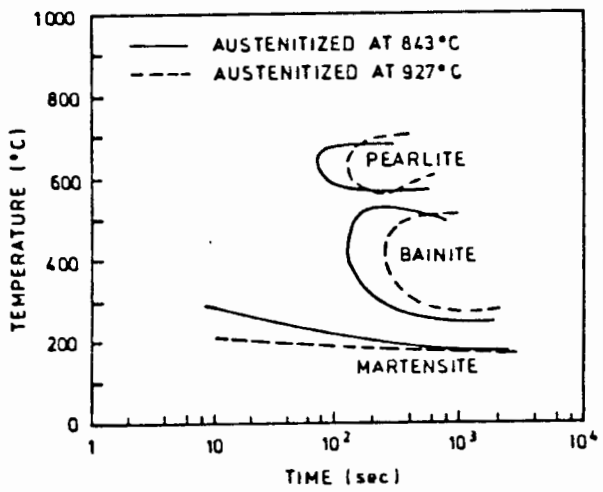

Figure 2.19 : Continuous cooling transformation diagrams for 1.5%Ni-0.3%Mo alloyed ductile iron austenitised at 927°C and 843°C (16)

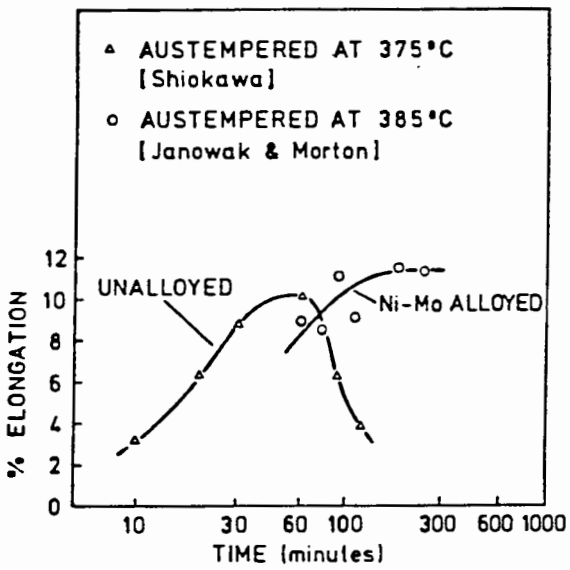

Figure 2.20 : Showing the effect of austempering time and alloying content on ductility (26, 27)

It is important to note, however, that as the amount of the alloying elements increases, the interdendritic volumes become more resistant to nucleation and the growth of ferrite platelets (these volumes have greater hardenability) and therefore do not recarburise to the extent that the remainder of the material recarburises. This is due to the tendency of alloying elements to alter the solubility of carbon in austenite.

Hence, when the austempered iron is cooled to room temperature, the unrecarburised interdendritic volumes transform to martensite, thereby embrittling the structure (23).

2.2.4.2 Segregation of Alloy Elements

Segregation of alloying elements during solidification is known to occur in ductile iron. Silicon will segregate to the graphite nodules and therefore it will have a lower concentration at the cell boundary. Manganese and molybdenum have the opposite effect (Figure 2.21).

The degree of segregation increases as the section size increases due to the slower solidification rate - this creates more time and longer freezing distances for segregations to occur. Cell boundaries would tend to become rich in carbon, manganese, chromium and molybdenum and low in silicon and nickel.

As manganese is a strong austenite stabilizer, the time for completion of the first reaction would be very long and therefore the bulk of the material would have reached the embrittling stage before the reaction is complete at the cell boundary.

Segregations can therefore seriously limit the commercialisation of austempered ductile irons as martensite and/or transformed austenite can preferentially occur at cell boundaries. Mechanical properties would, as a result, be significantly reduced (Figure 2.22).

To try and avoid alloy segregation a high nodule count is required. High nodularity results in a decrease in interdendritic spacing which in turn reduces alloy segregations and its effects.

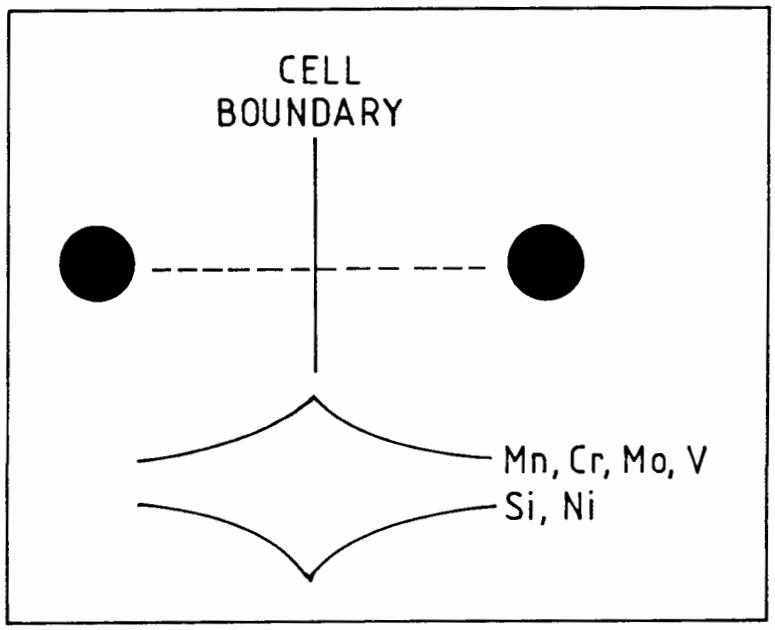

Figure 2.21 : Schematic representation of the relative segregations of some elements in austempered iron (10)

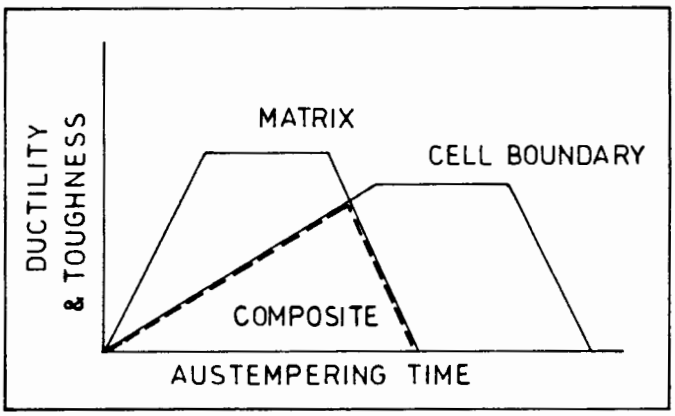

Figure 2.22 : Schematic illustration of the effect of segregations on the development of toughness with austempering time (10)

CHAPTER 3

A REVIEW OF ABRASIVE WEAR

3.1 INTRODUCTION TO ABRASIVE WEAR

Abrasive wear has been defined as wear by displacement from one of two surfaces which are in relative motion. The wear is caused by the presence of hard protruberances on the second contact surface, or by the presence of hard particles either between the surfaces or embedded in one of them.

Two modes of abrasive wear have been defined by Archard and Hirst (28)

a) mild wear
b) severe wear

In mild wear there is little indication of subsurface plastic deformation, any deformation being confined to regions very close to the rubbing interface. In severe wear, the crystal structure of the surface layers becomes heavily distorted and plastic deformation may extend to a considerable degree - 1mm.

Abrasive wear is commonly divided into three types:-

1. Gouging Abrasion involves the removal of relatively coarse particles from the metal wearing surface and is similar to the removal of metal by machining or grinding.
2. High Stress Abrasion involves removal of relatively fine (microscopic) particles from the wearing surface. This wear is believed to be caused by concentrated compressive stresses at the point of abrasive contact. High stress abrasive wear can occur under three body conditions where loose particles become trapped between two sliding or rolling surfaces which are close to one another. The crushing strength of the abrasive is exceeded, causing the particles to be reduced; hence the term "high stress".

3. Erosion or low stress abrasion occurs when small relatively free moving particles dynamically impinge or lightly rub against the wearing surface. This type of abrasion involves the formation of a groove with the displacement of microchips. The stressses are generally under two body conditions. The stresses are insufficient to cause fragmentation of the abrasive particles, hence the term "low stress".

Often a combination of more than one type of abrasion is responsible for the actual wear of a part in service; it is therefore sometimes difficult to determine which type of abrasion is dominant.

3.2 Simple Model of Abrasive Wear

Consider an abrasive particle in contact with a surface of a ductile material (Fig 3.1). According to Moore (29) two major processes take place:

1. The formation of a groove i.e. the material is displaced sideways to form ridges. There is no direct material removal.
2. The separation of particles in the form of primary wear debris or microchips.

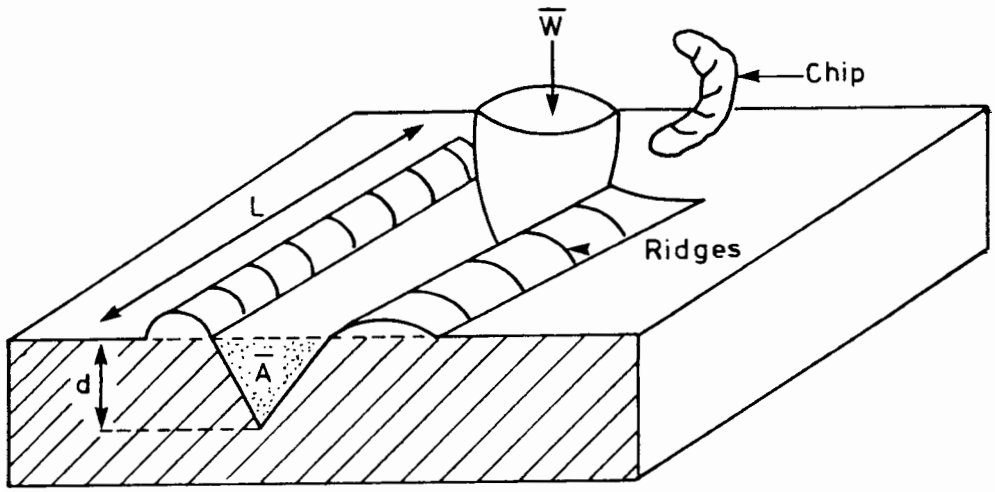

Figure 3.1 : Model of abrasive wear (30)

From Moore (31) the following equation can be derived:

$$V \quad K\,C\,L\,\frac{\delta}{H}$$

C - proportion of groove removed

L - sliding distance

K - proportion of abrasive particles that contact the surface

H - hardness

δ - proportionality constant

V - volume of material removed

This simple model of abrasive wear shows the following:

The volume of material removed from a wearing surface should be linearly dependant on:-

1. Sliding distance - this is generally true although there may be initial non-linear behaviour when the material deforms plastically and strain hardens to an equilibrium hardness.
2. Load per unit area, according to the second law of friction, where the greater the load the greater the friction, and in this case the greater the volume of material removed.

The volume of the material removed is, however:

1. Independent of the abrasive particle size.
2. Inversely dependent on the surface hardness. Surface hardness is generally taken as the most important physical characteristic to consider when selecting materials for abrasion resistance. This may be misleading in some cases as will be shown later.

3.2.1 Problems in the Mathematical Formulation

Kruschov (32) in his pioneering work on the relationship between hardness and abrasion resistance, showed that for pure metals the relative abrasion resistance increased linearly with hardness. This relationship did not hold true for heat treated alloy steels (Figure 3.2). A heat treated steel would have a lower relative abrasion resistance value than a metal of the same hardness. This was due to the material having a heterogenous structure, containing inclusions. These inclusion particles, which are frequently elongated or broken by plastic deformaton during processing, produce high local stress concentrations, which substantially increase the wear rate.

The other important physical parameter which the derived simple model for abrasion resistance does not take into account is toughness. In hard materials when the applied stress during abrasion is high, exceeding the elastic limit, microcracks are produced and propogate until fracture. A weaker more ductile material under the same stresses would undergo continuous material removal by ductile extrusion without the catastrophic rupture that would be caused by the cracks in the harder material.

The most recent approach to considering the mechanisms of abrasive wear is through the study of the effect of various microstructures on abrasion resistance. The microstructural approach to the problem allows consideration of the system as a whole, rather than the strictly defined physical parameters such as hardness, toughness, or yield strength.

Abrasion resistance is not an intrinsic mechanical property, and cannot be modelled by a simple mathematical approach. All wear events must be considered as parts of a tribological system. A systems analysis approach to wear is therefore needed.

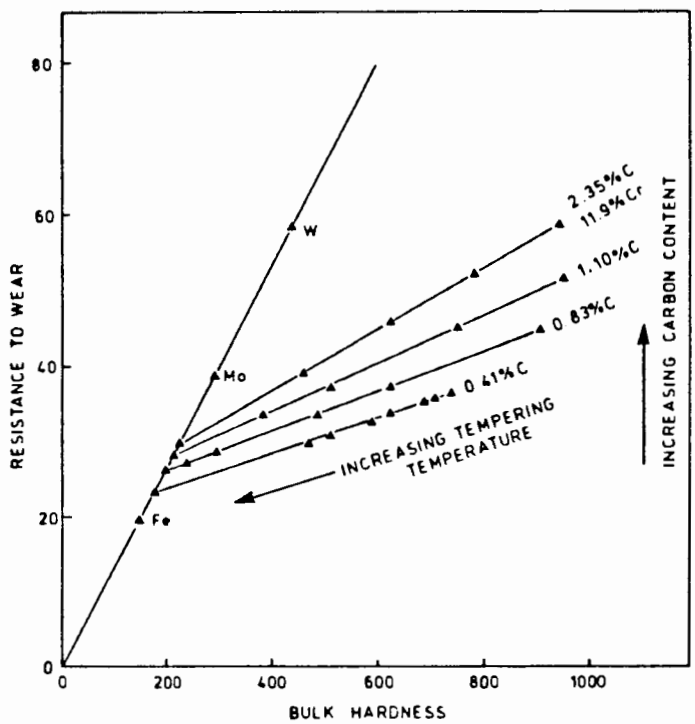

Figure 3.2 : The effect of hardness on the wear resistance of metals and heat treated steels (32)

3.3 MECHANISMS OF ABRASIVE WEAR

Wear mechanisms is the collective name for microevents, by which wear - according to a chosen definition - takes place. Since the removal of material in a tribological system can be the result of a great number of events, with a practically infinite number of combinations, there will be no end to finding, and naming, wear mechanisms.

Vingsbo (33) postulates that the fundamental phenomenon in material removal is fracture and can occur by four basic mechanisms:

1. Shearing of junctions
2. Microcutting
3. Impact
4. Fatigue

These four mechanisms can act alone or in combination with other phenomena, like heating, plastic deformation or corrosion, none of which, however, are specific to wear.

In abrasive wear, the fracture mechanism is predominantly microcutting (34), while the dominant interactive phenomenon is plastic deformation (35)

The nett effect of interaction between microcutting and plastic flow has been called "ploughing" (36) (Figure 3.3).

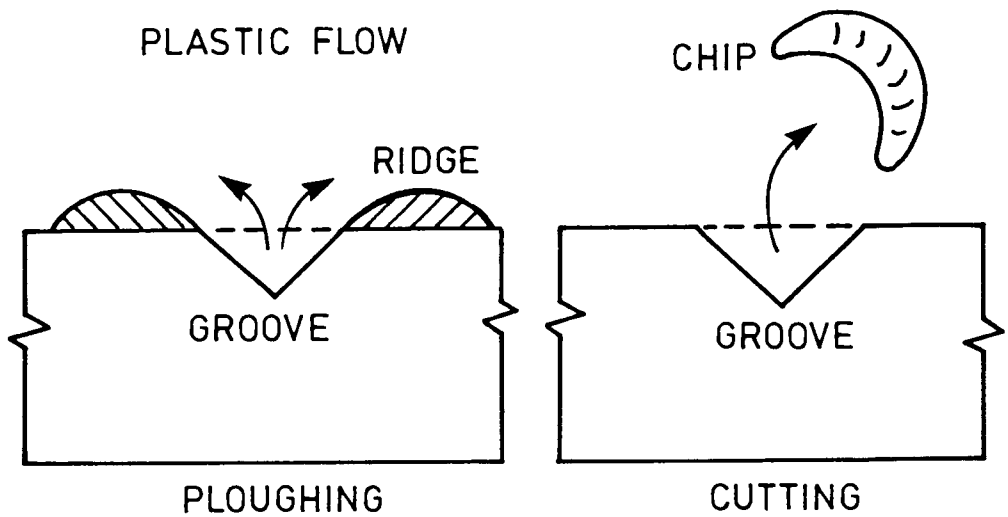

Figure 3.3 : Illustrating the mechanism of material removal during abrasion (36)

3.3.1 Microcutting

If a hard asperity or particle slides over a surface of a softer material under particular wear conditions, it may act as a microcutting tool. The cutting operation leads to removal of the material from the surface by the formation of chips, shavings, fragments, etc. By definition, the surface is worn, and it is left with a groove. The width and depth of the groove depends on the size of the cutting element and may vary from "atomically" small up to some transition region towards macrocutting.

3.3.1.1 Ploughing

In the general case, microcutting interacts with plastic deformation when a hard abrasive element acts as a ploughshare and drives up a pair of crests in ductile materials at the same time as it cuts a fragment.

In ductile irons, a large fraction of the work done by the abrasive element is consumed in plastic deformation, to some extent of the fragment, but mainly for crest formation.

In brittle materials the abrasive work during ploughing is mainly consumed as fracture work. In many cases brittle and ductile fracture are intermixed.

This interaction of the ductile and brittle mechanisms was used by Murray, Mutton and Watson (36) to explain the wear behaviour of heat treated steels. The plot of wear resistance against hardness for such materials indicates that they form a transition between ploughing and microcutting situations (Figure 3.4).

3.4 THE EFFECT OF HARDNESS

The hardness of a material is clearly important in determining abrasive wear because it determines the depth of penetration of the abrading particles. Kruschov (32) showed that the wear resistance of annealed commercially pure metals was directly proportional to their bulk hardness. This work was later extended to include various carbon steels and his findings showed that the behaviour of steels departed radically from the linear behaviour of pure metals (Figure 3.5). He made two important observations:-

1. For a given steel heat treated to different levels of hardness, the slope of wear resistance versus hardness was lower than for pure metals.
2. As the carbon content of steels was increased the line of wear resistance versus hardness was displaced to higher values of wear resistance.

More recent investigators (36,37) have extended this work to commercially pure annealed metals and carbon steels. Their findings as compared to Kruschov's work were:-

1. They agreed that the wear resistance of commercially pure metals increased linearly with hardness.
2. They disputed that the plot of wear resistance versus bulk hardness for carbon steels was linear and instead found that it falls on a series of curves as shown in Figure 3.6.
3. They agreed that the curves are displaced to a higher wear resistance as carbon content was increased.

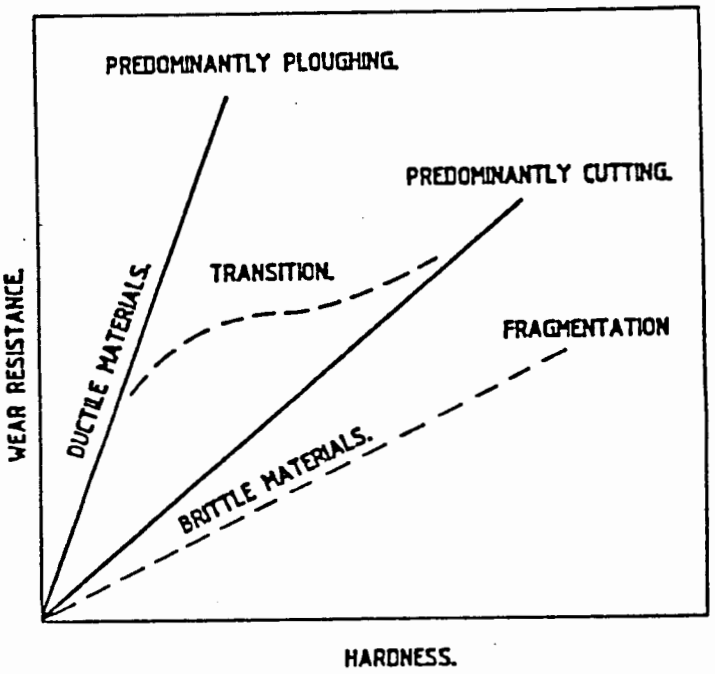

Figure 3.4 : Wear resistance versus hardness plots for ploughing, cutting and fragmentation modes of failure (36)

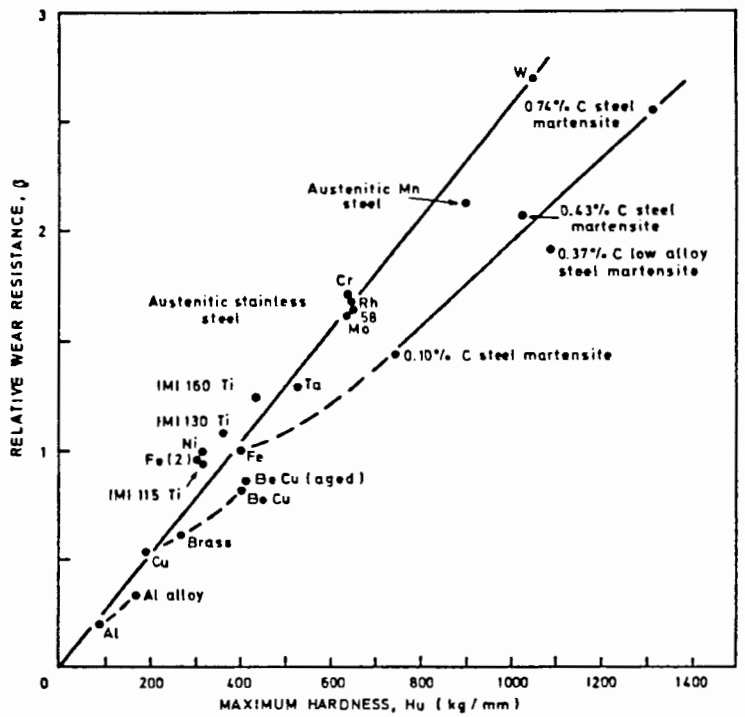

Figure 3.5 : Illustrating the effect of hardness on relative wear resistance of various materials (38)

The reason for this difference in behaviour of metals made some researchers think that the surface hardness could be a more realistic means of assessing the resistance to wear.

Kruschov (38) suggested that the surface of a metal becomes heavily cold worked during abrasion and may reach a limiting hardness for the material. Even though this was found to be more closely related to the wear resistance of a material than the bulk hardness there is still not a satisfactory relationship.

Comparisons of hardness values do however provide an approximate guide to relative wear behaviour among metals or alloys of similar microstructures.

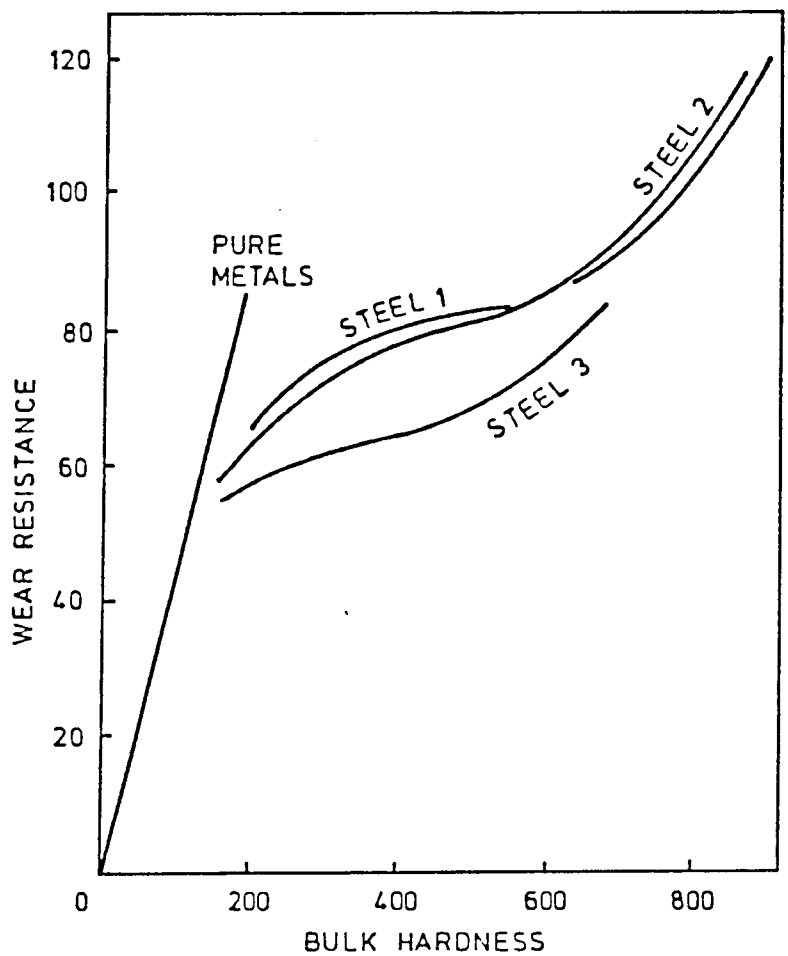

Figure 3.6 : The wear resistance of three steels quenched and tempered to different hardness levels. The sigmoidal shape of the plots is characteristic of carbon steels (36)

3.5 INFLUENCE OF MICROSTRUCTURE

From the preceding section it should be clear that abrasive wear resistance cannot be related to any one mechanical property of a material. What determines whether a material is going to abrade is the micro-interaction between a wearing indentor and the wearing material. The actual micro-mechanical characteristics at the point of contact will control wear, therefore the microstructure of any material plays a major role in its subsequent behaviour.

The effect of the microstructure can be divided into two broad categories:

1. The effect of the matrix structure. This includes the type of bulk matrix structure and the grain size of the matrix structure (the anisotropy).

2. The effect of inclusions - their shape, size, distribution. The effect of second or third phase particles and the possible elastic mismatch between inclusions and matrix.

Zum Gahr (39) has analysed fully these microstructural parameters affecting abrasion resistance.

3.5.1 The effect of the Matrix Structure

The matrix is responsible for the coherency and toughness of any material. In ferritic materials, wear resistance increases as microstructures are changed progressively from ferrite to pearlite, bainite to martensite. Correspondingly the bulk hardness also increases from ferrite to martensite.

Moore (40) also worked on the effect of the various matrix structures and concluded that the wear resistance is related to the metallurgical structure determined by composition and heat treatment. He concludes that it is the structure that determines the hardness and flow stess, and consequently the abrasion resistance. The results of his investigation show that for pearlitic steels containing over 10% by volume pearlite, wear resistance and bulk hardness are linear functions of the pearlite volume. For martensitic steels, wear resistance and bulk hardness are linear functions of the square root of the carbon weight percent. For non-pearlitic steels, the wear resistance is a function of the particle size and mean free ferrite path. Different microstructures, therefore, behave differently during wear. It is generally recognised that most ferrous martensitic materials exhibit abrasive wear resistance superior to ferritic, pearlitic or bainitic materials (Figure 3.7).

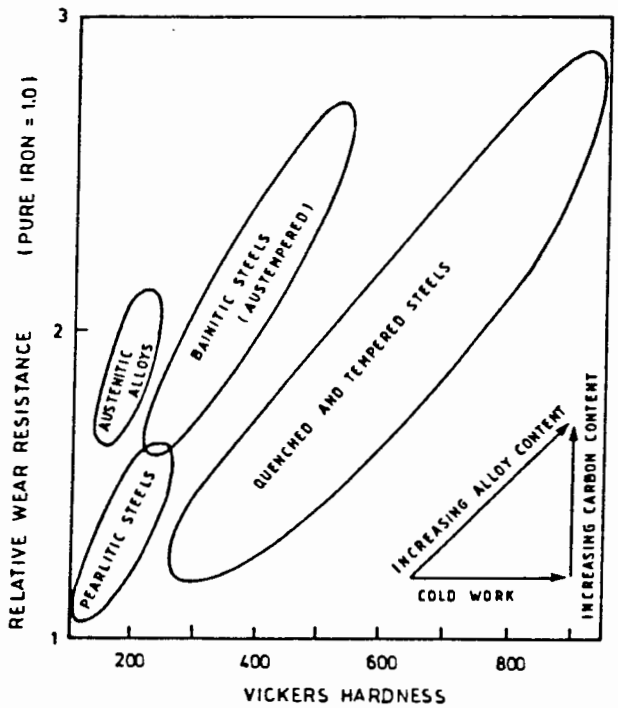

Figure 3.7 : Effect of structure, heat treatment and alloy content on the wear of steels. (Worn on 90 μm Al_2O_3 abrasive, $1MNm^{-2}$ applied load) (29)

3.5.2 Retained Austenite in the Matrix

Kar (41) found that bainitic microstructures containing substantial amounts of retained austenite exhibit better wear resistance than quenched and tempered martensite at similar hardness levels. He suggests that this may be related to the presence of high internal stresses in the quenched microstructures, thereby contributing to the poor fracture toughness and consequently low wear resistance.

Salesky (42) and Zum Gahr (39) suggest that retained austenite in the matrix increases abrasive wear resistance by two processes. Firstly, local stress induced transformation of the abrading surface raises the local hardness of the material thereby increasing the work hardening ability. Secondly, the soft and tough austenite acts as a crack inhibitor constraining any cracks that may initiate in the primary phase.

Allen et al (45) have also shown that the wear resistance of austenite stress is due primarily to the stress induced transformation of austenite to martensite giving increased strain to fracture, a high work hardening rate and a high fracture strength.

Kwok and Thomas (43), after studying the wear resistance of dislocated lath martensite with continuous interlath films of retained austenite, concluded that the reason for the enhancement of wear resistance by the retained austenite may be due to:

- the transformation-induced plasticity (TRIP), that can absorb energy for fracture and produce local compressive stresses that impede microcrack formation,
- the presence of the ductile austenite film between martensite laths which discourages microcrack nucleation and propagation,
- an increase in work-hardening coefficient through TRIP.

Bhat, Zackay and Parker (44) have suggested that the material having the best matrix properties for wear resistance would be a multiphase structure consisting of martensite and bainite with retained austenite. This would also give the optimum strength, hardness and toughness properties.

3.5.3 The Effect of Second Phase Particles

Larsen-Badse and Matthew (46) found that finely dispersed hard particles influence the flow stress of the material and thereby increase the abrasion resistance according to a Hall-Petch type relation, where the abrasion is inversely proportional to the square root of the distance between the particles. They conclude that coarse particles only contribute to abrasion resistance because they directly offer a hard surface. Thus ideally a fine distribution of spherical carbides is required for abrasion resistance.

However, the cohesion between precipitates and matrix increases as the shape changes from spheroids to platelets to needles. The ideal carbide shape to prevent pullout of carbides is thus the needle type. To obtain both low mean free path through the matrix and good cohesion, it is therefore necessary to have a high volume fraction of small, needle-like carbides (47).

Optimum matrix structure can, however, only be determined from consideration of the wear system in which the material operates. The general trend is that when carbides are harder than the abrasive and loads are high, then an austenitic matrix can give improved abrasion resistance and toughness. Where carbides are softer than the abrasive then martensitic irons give better abrasion resistance.

Sare (48) concludes that the wear rate is a balance between carbide removal and matrix removal, the slower of the two governing the overall wear rate. In low-stress abrasion, the carbides will retain sufficient support to resist pullout and fracture as preferential wear of the matrix will be slight, and gradual attrition of the carbides will thus control the wear rate. Preferential wear of the matrix becomes more significant under high-stress conditions, and carbides will be more easily pulled out and fracture - the wear of the matrix thus governing the rate.

3.6 TESTING TECHNIQUES

As stated by Uetz, Sommer and Khosrawi (49), "The ultimate assessment of the wear resistance of materials can only be obtained in service." Service tests are, however, time consuming and expensive, so some form of simulated tests in the laboratory must be used particularly in a programme in which new materials are tested.

The requirements of a meaningful wear test include:

- reproducability
- differentiability
- transferability

A fundamental problem of accelarated laboratory wear tests is that unless they simulate the wear mechanisms of the field application, the data produced has doubtful validity. (50)

3.6.1 Laboratory Tests

There are many laboratory testing techniques for the assessment of abrasive wear resistance of materials. These techniques are generally associated with the type of wear produced, of which high stress and low stress are two types.

In high stress systems laboratory apparatus is generally of the pin-on-disc type. A pin sample is loaded against a rotating disc of abrasive paper and the specimen traverses the disc, so describing a spiral path on the paper; thus it is always rubbed by fresh abrasive.

Variations of this type of apparatus include a belt grinder of the linisher type, where the specimen is moved across the rotating belt thus describing a helix on the abrasive paper. A vertical milling type of apparatus if also used where abrasive paper is bonded onto a platform and the specimen under load describes a series of passes across this flat table. Each pass is displaced by the width of the sample so that fresh abrasive is used each time.

In low stress systems the dominant abrasive wear testing apparatus is the sand/rubber wheel abrasion tester. This apparatus has the distinction of being the only abrasive wear testing device as yet covered by an internationally recognised standard specification. The specimen is loaded against the horizontal diametral line of the rubber wheel, and rounded quartz grain sand is introduced as a sand curtain between the wheel and the sample.

Apart from these two main categories of abrasion tests (viz. high stress and low stress) there are various other test methods. These can be broadly divided between those that study mechanisms, such as single pass diamond scratch tests, and those which attempt to simulate more closely the field applications, such as pilot plant ball mill tests.

3.6.2 Variables in the Wear Environment

Load

In two-body abrasive wear, weight loss varies linearly with nominal load. Moore (40) states that volumetric wear is directly proportional to the nominal load up to a critical load which is determined by the onset of massive deformation of the specimen or instability of the abrasive surface. For brittle materials, the wear mechanism changes at this point from plastic deformation to fracture.

Sliding Velocity

The effect of speed on wear against a fixed abrasive is associated with the material's dynamic properties through strain rate sensitivty resulting in change in the wear mechanisms (30). Velocity variations may also cause the particle loading to change, either through contacting particle flow dynamic effects or through larger range effects associated with strain rate stiffening of the abrasive medium.

Results from previous work have shown that an increase in velocity above 300 mms^{-1} has little effect on the wear rate as shown in Figure 3.8 (30).

Wear Path Length

Weight loss is found to increase linearly with sliding distance after initial non-linear behaviour. The non-linear portion may correspond to plastic deformation and strain hardening of the surface to equilibrium hardness (52), or embedding of abrasive particles in the surface of a specimen leading to an initial increase in its weight (53-55).

Grit Size

Larsen Badse (51) shows that the diameter of the abrasive influences wear. His results indicate that the wear rate increases with grit size until a critical diameter is reached (Figure 3.9). Above this volume the wear is found to increase much more slowly with grit size or to be independent of this variable.

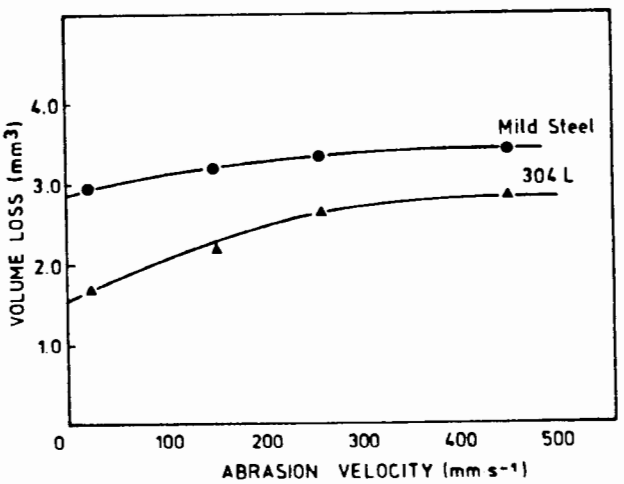

Figure 3.8 : The effect of abrasion velocity on volume loss during abrasion (30)

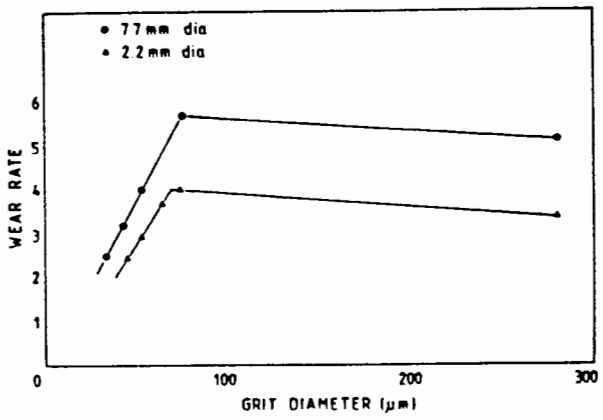

Figure 3.9 : The effect of abrasive grit size on wear rate (51)

CHAPTER 4

EXPERIMENTAL TECHNIQUES

4.1 MATERIALS

Two grades of commercially available spheroidal cast iron, namely grades SG42 and SG60, were examined during this study. Grade SG42 had a fully ferritic matrix and grade SG60 a ferritic/pearlitic matrix. Both grades had a nodule count in excess of 110 nodules/mm^2. This was sufficiently high to indicate a good quality of spheroidal cast iron.

The chemical composition of the two materials, grade SG42 and grade SG60, as well as the chemical compositions of the proprietary abrasion resistant alloys, are given in Table 4.1.

TABLE 4.1 : Chemical Analyses of Materials Used (wt %)

MATERIAL	C	Si	Mn	S	P	Cr	Ni	Mo	Cu	Al	Mg
Mild Steel	0.15	0.08	0.44			0.02	0.03	0.01			
SG42	3.7	2.2	0.1	0.02	0.05						0.037
SG60	3.6	2.1	0.25	0.05	0.05				0.8		0.03
Alloy A	0.48	0.14	0.86			0.01	0.01	0.01			
Alloy B	0.39	0.17	0.85	0.018	0.012	0.43	0.60	0.16	0.05	0.038	
Alloy C	0.35	0.26	0.59			0.89	0.02	0.19			
Alloy D	0.25	0.02	0.02			8.00	3.00	0.01			
Alloy E	0.71	0.31	0.55	0.026	0.012	0.28	0.11	0.03	0.18	0.010	
Hadfield	1.25		12.0								

4.2 SAMPLE PREPARATION

All the necessary samples required for testing were made in the laboratory workshop. Standard Hounsfield tensile specimens of diameter 4.51 mm and gauge length 22.55 mm were made. Lengths of square bar, 10x10 mm were machined. These lengths were used to make Charpy specimens as well as 25 mm long specimens. These shorter lengths were used for microstructural analysis, abrasion testing and X-Ray analysis.

4.3 HEAT TREATMENTS

4.3.1 Decarburisation

Prior to any heat treatment of specimens,a study was carried out to determine the effects of decarburisation during the austenitising process.

The surfaces of the specimens were polished down to a 1 μm and coated with two commercially available protective ceramic coatings. Only one half of each specimen was coated; the other half was left in the polished condition. Type A coating is heat resistant up to 900°C and Type B up to 1100°C. Each specimen was first coated with Type A, allowed to dry, and then coated with Type B.

After austenitising at 900°C for 60 minutes the specimens were austempered at 350°C for 30 minutes. They were then cleaned and cross sections taken of the uncoated and coated sides. Microhardness values, using a load of 25 grams, were taken at various depths below the exposed surface. This enabled the depth to which decarburisation occurred to be determined. The extent and depth of decarburisation is indicated by a fall in hardness values in the surface layers.

Both grades SG42 and SG60 were tested. The results are shown in Figures 4.1 and 4.2.

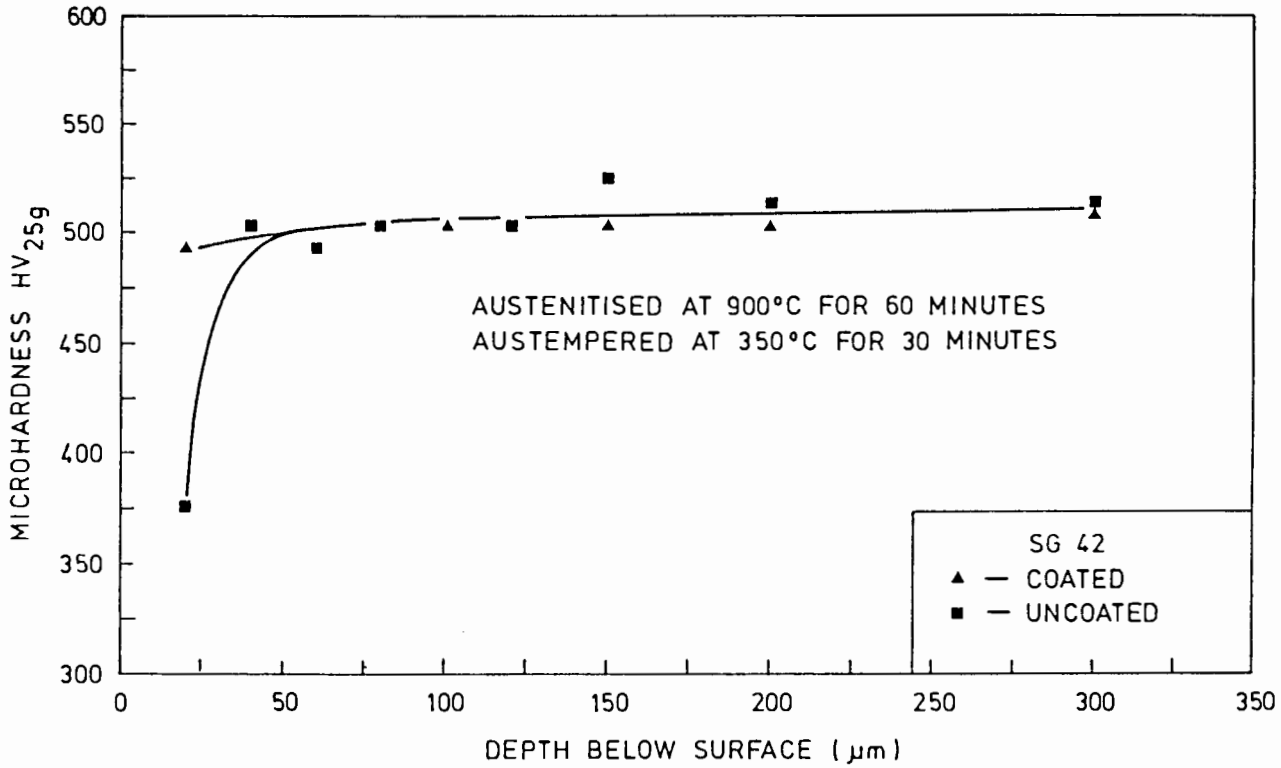

Figure 4.1 : Showing the effect of decarburisation on the microhardness of the surface layers following austenitising for grade SG42

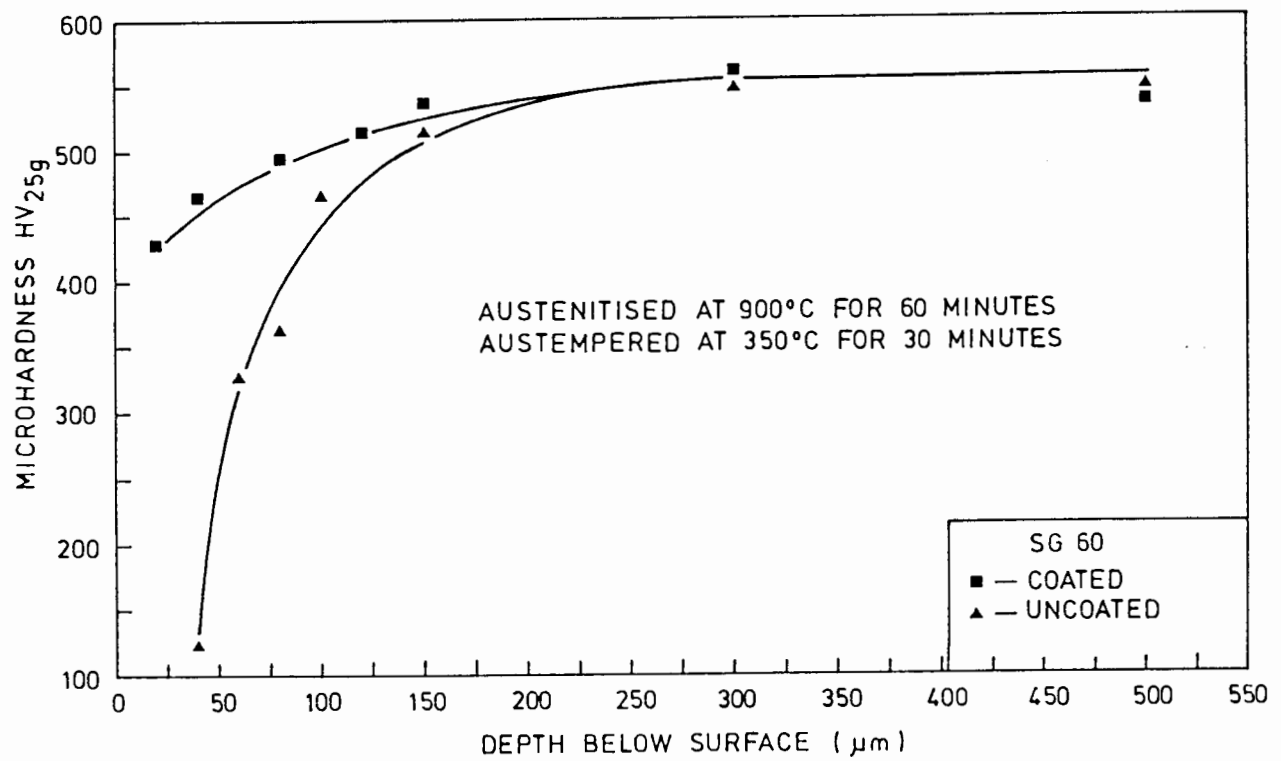

Figure 4.2 : Showing the effect of decarburisation on the microhardness of the surface layers following austenitisation for grade SG60

From the results it is apparent that the coatings were effective in preventing and/or slowing down decarburisation. Both uncoated specimens showed decarburisation. The coated grade SG42 material did not appear to have suffered any decarburisation whilst the coated grade SG60 showed partial decarburisation to a depth of 150 m. Grade SG60 has the greater susceptibility to decarburisation. This is probably due to the higher carbon concentration present in the matrix of the austenitised grade SG60 material as compared to the grade SG42 material which initially has a fully ferritic matrix.

All specimens were therefore coated with the ceramic coatings before being heat treated.

4.3.2 Furnaces

All austenitising heat treatments were performed in two muffle furnaces. Both furnaces had Nitrogen purging facilities and during heat treatment a flow rate of 2 cm^3/sec. was maintained throughout. All austenitisation times were preceded by a 20 minute soak of the specimen at the austenitising temperature. Austenitisation times varied from 2 minutes to 120 minutes at temperature and austenitisation temperatures from 800°C to 950°C. The furnace temperatures were controlled to an accuracy of ± 2°C of the preset temperature.

4.3.3 Salt Baths

The specimens were transferred to the salt bath with steel tongs as quickly as possible; approximately 1-3 seconds. This was to ensure that the cooling rate was sufficient to avoid the formation of pearlite during cooling. The poor hardenability of the unalloyed spheroidal cast iron, especially the ferritic SG42, made this step the most critical of the whole heat treatment process.

All austempering was performed in two salt baths and specimens were heat treated in the range from 160°C to 500°C. Austempering times varied between 2 minutes to 240 minutes. The salt baths could be accurately controlled to within ± 2°C of their preset temperature.

4.4 MECHANICAL TESTING

Mechanical properties were determined for a range of heat treatments. These included a comprehensive set of tensile tests for the two austempering temperatures of 250°C and 350°C and austempering times between 2 minutes to 120 minutes. Both grades SG42 and SG60 were tested.

Tensile testing: Tensile tests were performed on a ZWICK 150 kN tensile testing machine at a strain rate of 15mm/min. Three tests were carried out for each heat treatment and the average value recorded.

Hardness testing: Hardness was measured using a Vickers diamond pyramid indentor using a 30kg load. The average value of four tests on each specimen was recorded. Microhardness tests were performed using a Shimandzu diamond pyramid indentor. An average of five readings was taken, using loads ranging from 25 to 200 grams. Taper sections of various austempered specimens were used to determine variation in hardness at different depths below the specimen surface.

Toughness measurements were conducted using Charpy V-notch specimens. The toughness tests were limited to a smaller range of austempered specimens than the tensile tests. No Charpy testing on specimens austempered for different times was performed.

The object of mechanical testing was to determine how the properties of the materials were affected by different heat treatment temperatures and times, and whether the retained austenite, acicular ferrite and/or martensite had any effect on tensile strength and toughness of the material.

4.5 ABRASION TESTING

Dry abrasion testing was performed on a variety of austempered ductile irons and an assortment of other proprietary abrasion resistant alloys. This enabled austempered spheroidal cast irons to be compared with other abrasion resistant alloys. Normalised mild steel was used as the standard.

The abrasion rig was an extensively modified Rockwell disc/belt sanding machine. It was modified to function as a semi-automatic abrasion testing machine (Figures 4.3 and 4.4).

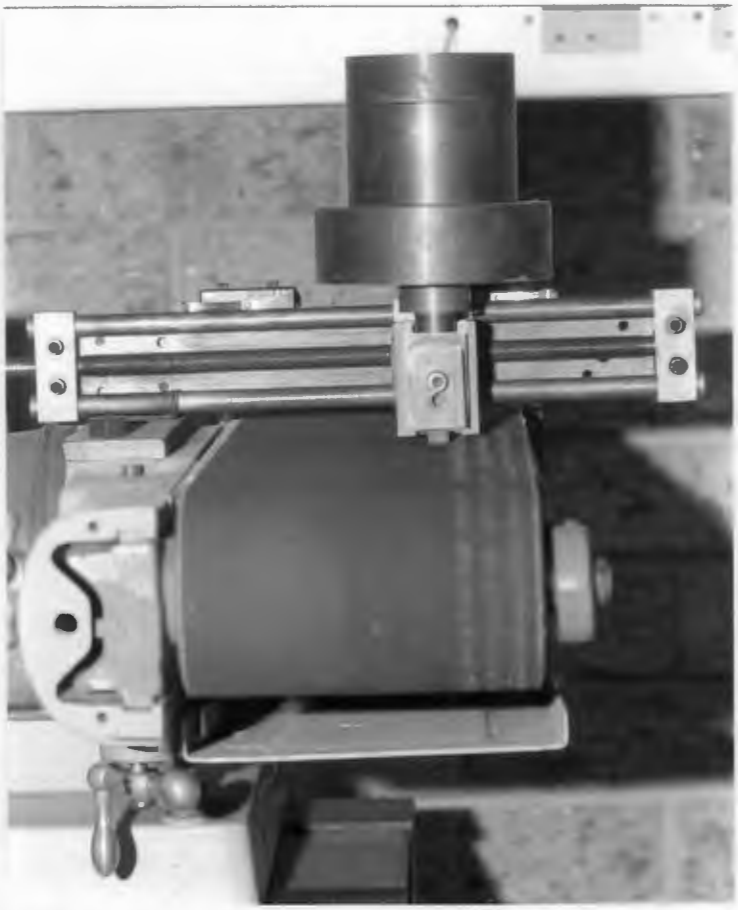

Figure 4.3 : Frontal view of the Linisher abrasion tester

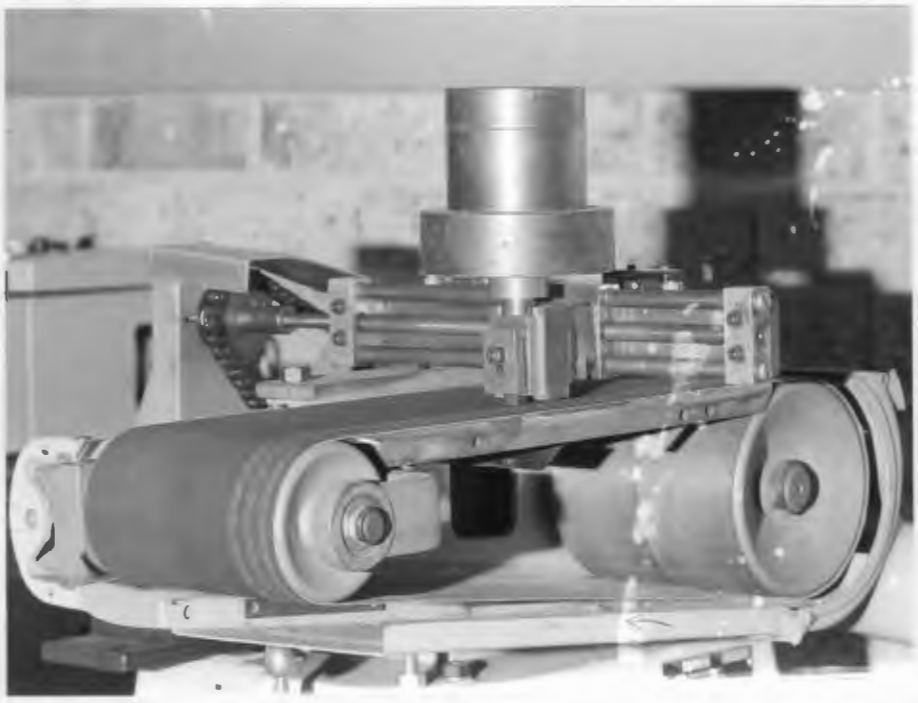

Figure 4.4 : Side view of the Linisher abrasion tester

It involves the principle of abrading a dead loaded specimen, 10x10x15 mm in length, against the surface of a bonded abrasive belt. The continuous belt runs horizontally at a constant velocity while the specimen is made to traverse normal to the direction of belt movement; thus the specimen abrades against unworn particles all the time.

Each sample was run in on old abrasive belts until the abraded surface was flat and uniform. The leading edge of each sample was marked so that in subsequent tests the samples were always aligned in the same way. After running in, the samples were ultrasonically cleaned in alcohol, dried and the initial mass recorded. The samples were then abraded in accordance with the test parameters given, ultrasonically cleaned, dried and re-weighed. Each sample was tested in this manner five times. The loss in weight was converted to volume loss and the wear resistance was calculated relative to mild steel using the reciprocal of volume loss,i.e.

$$\text{Relative abrasion resistance (RAR)} = \frac{\text{Volume loss of mild steel}}{\text{Volume loss of specimen}}$$

In this way the relative abrasion resistance (RAR) of the material could be compared. The reproducibility of the test was found to be within ± 4%. This is consistent with other pin on disc testing equipment.

The actual conditions which were employed for testing were:

Load	3.2Kg
Length of abrasion path	14.64m
Mean Diameter of abrasive particles	300 μm
Type of abrasive	Al_2O_3
Velocity of belt	$0.28ms^{-1}$

Before and after abrasion, the austempered ductile iron specimens were analysed for retained austenite. This enabled the effect of abrasion on transformation of the retained austenite to martensite to be studied.

Microhardness of taper sections of the ADI were taken to determine the depth to which the retained austenite transformed to martensite during abrasion.

4.5.1 Selection of Speed, Load, Abrasion Path Length and Grit Size

It was decided that the speed at which the rate of volume loss for mild steel and 304L stainless steel did not alter significantly with increasing speed, should be chosen for the test (Section 3.6.2). A speed of 280 mm/sec was therefore chosen for the dry abrasion testing.

In order to select the load, a comparison was made of the percentage of austenite to martensite transformation under different loading conditions. From the results in Figure 4.5 it can be seen that the change in loads had little effect on the final amount of retained austenite following abrasion. A load of 3.2kg was finally chosen as this fell in the middle of the range of loads tested and proved to be convenient.

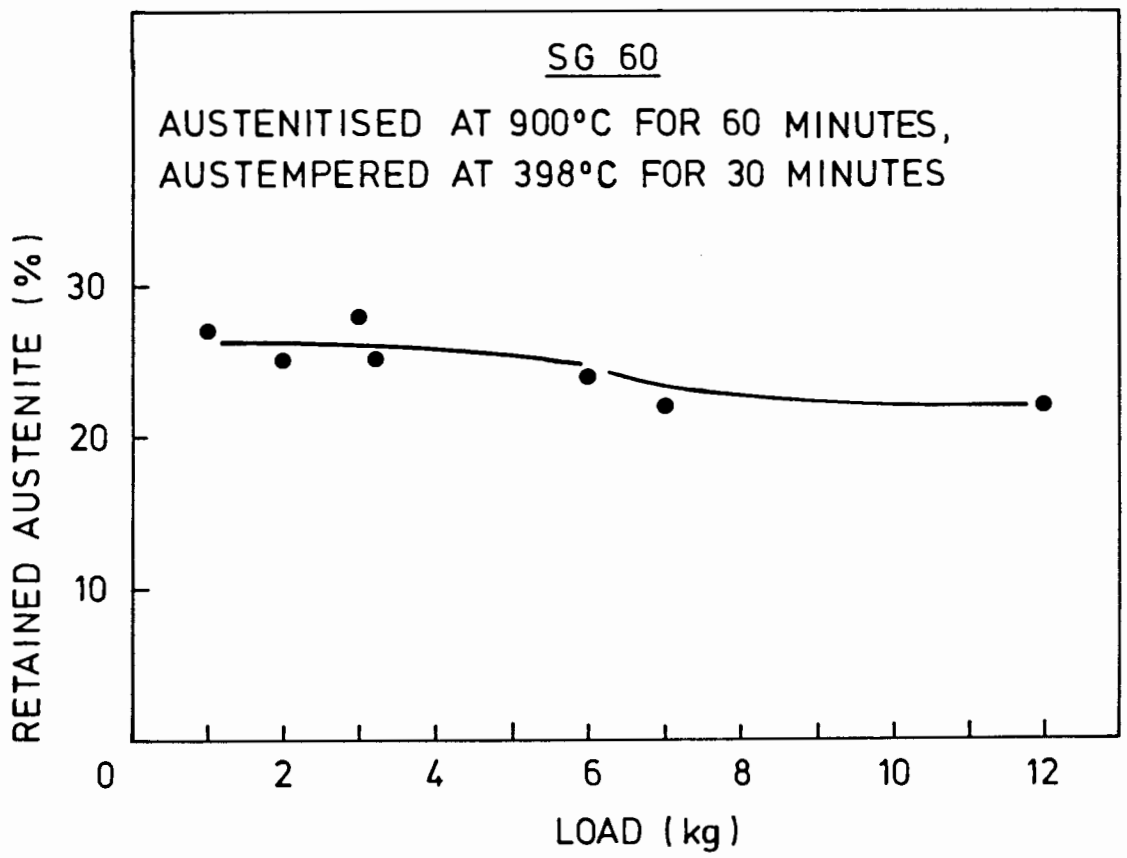

Figure 4.5 : The effect of load on percentage of retained austenite after abrasion at 2.8 ms^{-1}

An abrasion path length of four times 3.64m (i.e. a total of 14.64m) was chosen because it gave good measurable and reproducible volume losses of material.

It was decided to use 80 grit alumina (300 μm) as the abrasive owing to reasons discussed in Section 3.6.2 and also due to the easy availability of this size abrasive belt.

4.6 MICROSTRUCTURAL EXAMINATION

Heat treated specimens, as well as abraded specimens, were examined using both optical and scanning electron microscopes. A Nikon microscope was used for optical microscopy and a Cambridge 200 SEM for electron microscopy. All specimens were finally polished using a 0.25 m diamond paste and etched in a 2.5% Nital solution for a few seconds prior to microscopic observation.

Single and multiple particle abrasion track specimens were examined under the scanning electron microscope. The single particle abrasion track specimens were initially polished to 1 μm and etched with 2.5% nital solution for a few seconds. This allowed the wear tracks as well as the etched microstructure of the specimens to be studied.

X-ray analysis was performed using molybdenum radiation and was carried out on a Phillips diffractometer. Retained austenite measurements were made using the integrated intensities of two suitable diffraction peaks. The austenite/ferrite diffraction lines best suited are the (200) of the ferrite and the (220) reflection of the austenite. Retained austenite measurements were made in accordance with the recommended procedure of the manufacturer (Appendix 1). X-ray analysis was performed on specimens polished using a 0.25 μm diamond paste and etched in a 2.5% Nital solution for a few seconds. Specimens were ultrasonically cleaned and dried prior to analysis after abrasion.

CHAPTER 5

RESULTS AND DISCUSSION

HEAT TREATMENTS

5.1 AUSTENITISATION TEMPERATURE AND TIME

From the literature review it appears that the austenitisation temperature was important in determining whether the material could be successfully austempered or not. The austenitising temperature and time at temperature affect the amount of carbon taken into solution in the austenite. This in turn plays an important role in determining the hardenability and the final amount of stabilised austenite that can occur in the matrix after austempering.

5.1.1 Microstructural Examination

Generally the microstructures resulting from the austentising and austempering heat treatments consist of graphite spheroids in a basic matrix of acicular ferrite and retained austenite. However, such structures were only consistently obtained for all austempering temperatures when the austenitising temperature exceeded 900°C. Table 5.1.

Below an austenitising temperature of 900°C, other transformation products, e.g. pearlite, were apparent, particularly in the grade SG42 material.

For example, austenitising grade SG42 at 850°C gave two different microstructures depending on the austempering temperature. A 250°C austemper gave a pearlitic matrix (Figure 5.1 (a)). A 342°C austemper gave an acicular ferrite and retained austenite matrix (Figure 5.1 (b)).

TABLE 5.1 : Effect of Austenitising Temperature on Matrix Structure
Austenitised for 60 minutes

AUSTENITISING TEMPERATURE °C	MATRIX STRUCTURE			
	Austempered at 250°		Austempered at 350°C	
	Grade SG42	Grade SG60	Grade SG42	Grade SG60
800	Pearlite	Pearlite	Pearlite	Pearlite
850	Pearlite Fig 5.1 (a)	Acicular ferrite and retained austenite	Acicular ferrite and retained austenite Fig 5.1 (b)	Acicular ferrite and retained austenite
900 and 950	Acicular ferrite and retained austenite	Acicular ferrite and retained austenite	Acicular ferrite and retained austenite	Acicular ferrite and retained austenite

Micrographs showing the effect of austenitising time at 900°C on the resulting structure are shown in Figures 5.2 (a) and (b).

From Figures 5.2 (a) and (b) the austenitising time appeared to play a significant role in increasing the amount of retained austenite present in the matrix structure for both grades SG42 and SG60. As the austenitising time increased the volume of retained austenite increased. Consequently the matrix became coarser and large blocks of retained austenite were present at austenitising times of 60 minutes (Figure 5.2 (b)).

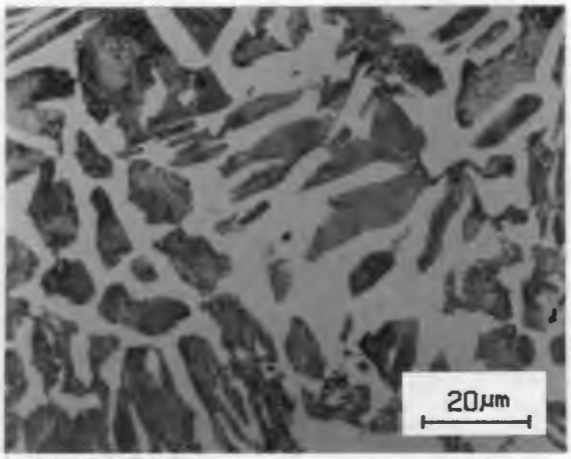

(a) Austempered at 250°C. Pearlite

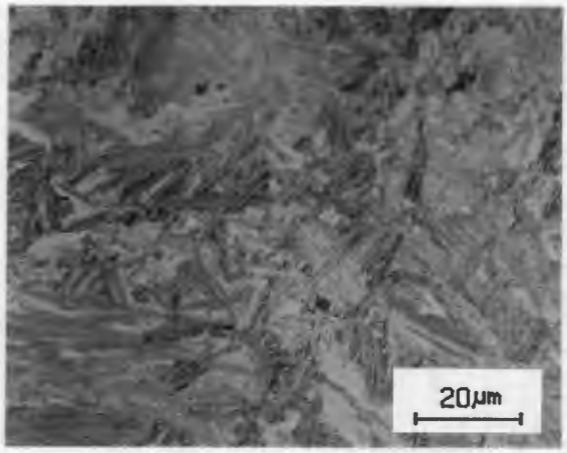

(b) Austempered at 342°C. Acicular ferrite and retained austenite

Figure 5.1 : Optical micrographs of grade SG42 iron, austenitised at 850°C for 60 minutes, illustrating the effect of the austempering temperature on the resulting matrix structure. Etched in Nital. (x720)

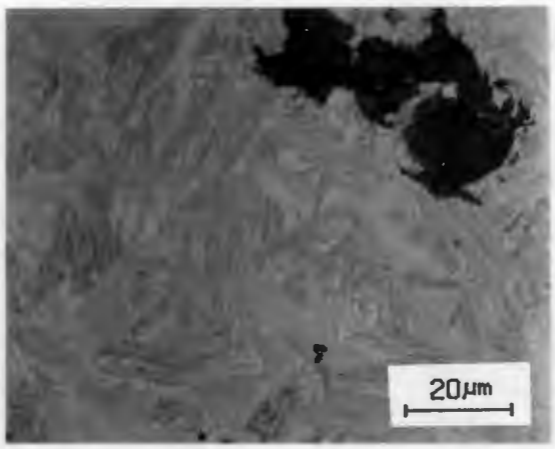

(a) Austenitised for 10 minutes

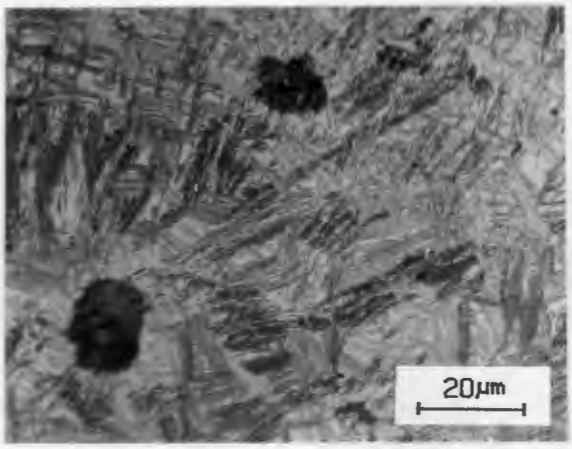

(b) Austenitised for 60 minutes

Figure 5.2 : Optical micrographs of grade SG42 iron, austempered at 342°C, illustrating the effect of austenitising time on the resulting matrix structure. Etched in Nital. (x720)

5.1.2 X-Ray Diffraction

The results showing the effect of austenitising temperature on retained austenite present in the matrix of the two grades, SG42 and SG60, are illustrated in Figures 5.3 and 5.4, and Table 5.2. Measurements were taken on specimens austempered at 250°C, 342°C and 350°C.

Following austenitising at a temperature of 800°C no retained austenite was present in either grade SG42 or SG60 for austempering temperatures of 250°C and 342°C.

Austenitising at 850°C resulted in no retained austenite in grade SG42 austempered at 250°C, but 16% austenite when austempered at 350°C. Grade SG60 had retained austenite present after austenitising at 800°C and austempering at either 250°C or 350°C.

Above an austenitising temperature of 850°C, the amount of retained austenite found in the matrix increased with increasing austenitising temperatures for both grades and all austempering temperatures.

It was also noticeable that above an austenitising temperature of 900°C the rate of increase of retained austenite slowed down considerably, particularly for the lower austempering temperature of 250°C.

The amounts of retained austenite found in specimens austempered at 350°C were always greater than for the specimens austempered at 250°C for equivalent austenitising temperatures. For example, at 950°C, and austempered at 342°C, grade SG60 had 45% retained austenite present, but at an austemper of 250°C only 25% was present.

Grade SG60 always showed consistently higher retained austenite percentages than grade SG42 austenitised at different temperatures. For example when austenitised at 950°C, and austempered at 342°C, grade SG60 had 45% retained austenite present, while grade SG42, for a similar heat treatment, had 30% present.

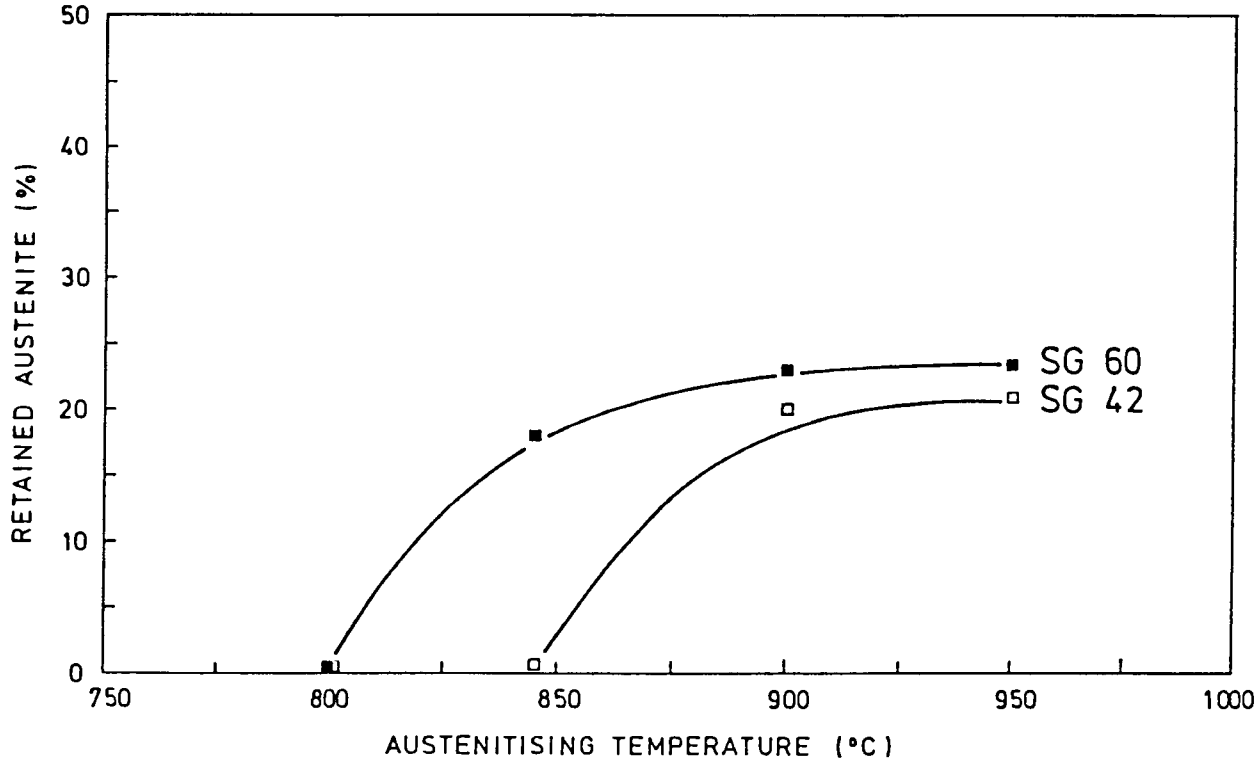

Figure 5.3 : Retained austenite quantities found in grades SG42 and SG60 austenitised for 60 minutes at various temperatures. Austempered at 250°C for 30 minutes

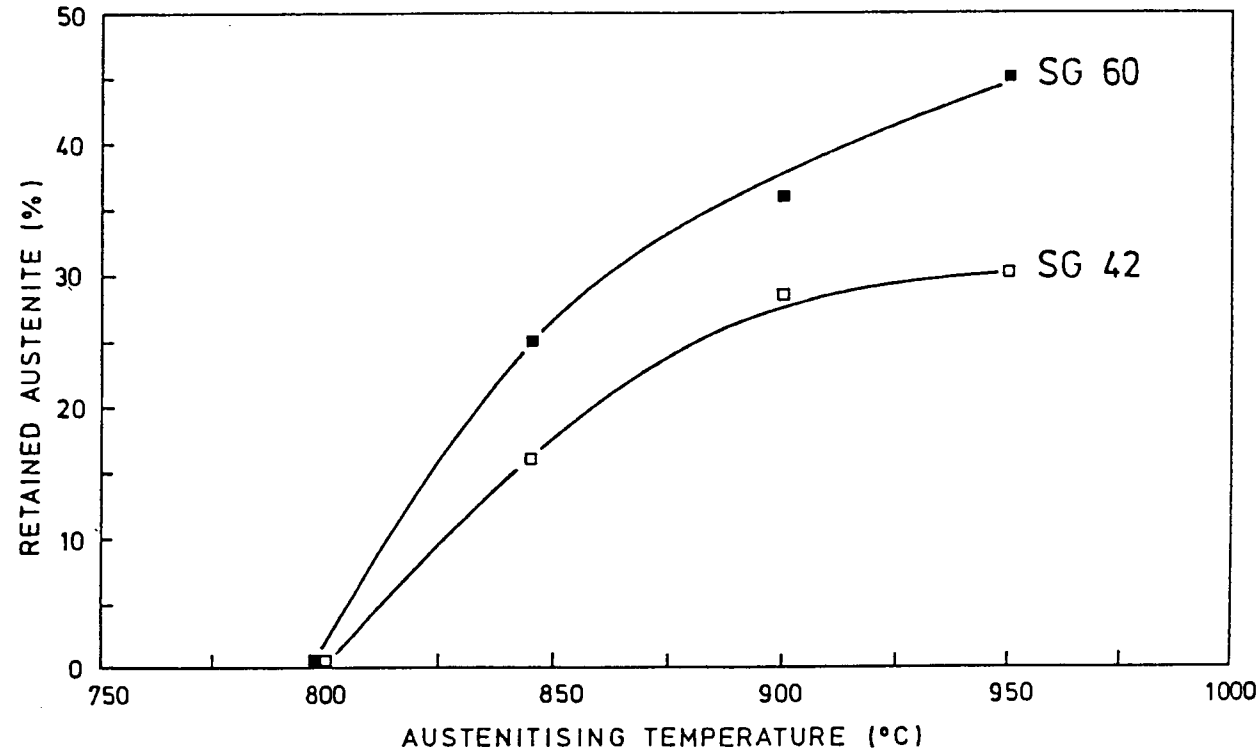

Figure 5.4 : Retained austenite quantities found in grade SG42 and SG60 austentised for 60 minutes at various temperatures. Austempered at 342°C for 30 minutes

TABLE 5.2 : The effect of austenitising temperature on percentage retained austenite in the matrix. Austenitised for 60 minutes.

AUSTENITISING TEMPERATURE °C	% RETAINED AUSTENITE IN THE MATRIX			
	Austempered at 250°		Austempered at 350°C	
	Grade SG42	Grade SG60	Grade SG42	Grade SG60
800	0	0	0	0
850	0	18	16	25
900	19	23	28	35
950	21	25	30	45

The effect of austenitising time, at an austenitising temperature of 900°C, also effected the amount of retained austenite following austempering at 250°C and 350°C for 30 minutes. Figures 5.5 and 5.6.

As the austenitising times increased from 2 minutes to 120 minutes, the amount of retained austenite in the matrix increased. For an austemper at 342°C, retained austenite in grade SG60 increased from 30% after 10 minutes, to 35% after 120 minutes.

The same trend occurred for the 250°C austemper, although the amounts of retained austenite were less. For grade SG60, retained austenite increased from 19% after 10 minutes, to 24% after 120 minutes. For grade SG42 the increase was from 14% after 10 minutes, to 21% after 120 minutes.

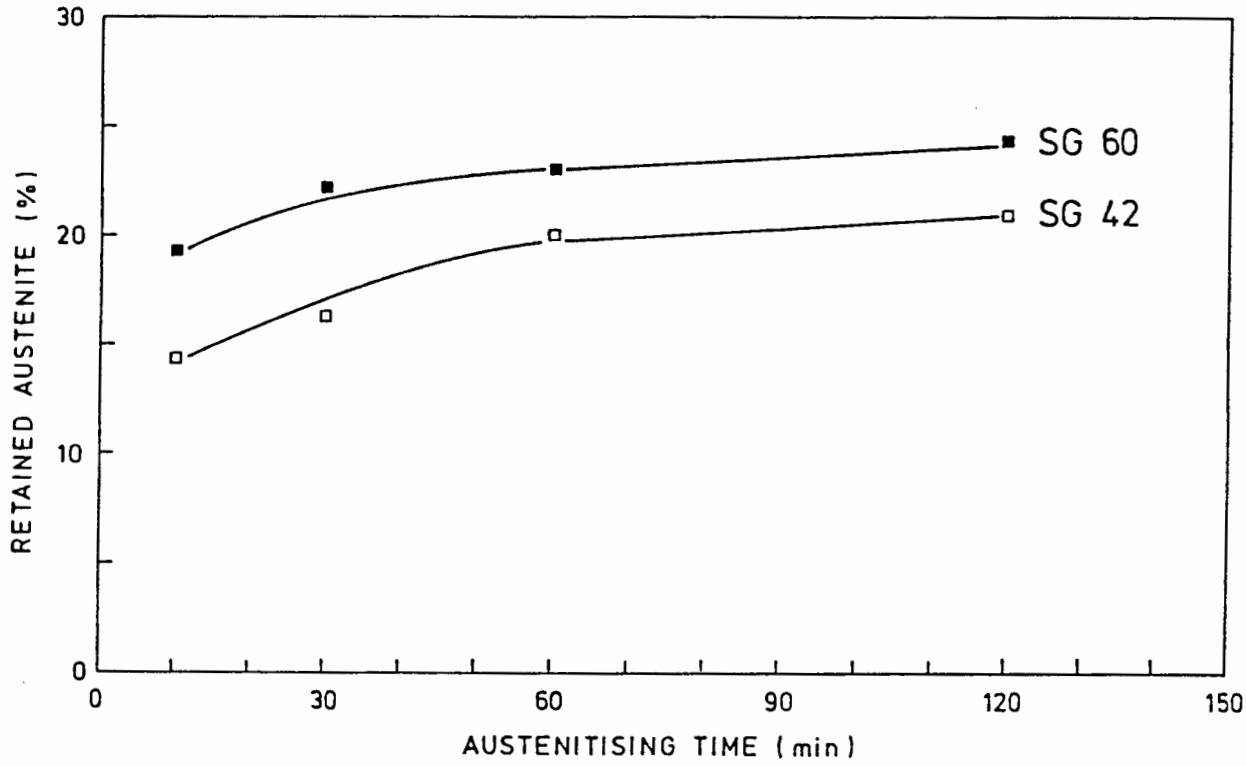

Figure 5.5 : Retained austenite quantities found in grades SG42 and SG60 austenitised at 900°C for various times. Austempered at 250°C for 30 minutes

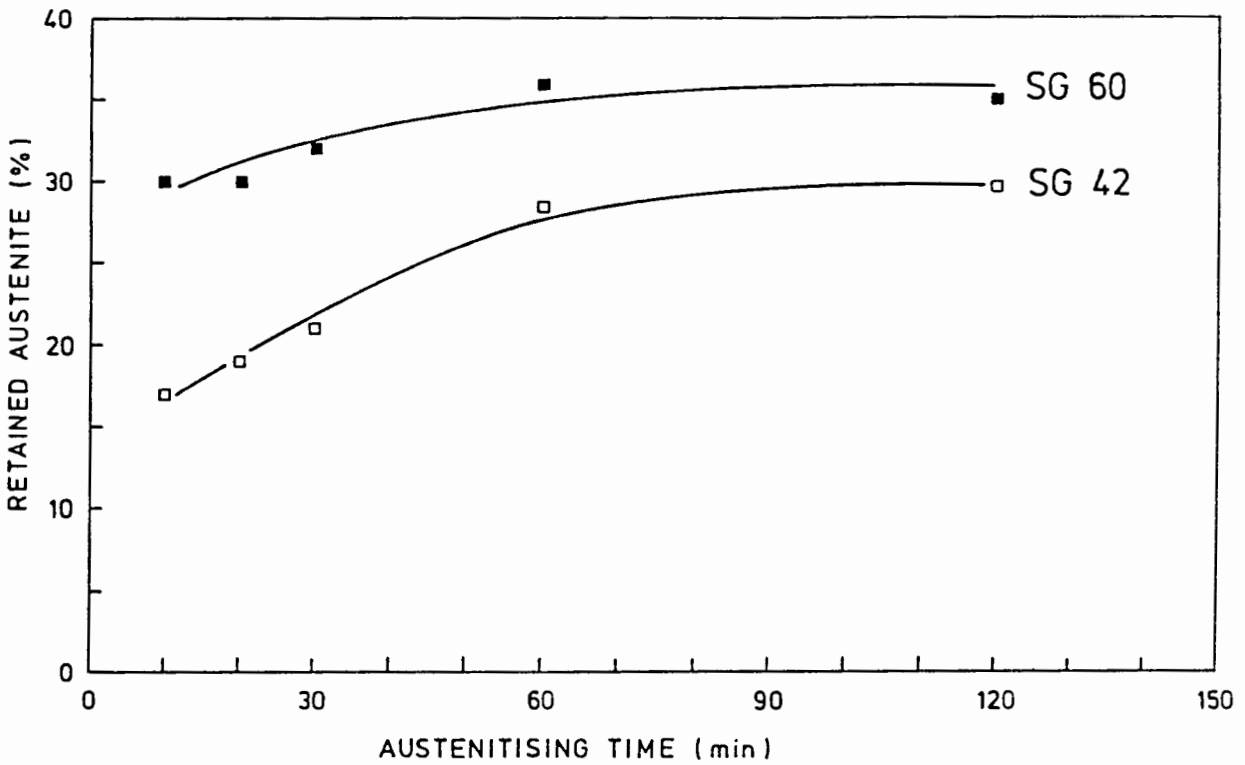

Figure 5.6 : Retained austenite quantities found in grades SG42 and SG60 austenitised at 900°C for various times. Austempered at 342°C for 30 minutes

5.1.3 Discussion

Austenitisation is important as it determines the amount of carbon that can and will be dissolved into the austenite matrix. The greater the carbon content of the austenite the higher the hardenability and the lower the critical cooling rate to avoid pearlite formation. The carbon content of the austenite also determines how much austenite will be stabilised following austempering treatments. The higher the carbon content of the austenite the greater the depression of the M_S temperature. The M_S temperature can be depressed to well below room temperature resulting in substantial quantities of austenite being retained on cooling the iron to room temperature.

It is important to remember however, that the austempering reaction itself, affects the carbon content of the austenite. Thus the final amount of carbon in the austenite is dependent on both the austenitising as well as the austempering temperatures and times.

5.1.3.1 Austenitising Temperatures

It is apparent from the results that the austenitising temperature plays an important role in determining whether or not the material can be successfully heat treated.

The austenitisation temperature has to be high enough to ensure that the material being heat treated is in the austenite region of the Fe-C-Si phase diagram. From Figure 2.3, Section 2.1.3, it is apparent that at 800°C the fully austenitic region is not attained for either the ferritic grade SG42 or the pearlitic/ferritic grade SG60 iron. Accordingly, no acicular ferrite or retained austenite is expected - only ferrite and/or pearlite. This is apparent in Figures 5.3 and 5.4 and Table 5.1, which show that no retained austenite is present.

At 850°C, two different results are obtained for the two austempering temperatures for grade SG42. According to the phase diagram, 850°C is still below the fully austenitic region for a ferrite matrix material. The amount of carbon rejected into the austenite under these conditions would therefore be negligible and no retained austenite is expected upon cooling, only ferrite and possibly pearlite. This is indeed the case for results obtained for the 250°C austemper but not the 350°C austemper.

To explain this discrepancy it is necessary to study the kinetics of the austempering reaction.

The austempering reaction itself rejects carbon into the austenite as the transformation proceeds, i.e. the acicular ferrite platelets grow. At low austempering temperatures e.g. 250°C, the carbon diffusion rate is relatively slow and very little carbon is rejected by the growing ferrite into the austenite. The carbon appears to be rejected as epsilon-carbide in or alongside the ferrite needles. As no austenite has been stabilised by the rejected carbon, no retained austenite should be present upon cooling. From results in Figure 5.1 (a) and 5.3 this is what appears to have occurred.

At 350°C however, the diffusion rate of carbon is greater than at 250°C and enrichment of the austenite can occur. This enrichment stabilises the austenite and upon cooling an acicular ferrite and retained austenite matrix is observed (Figures 5.1 (b) and 5.3).

The retained austenite present in grade SG42 at 850°C is therefore not related to the austenitising temperature but rather to the kinetics of the austempering reaction. (To be discussed in more detail in Section 5.2.5).

At 850°, for grade SG60, the material is now within the austenite region and hence an acicular ferrite and retained austenite matrix is expected after austempering. At 900°C and above both grades SG42 and SG60 are within the austenite regions and as can be seen from Table 5.1, retained austenite and acicular ferrite is present following austempering. Figures 5.3 and 5.4 confirm the presence of retained austenite in the austempered structures.

The levelling off in the rate of increase of retained austenite with higher austenitising temperatures is probably due to the higher rate of carbon diffusion at higher temperatures. After 60 minutes at 950°C the maximum amount of carbon possible in the matrix would most probably have been reached whereas at lower temperatures more time would be needed to attain carbon saturation of the matrix. The levelling off of austenite percentages in the austempered specimens is therefore due to the saturation limit of carbon in the austenite being reached sooner at higher austenitising temperatures.

This explanation is supported by the results obtained when austenitising temperatures were varied.

Grade SG60 will tend to have more retained austenite in the austempered matrix than grade SG42 for equivalent austenitising temperatures and times. This is due to the original matrices of these two materials. Grade SG60 has a pearlitic/ferritic matrix when in the unheat treated state and grade SG42 has a fully ferritic matrix before heat treatment. Upon austenitisation the cementite, from the pearlite, can go into solution relatively quickly as carbon, thereby enriching the austenite in grade SG60. This carbon is over and above any carbon diffusing from the graphite spheroids. As ferrite has negligible carbon, grade SG42 upon austenitisation will have to receive all its carbon from graphite spheroids - a much more time dependant and thermodynamically unfavourable reaction.

5.1.3.2 Austenitisation Time

The longer the austenitisation time the greater the amount of retained austenite present in the structure after austempering. This is apparent from retained austenite measurements and micrographs, i.e. large 'blocks' of retained austenite are visible and the matrix appears to be coarser.

This is is due to the increase of carbon in the austenite with increasing austenitising time. The diffusion of carbon into the austenite is time dependent and for longer soaking times more carbon is able to diffuse into the austenite matrix. Eventually the carbon saturation will reach a limit due to the matrix being unable to accommodate any further carbon. At 900°C this is approximately 0.83% (9). Higher carbon concentration in the matrix inhibits growth of ferrite plates. The matrix will therefore have a coarser appearance due to more stabilised austenite and less ferrite plate growth.

As carbon saturation of the matrix occurs with time at austenitising temperature, the amount of retained austenite in the matrix, following austempering, tends towards a maximum as would be expected. This can be seen to occur in Figures 5.5 and 5.6 for both grades SG42 and SG60. At an austempering temperature of 900°C this levelling off starts to occur after about 60 minutes.

5.2 AUSTEMPERING TEMPERATURE AND TIME

The austempering temperature and time appear to have an important effect on the final nature of the heat treated material. Austempering conditions determine the microstructures, the quantities of stabilised austenite as well as the mechanical properties of the material.

All austempering temperatures and times were performed following a 60 minute soak at the austenitisation temperature of 900°C. These conditions allowed satisfactory austenitisation - see Section 5.1.

5.2.1 Microstructural Examination

The microstructures produced after a 30 minute soak between austempering temperatures of 250°C and 375°C for grade SG42 iron are shown in Figures 5.7 (a-e).

At the lower austempering temperatures, noticeably below 300°C, the structure consists of very fine ferrite needles/platelets interspersed in retained austenite. As the transformation temperature is raised the ferrite plates become progressively coarser and more feathery in appearance. At an austempering temperature of 375°C, nodules of fine pearlite were observed in the ferrite/austenite matrix. Grade SG42 austempered at 400°C was found to have a fully pearlitic matrix.

The same trend is evident in the scanning electron micrographs of grade SG42 for the same austempering conditions. Figures 5.8 (a-e). The ferrite platelets can be seen to become coarser and more feathery. At 400°C, in Figure 5.8 (e), the microstructure is totally pearlitic.

The microstructures observed in grade SG60 iron, austempered at similar temperatures and times were almost identical except that no pearlite colonies were found in specimens transformed at 375°C. A fully duplex ferrite/austenite matrix was maintained until a transformation temperature of approximately 450°C was reached. Small volumes of pearlite were then observed in the structure

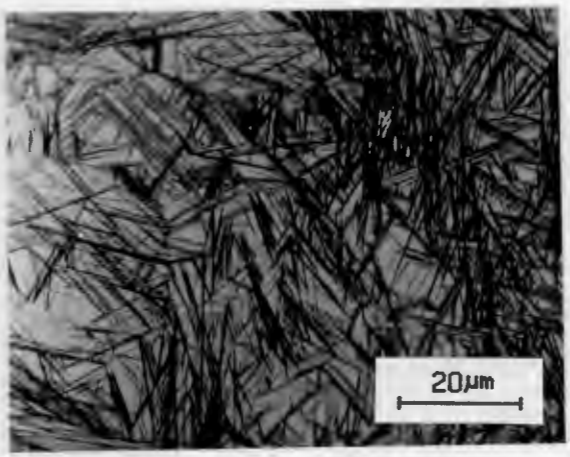

(a) Austempered at 250°C

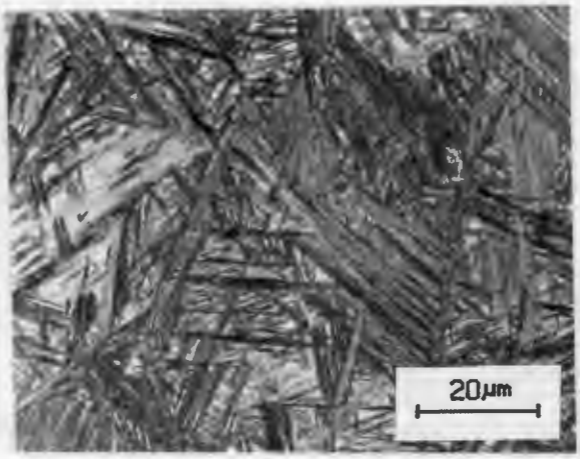

(b) Austempered at 300°C

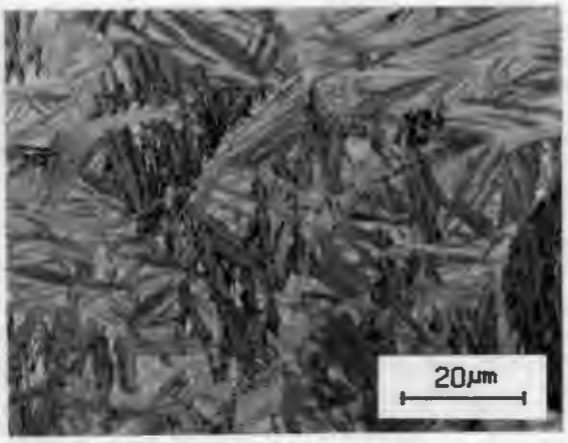

(c) Austempered at 325°C

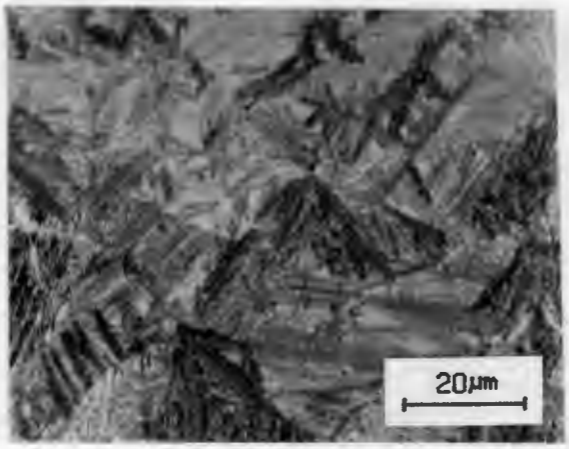

(d) Austempered at 355°C

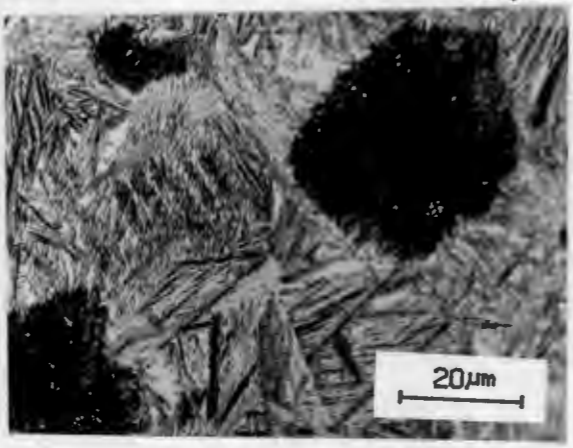

(e) Austempered at 375°C

Figure 5.7 : Optical micrographs for grade SG42, austenitised at 900°C for 60 minutes, illustrating austempering temperature on the resulting microstructure. Etched in Nital. (x1000)

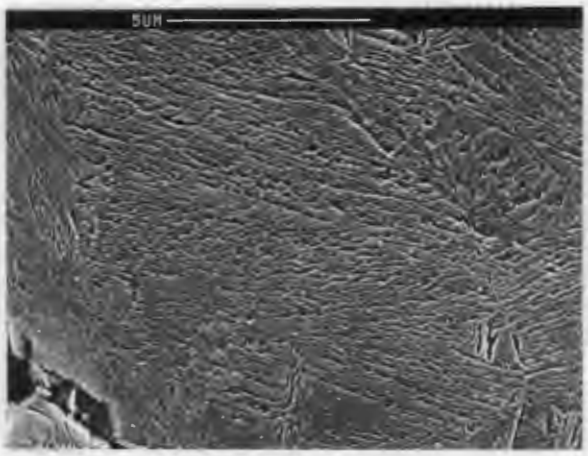

(a) Austempered at 300°C

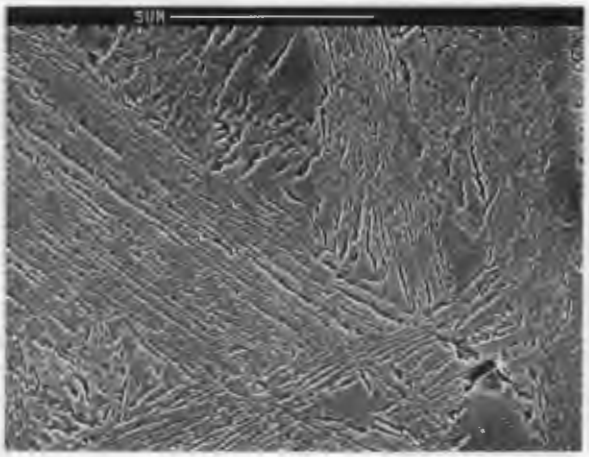

(b) Austempered at 325°C

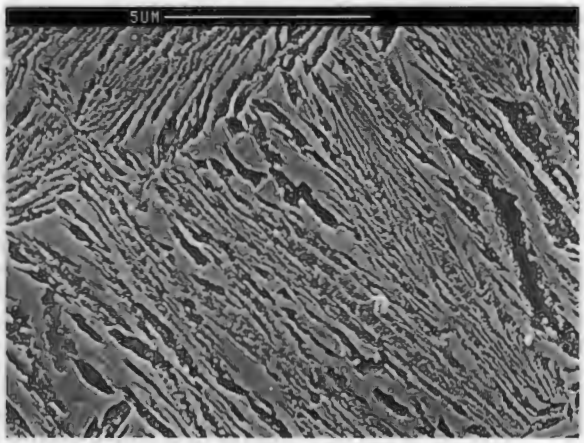

(c) Austempered at 355°C

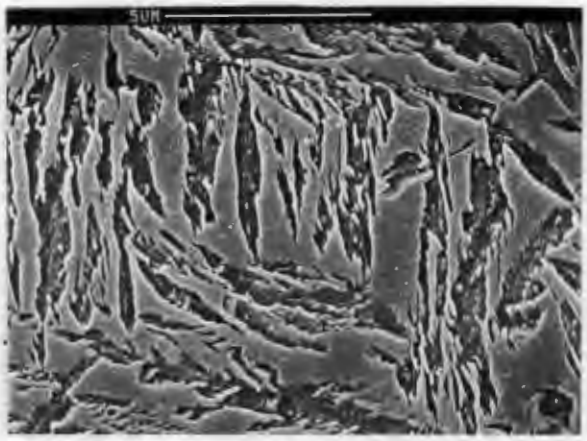

(d) Austempered at 375°C

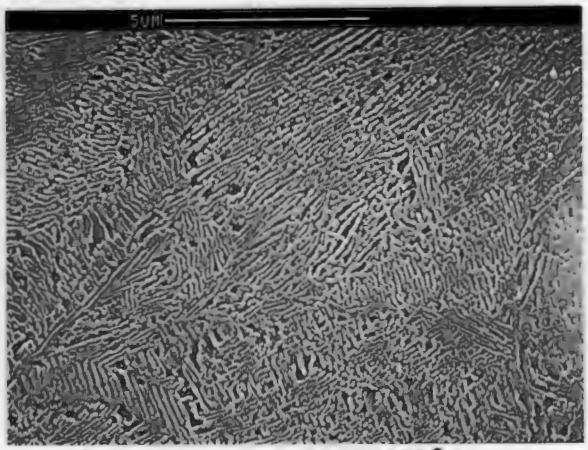

(e) Austempered at 400°C

Figure 5.8 : Scanning electron micrographs for grade SG42, austenitised at 500°C for 60 minutes, illustrating the effect of austempering temperature and the resulting microstructure. Etched in Nital.

Figure 5.9 (a-d) shows microstructures produced after soaking times varying from 6 minutes to 60 minutes at 355°C for grade SG42.

The basic ferrite/austenite matrix structure was modified for short austempering times, usually less than 30 minutes, by the appearance of martensitic needles. The amount of martensite decreased with increasing austempering times. Similar three phase matrix microstructures were observed in both grades of spheroidal cast iron transformed at all austempering temperatures for short perods of time.

As the length of austempering times increased, the volume of acicular ferritic platelets increased. This trend can be clearly seen in the scanning electron micrographs for grade SG42 from 10 - 120 minutes (Figure 5.10 (a-e)). At the short austempering times, large islands of retained austenite and/or martensite are visible. These get smaller at longer austempering times. After 120 minutes the matrix is a finely interspersed mixture of acicular ferrite platelets and retained austenite.

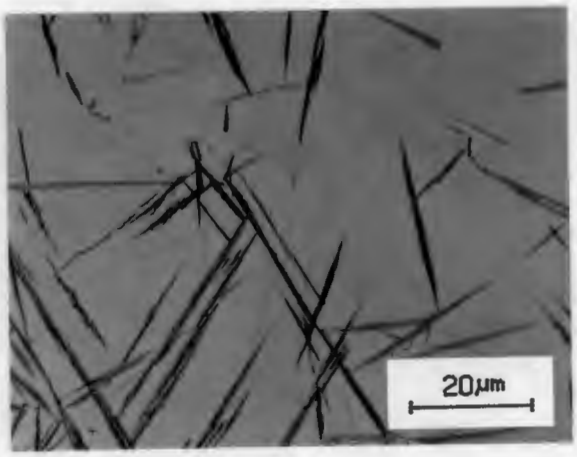

(a) Austempered for 6 minutes

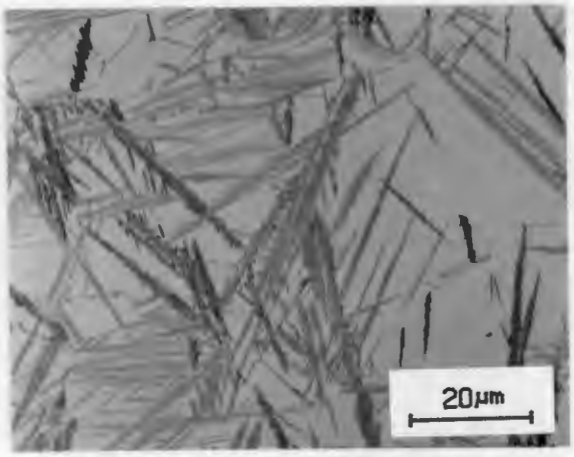

(b) Austempered for 10 minutes

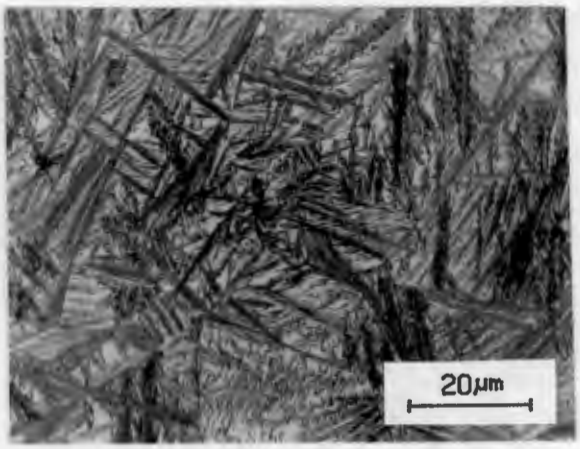

(c) Austempered for 20 minutes

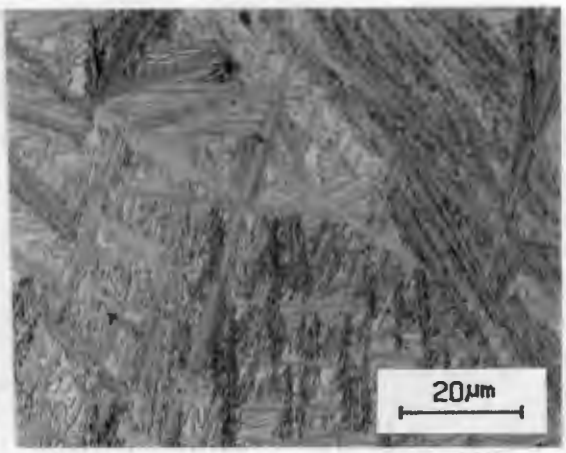

(b) Austempered for 60 minutes

Figure 5.9 : Optical micrographs for grade SG42, austenitised at 900°C for 60 minutes and austempered at 355°C for various times, illustrating the growth of acicular ferrite plates. Etched in Nital. (x1000)

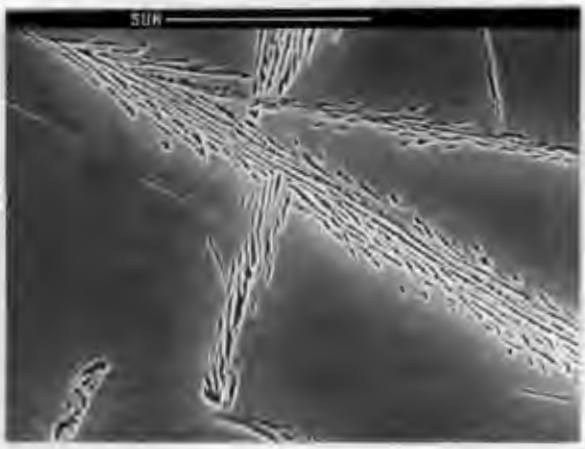

(a) Austempered for 10 minutes

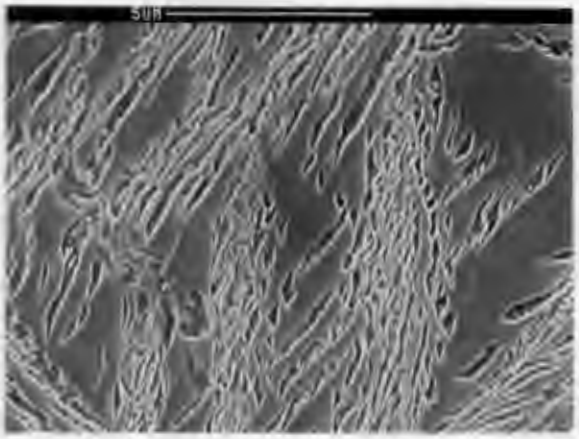

(b) Austempered for 20 minutes

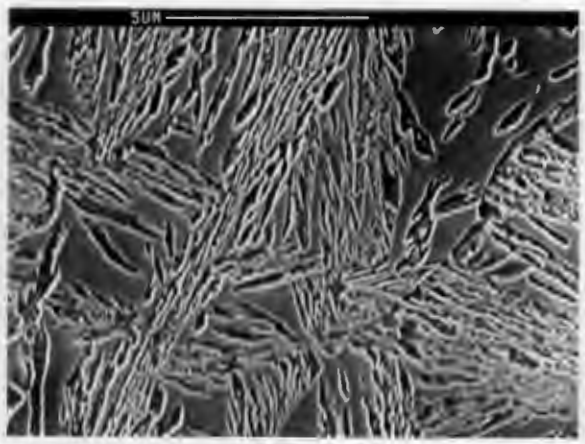

(c) Austempered for 30 minutes

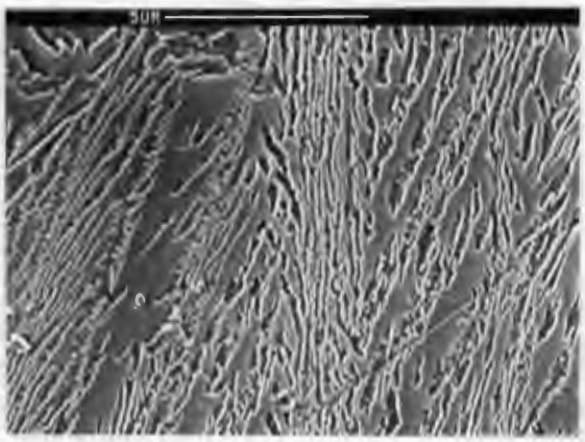

(d) Austempered for 60 minutes

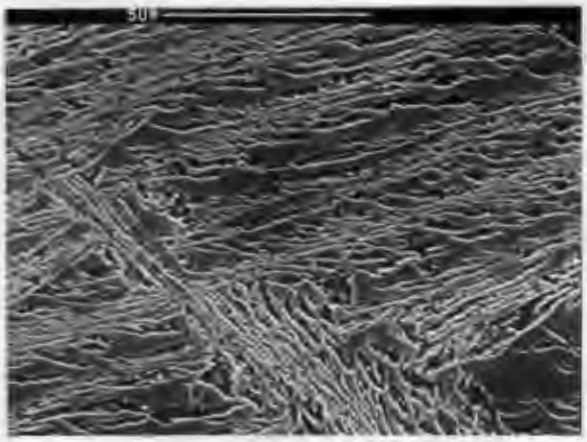

(e) Austempered for 120 minutes

Figure 5.10 : Scanning electron micrographs for grade SG42, austenitised at 900°C for 60 minutes and austempered for various times, illustrating the growth of acicular ferrite plates. Etched in Nital.

5.2.2 X-Ray Diffraction

Figures 5.11-5.16 show the results obtained for specimens austempered at different temperatures and times.

As the austempering temperature is raised from 250 °C the amount of retained austenite was found to increase from around 15% to a maximum of 45-50% in the case of grade SG60 at a temperature of approximately 420°C, and to 30-35% for grade SG42 at 350°C (Figures 5.11 and 5.12). The results were obtained from specimens that had been austempered for 30 minutes at each temperature.

At higher temperatures the quantity of retained austenite in both grades fell sharply towards zero. The amount of retained austenite in grade SG60 and grade SG42 was found to be similar for the temperature range 250°C - 350°C.

The amount of retained austenite was also found to be dependent on the time at austempering temperature. Figure 5.13 shows the increasing amount of retained austenite due to the increase in transformation time from 2 minutes to 30 minutes for grade SG60 iron austempered at 355°C. There was an increase in retained austenite from 12% to 43%. Further holding time at this temperature resulted in a slight decrease in the measured value of retained austenite. A similar result was found for grade SG42 iron austempered at 355°C (Figure 5.14).

When both grade SG42 and SG60 were austempered at 250°C however, the time taken to reach maximum retained austenite was longer - approximately 60 minutes. The quantity of retained austenite was also found to be lower, 30% for grade SG60 and 25% for grade SG42 (Figures 5.15 and 5.16).

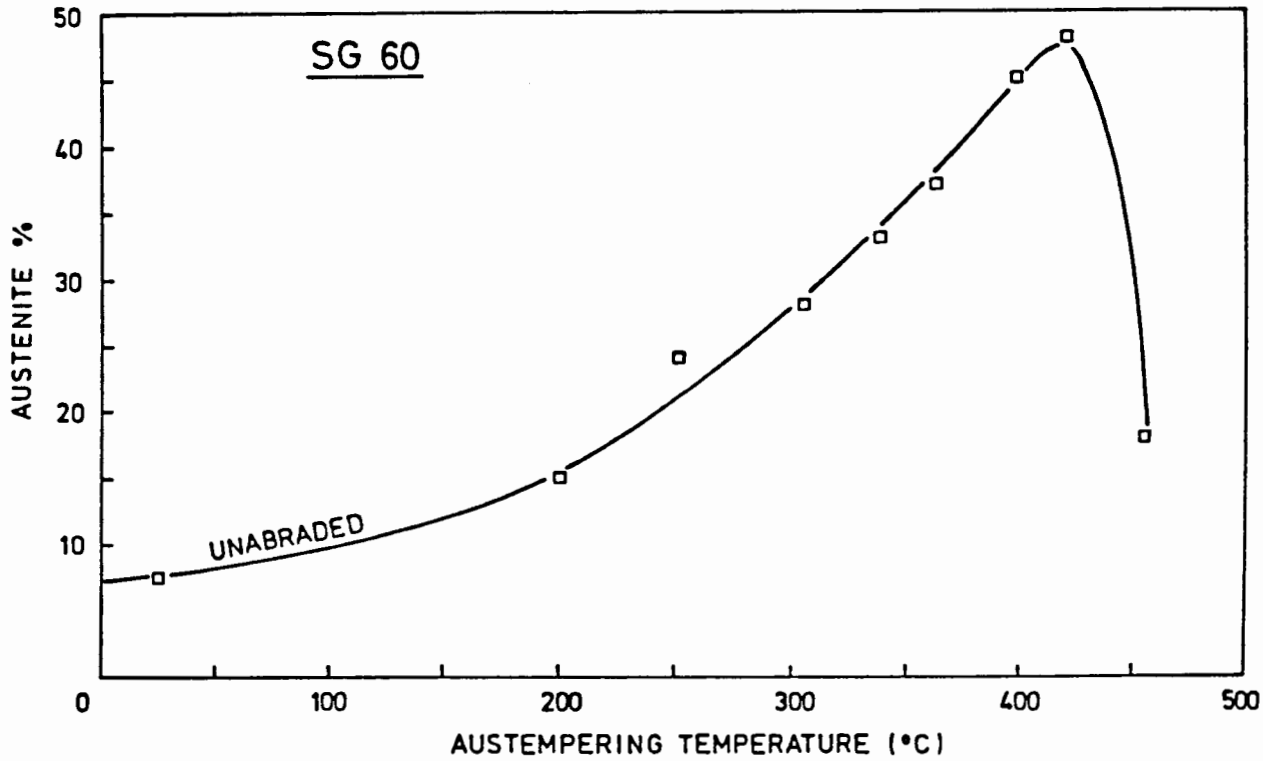

Figure 5.11 : Retained austenite quantities found in grade SG60 iron austempered for 30 minutes at various temperatures. Austenitised at 900°C for 60 minutes

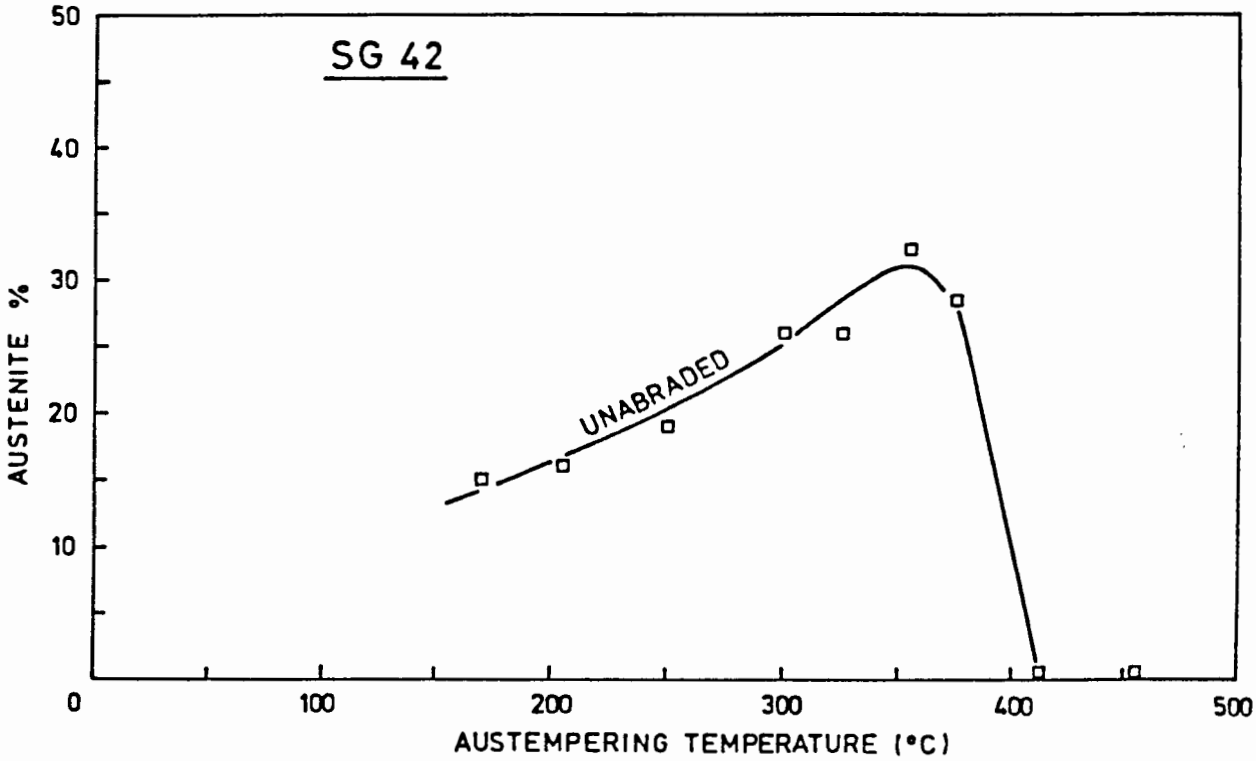

Figure 5.12 : Retained austenite quantities found in grade SG42 iron austempered for 30 minutes at various temperatures. Austenitised at 900°C for 60 minutes

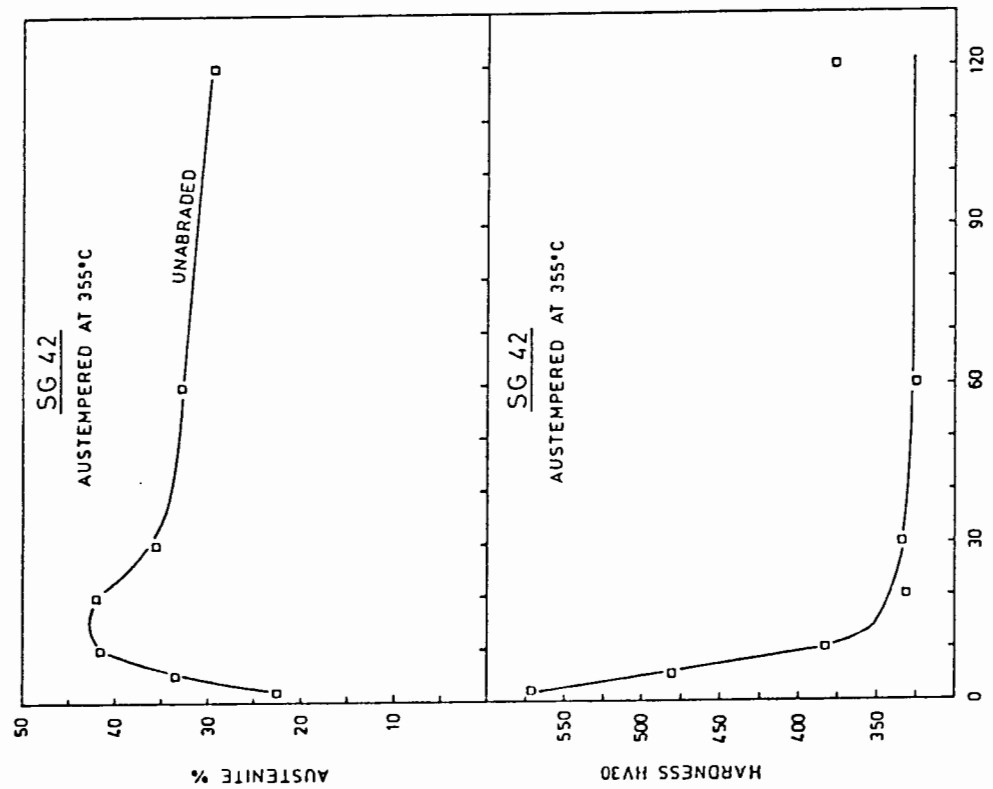

Figure 5.14 : Retained austenite and hardness values for grade SG42 with austempering temperature of 355°C. Austenitised at 900°C for 60 minutes

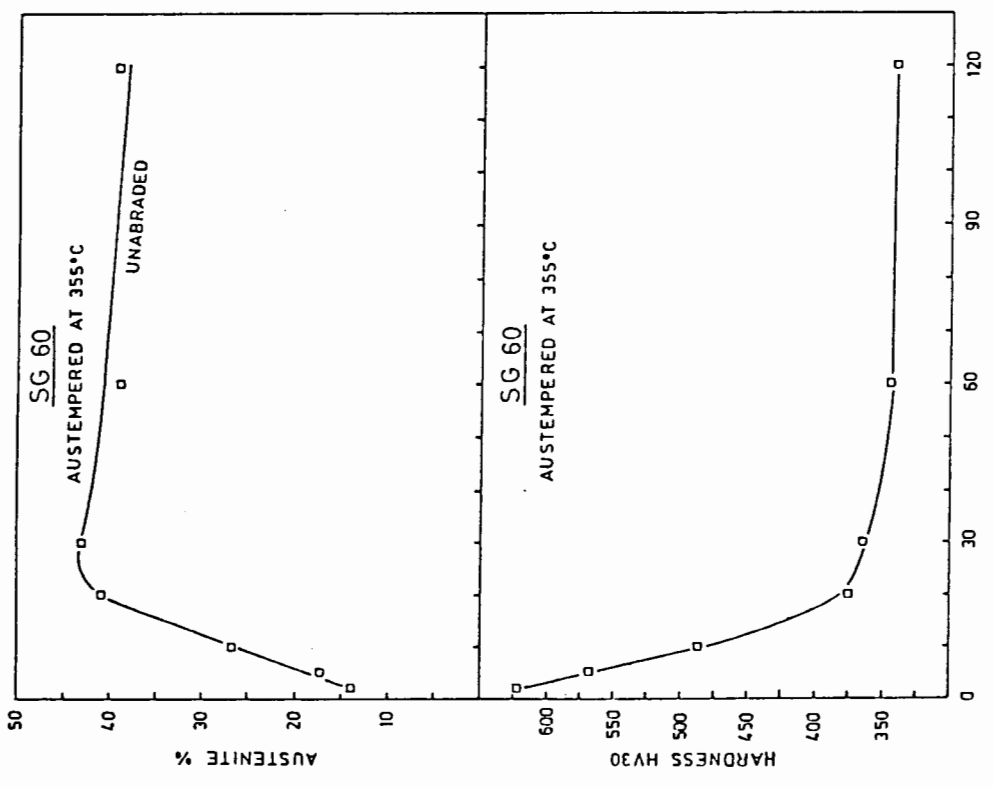

Figure 5.13 : Retained austenite and hardness values for grade SG60 with austempering temperature of 355°C. Austentitised at 900°C for 60 minutes

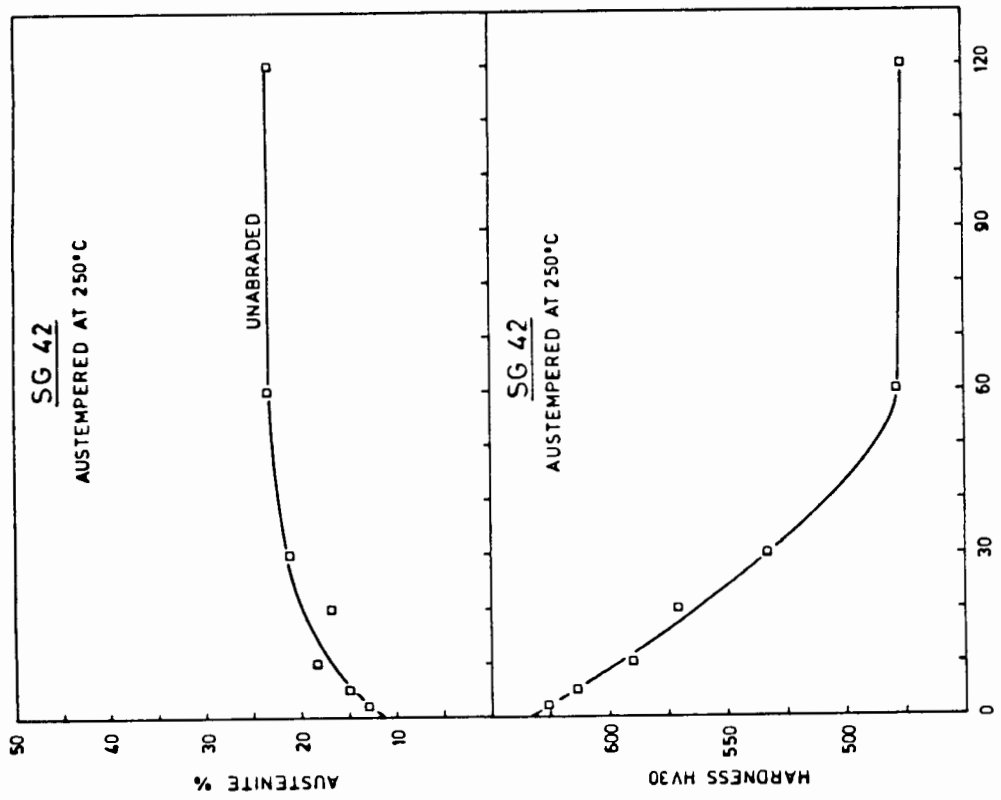

Figure 5.16 : Retained austenite and hardness values for grade SG42 with austempering temperature of 250°C. Austenitised at 900°C for 60 minutes

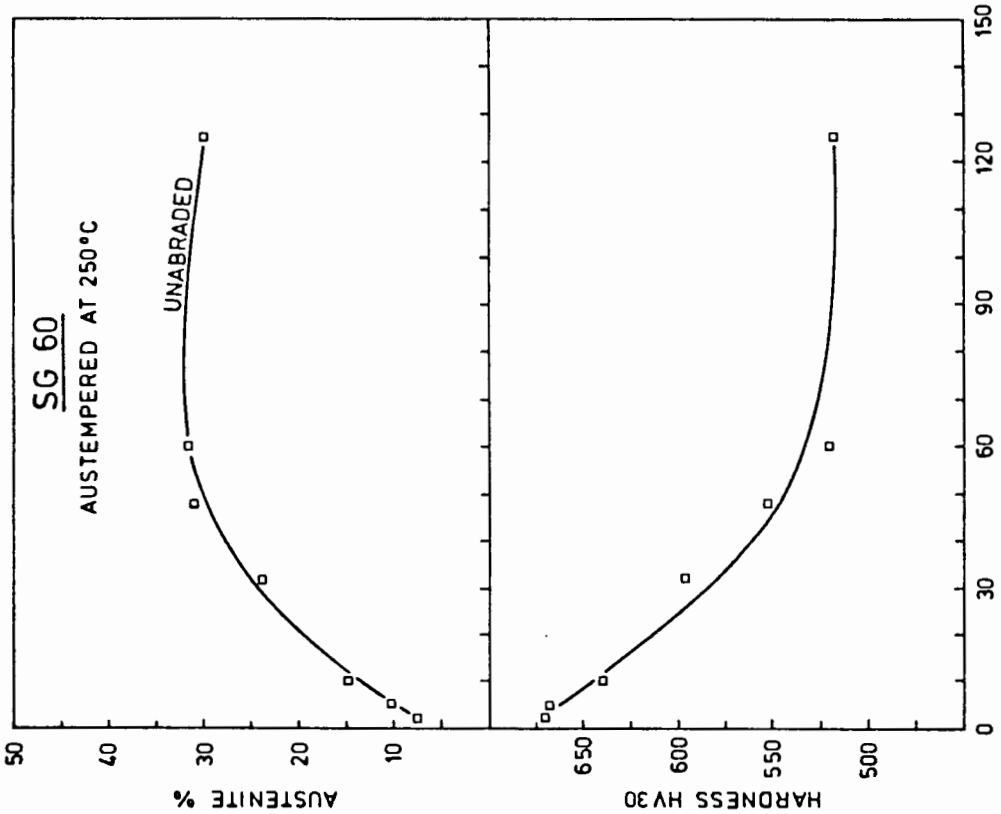

Figure 5.15 : Retained austenite and hardness values for grade SG60 with austempering temperature of 250°C. Austentitised at 900°C for 60 minutes

5.2.3 Hardness Survey

As the morphology and the constitution of the austempered microstructures alter there is a parallel change in hardness (Figure 5.17).

As the austempering temperature is increased from 250°C to 450°C the hardness falls from approximately 500 HV30 for both grades SG42 and SG60. Grade SG42, austempered at 370°C, had a hardness of approximately 300 HV30 whilst a similar hardness was found for grade SG60 at 420°C. Further increases in austempering temperature result in a slight increase in hardness for both grades as the amount of retained austenite falls and another harder transformation product, pearlite, makes its appearance in the structure.

It is noticeable that the hardness values measured for grade SG60 iron were always higher than those for grade SG42 at all austempering temperatures.

A large variation in hardness occurs with changes in holding times, at an austempering temperatures of 355°C and 250°C, for both grades. In each case the hardness decreases sharply as the holding time is increased to approximately 30 minutes at 355°C and 60 minutes at 250°C. This decrease parallels a decrease in the amount of martensite in the structure of these irons and with a corresponding increase in the amount of ferrite and retained austenite. Holding times of up to two hours do not appear to significantly change the minimum hardness obtained at each temperature.

The change in hardness was found to be greater for the higher austempering temperatures.

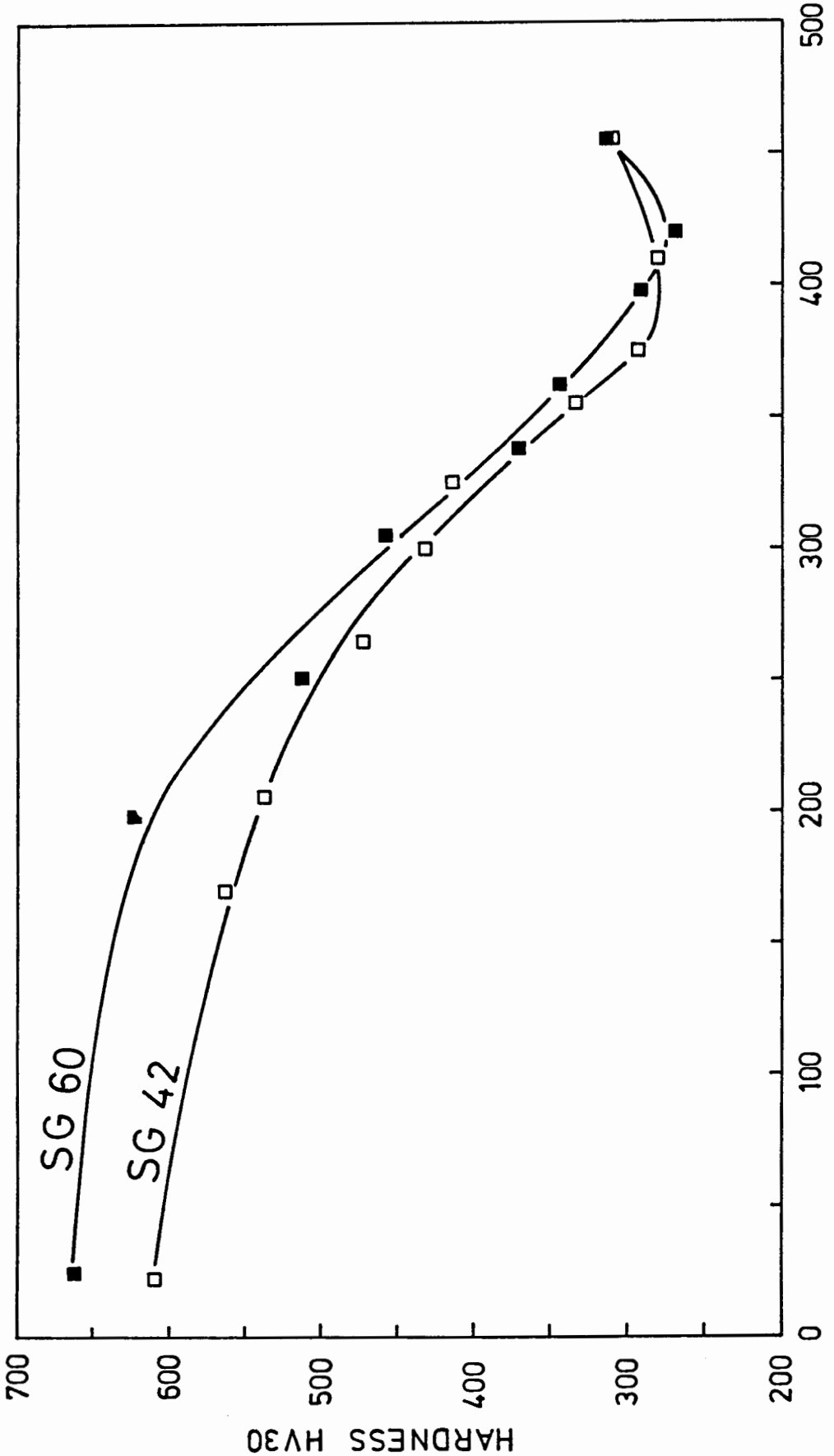

Figure 5.17 : Hardness of grades SG42 and SG60 with austempering temperatures. Austempered for 30 minutes at temperature. Austenitised at 900° for 60 minutes

5.2.4 Mechanical Testing

The results of tensile tests carried out on grades SG42 and SG60 irons for different austempering temperatures and times are shown in Figures 5.18 and 5.19.

It is clear that the highest strength levels are associated with the lower austempering temperatures, i.e. 250°C and 300°C. Tensile strength of 1300 MPa for grade SG60 and 1100 MPa for grade SG42 after austempering for 60 minutes at 250°C are attainable. As the austempering temperatures are increased the tensile strengths decrease. Grade SG60 has a tensile strength of 900 MPa after 60 minutes austempering at 400°C and grade SG42 a strength of 853 MPa after 60 minutes austempering at 350°C.

Holding times of 30 minutes at 250°C and 350°C produce the highest tensile strength for both grades.

The increase in tensile strength appears to parallel the decrease in the amount of martensite in the structure in these irons and a corresponding increase in the amounts of ferrite and austenite. It would normally be expected that a fully martensitic structure would have the higher tensile strength. However, it was observed that the specimens containing substantial quantities of brittle martensite tended to fail at the change in section of the tensile test. Thus the recorded results may be somewhat lower than the true strength levels.

Further mechanical tests were done for a much smaller range of austempering temperatures for an austempering time of 30 minutes. The selected temperatures of 250°C, 350°C and 400°C are shown in Table 5.3. This Table also includes the mechanical properties of the proprietary abrasion resistant alloys that were used for abrasion testing (Chapter 6). Results show that as the austempering temperature is raised from 250°C, the toughness values, measured by the notched Charpy test, and elongation improve.

TABLE 5.3 : Mechanical Properties of Austempered Irons and Steels

GRADE	AUSTEMPERING TEMPERATURE °C	HARDNESS HV30	LONGITUDINAL CHARPY ENERGY J	TENSILE STRENGTH Nmm^{-2}	% ELONGATION
SG42 (As received)		136	15.0	390	13.0
SG42	250	500	3.5	1000	6.3
SG42	300	414	5.0	1090	6.4
SG42	325	359	5.8	1089	6.1
SG42	350	334	6.0	954	6.3
SG42	375	312	9.0	981	6.1
SG42	400	290	3.8	917	6.9
SG60 (As received)		229	2.5	618	4.2
SG60	250	513	4.0	1318	6.3
SG60	300	459	5.0	1236	8.2
SG60	325	370	9.0	1248	8.8
SG60	350	366	6.0	1200	8.0
SG60	375	350	11.0	983	10.4
SG60	400	317	12.0	1037	11.0
Abrasion Alloy A		211	4	668	27
Abrasion Alloy B		437	15	1450	15
Abrasion Alloy C		457	13	1302	9
Abrasion Alloy D		547	78	1700	15
Abrasion Alloy E		550	15.7	1589	16.7
Abrasion Alloy E		710	7.3	1699	7.6
Hadfield Steel		236			

Austenitising carried out at 900°C for 60 minutes. All testing carried out at room temperature.

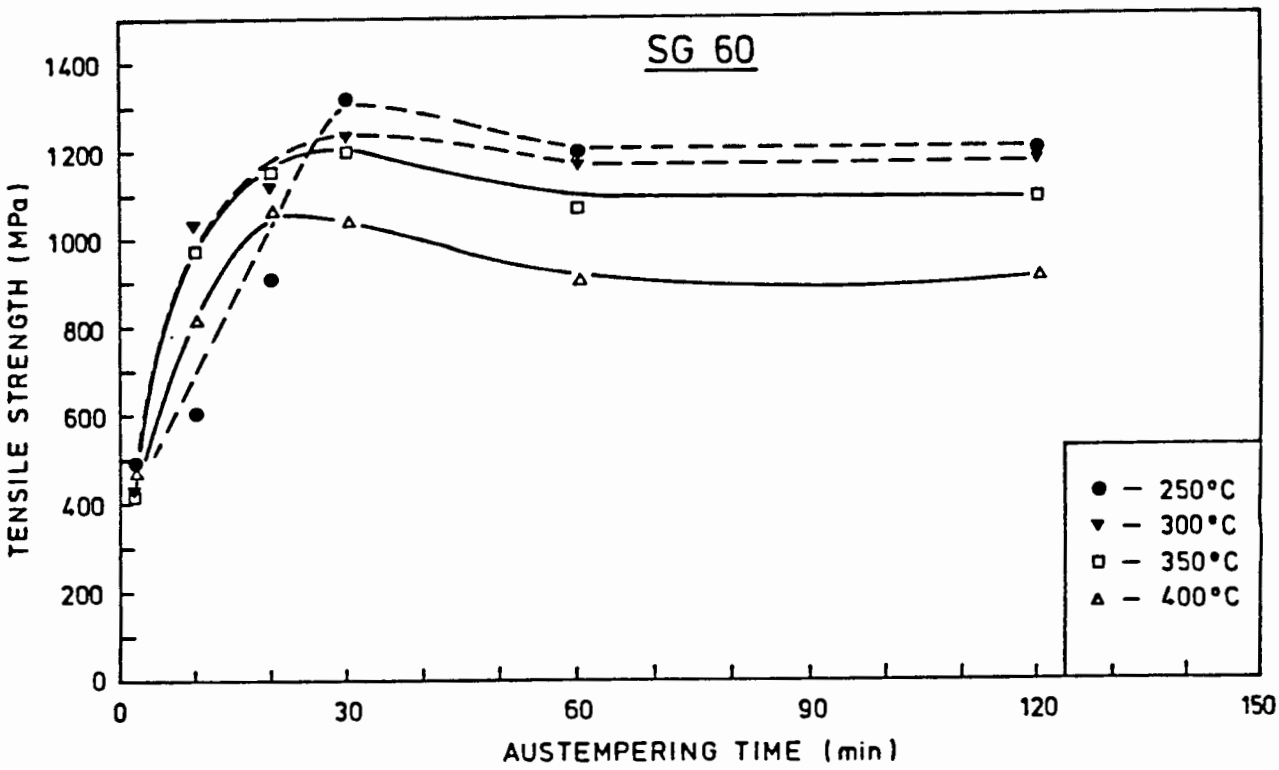

Figure 5.18 : Tensile strengths of grade SG60 for various austempering temperatures at various austempering times. Austempered for 30 minutes at temperature. Austenitised at 900°C for 60 minutes

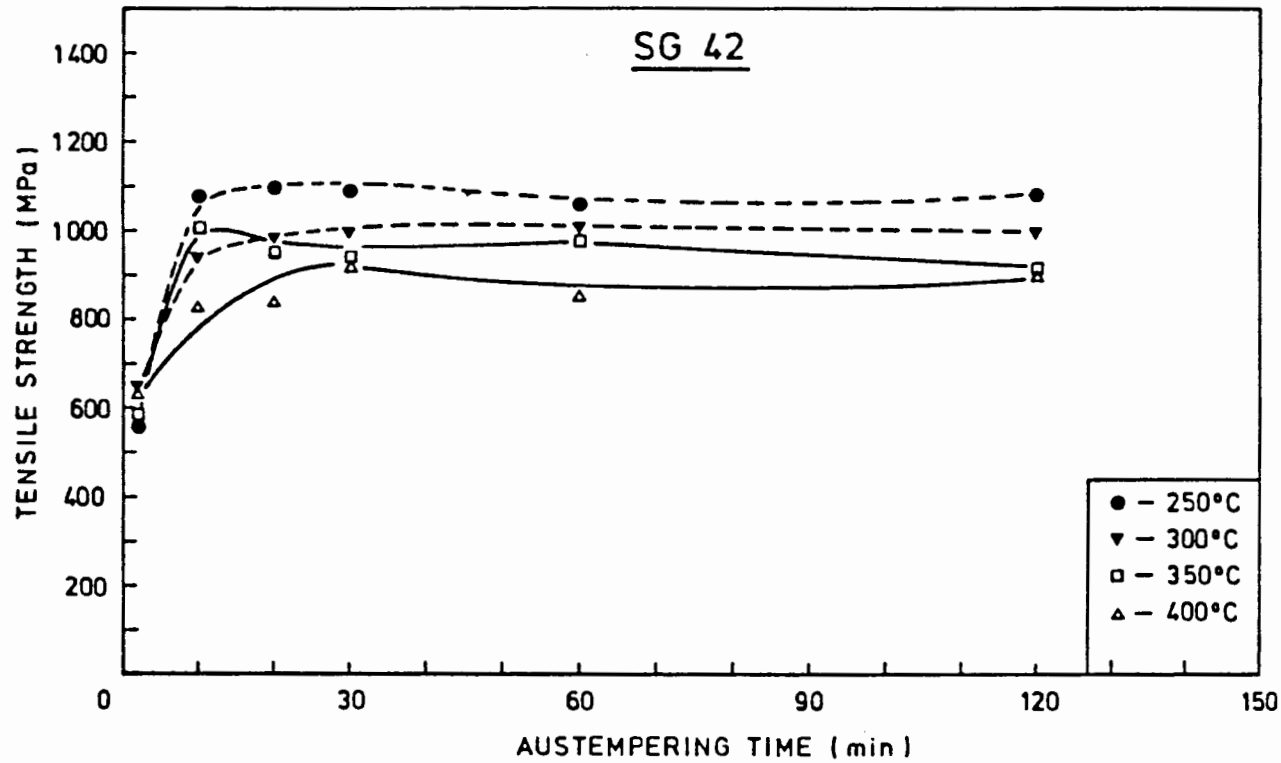

Figure 5.19 : Tensile strengths of grade SG42 for various austempering temperatures at various austempering times. Austempered for 30 minutes at temperature. Austenitised at 900°C for 60 minutes

It is noticeable that the toughness of the grade SG60 iron is improved by austempering whereas that of the grade SG42 is lowered. This suggests that a soft ferritic matrix is tougher than a stronger and harder duplex ferrite/austenite matrix. In the case of grade SG60 the duplex ferrite/austenite matrix is shown to be tougher than an essentially softer and less strong pearlitic matrix.

5.2.5 Discussion

The austempering heat treatment affects both the carbon content of the matrix and hence the amount of stabilised austenite upon cooling as well as the morphology of the matrix structure. During the austempering process ferrite is nucleated leading to the carbon enrichment of the remaining austenite (2).

The high silicon content of the iron stabilizes the austenite preventing the precipitation of iron carbide. Eventually, further ferrite formation is inhibited by the high carbon content of the remaining austenite. The high carbon content of the austenite can depress the M_S to below room temperature and therefore result in substantial quantities of austenite being retained on cooling to room temperature.

5.2.5.1 The Austempering Temperature

The austempering temperature affects the kinetics of the transformation reaction. As the austempering temperature is lowered from around 400°C the ferrite plates become finer and more acicular and the amount of retained austenite less. There is an increase in hardness and strength but a decrease in toughness.

As explained in section 5.1.3.1 the rate of carbon diffusion from the growing ferrite plates decreases with decreasing austempering temperatures. Hence at low austempering temperatures, below 300°C, the carbon being rejected by the growing ferrite plates cannot diffuse into the austenite due to the low diffusion rate.

The carbon appears to be rejected as epsilon-carbide ($Fe_{2.4}C$) in or alongside the ferrite plates. Very little austenite is therefore stabilized by this rejected carbon. Most of the carbon present in the austenite would therefore be as a result of the austenitization process. Lower values of retained austenite are therefore expected at lower austempering temperatures for fixed austempering times. This is apparent from Figures 5.11 and 5.12.

The higher hardness at these lower temperatures is the result of a number of factors (Figure 5.17).

- The lower austempering temperature leads to a finer matrix structure of ferrite plates in retained austenite. Nucleation of the ferrite plates is more favourable at lower temperatures but plate growth is inhibited. A finer matrix structure results which in turn has a higher hardness than its coarser counterpart (Figures 5.7 (a) and (b) and 5.8 (a)).

- The hard epsilon-carbide phase precipitated inside the ferrite platelets will increase the hardness.

- If the carbon content of the austenite is not high enough to depress the M_s to below room temperature, some martensite will occur in the matrix upon cooling. The hard martensite will in turn increase the bulk hardness of the material.

The finer matrix structure and the epsilon carbide would explain the higher tensile strengths at lower austempering temperatures while the absence of large amounts of the soft austenite phase would decrease the toughness of the material (Table 5.3 and Figures 5.18 and 5.19).

Austempering time also determines the amount of carbon rejected into the austenite. Hence too short an austempering time would lead to austenite being unstable at room temperature. This is discussed in section 5.2.5.2.

At austempering temperatures above 300°C the reaction kinetics of the austempering reaction change. The rate of carbon diffusion increases and hence carbon can diffuse more easily from the growing ferrite plates into the austenite. This in turn leads to a more thorough enrichment of the austenite. Stabilisation of the austenite is therefore more rapid and successful at higher temperatures.

The consequence is higher amounts of retained austenite for higher austempering temperatures at fixed austempering times (Figures 5.11 and 5.12).

The ease of austenite stablisation will also minimise the chances of martensite formation due to a Ms above room temperature. This is however also dependant on austempering time (Section 5.2.5.2).

The higher ferrite plate growth at higher austempering temperatures will produce a coarser and more feathery matrix structure (Figure 5.7 (c-e) and 5.8 (b-d)).

Hardness values at higher austempering temperatures are bound to be lower. This is due to the greater amount of the soft retained austenite phase that is present and the coarser matrix structure. The absence of epsilon-carbide and the decreased probability of martensite formation would also contribute to a decrease in hardness.

A decrease in tensile strength occurs due to a coarser matrix structure, the absence of epsilon-carbide and easier dislocation movement due to the FCC nature of the austenite, while an increase in toughness occurs due to the greater volume of the tough austenite phase present at higher austempering temperatures.

5.2.5.2 Austempering Time

The austempering time will determine the growth of the acicular ferrite platelets i.e., the transformation reaction and hence the amount of carbon that can diffuse into the austenite matrix.

For long austempering times the austenite becomes destabilized, leading to iron carbide precipitation in the matrix. If, on the other hand, the transformation process is prematurely interrupted by cooling to room temperature before full austenite stabilisation is complete, some martensite wil be found in the matrix along with ferrite and austenite.

From Figures 5.13 - 5.16 it is appparent that full stabilisation of the austenite has not occuurred at the shorter austempering times. For grades SG42 and SG60 at 355°C austemper the full stabilisation would appear to occur after approximately 30 minutes while at 250°C austemper this is 50 minutes.

As previously explained, stabilisation of the austenite is dependant on the rate of diffusion of carbon from the ferrite into the austenite. This rate of diffusion is temperature dependant and hence stabilisation is expected to occur sooner at 355°C than at 250°C.

Prior to stabilisation any unstabilised austenite, i.e. Ms above room temperature, would be expected to change to martensite upon cooling to room temperature. The shorter the austempering time the greater the quantity of unstabilised austenite which is present and hence the greater the amount of martensite present in the matrix. This is borne out by the hardness results in Figures 5.13 - 5.16.

As the holding times decrease from 30 minutes to 2 minutes for the 355°C austempered materials and from 50 to 2 minutes for the 250°C austempered materials, the hardness rises sharply. At 2 minutes the hardness values approach those of pure martensite: greater than 700 HV30.

From the optical micrographs (Figures 5.9 (a-e)) and the scanning electron micrographs (Figures 5.10 (a-e)) it is also apparent that as the holding times increase from 2 minutes to 30 minutes, at a 355°C austemper, the volume and nature of the ferrite plates changes. The ferrite platelets grow into the austenite and with increasing lengths of time multiply and enlarge. After approximately 60 minutes the matrix stabilises and no more growth of ferrite is apparent. At this point the high carbon content of the austenite in the matrix inhibits further growth.

For long austempering times it is expected that the austenite will become destabilised leading to iron carbide precipitation in the matrix (2). From the results at the austempering temperatures of 355°C and 250°C this was not observed to occur for austempering times as long as 120 minutes.

CHAPTER 6

DRY ABRASION - RESULTS AND DISCUSSION

6.1 DRY ABRASION

A summary of the results of dry abrasion testing is shown in Table 6.1 and in Figure 6.1. From Table 6.1 it is apparent that the dry abrasion resistance of the two grades of austempered spheroidal irons is vastly superior to those in the as-received condition. Abrasion resistance also appears to be related to austempering temperatures. For example specimens austempered at 250°C have higher RAR values than those austempered at 350°C.

TABLE 6.1 : Results of abrasion testing

MATERIAL	STRUCTURE	HARDNESS HV30	RELATIVE ABRASION RESISTANCE (RAR)
Mild steel	Ferrite and pearlite	140	1.00
SG42 (as received)	Ferrite	136	0.89
SG60 (as received)	Ferrite, pearlite	229	1.08
Abrasion alloy A	Ferrite and pearlite	211	1.25
Abrasion alloy B	Tempered martensite	437	1.36
Abrasion alloy C	Tempered martensite	457	1.42
Abrasion alloy D	Tempered martensite	547	1.84
Abrasion alloy E	Tempered martensite	550	1.79
Abrasion alloy E	Tempered martensite	710	1.98
Hadfield steel*	Austenite	236	2.03
SG60 Austempered 362°C	Ferrite, austenite, carbon	366	1.77
SG42 Austempered 356°C	Ferrite, austenite, carbon	344	1.82
SG60 Austempered 255°C	Ferrite, austenite, carbon	550	2.58
SG42 Austempered 250°C	Ferrite, austenite, carbon	510	2.63

* Tested previously in Materials Engineering Department - U.C.T.

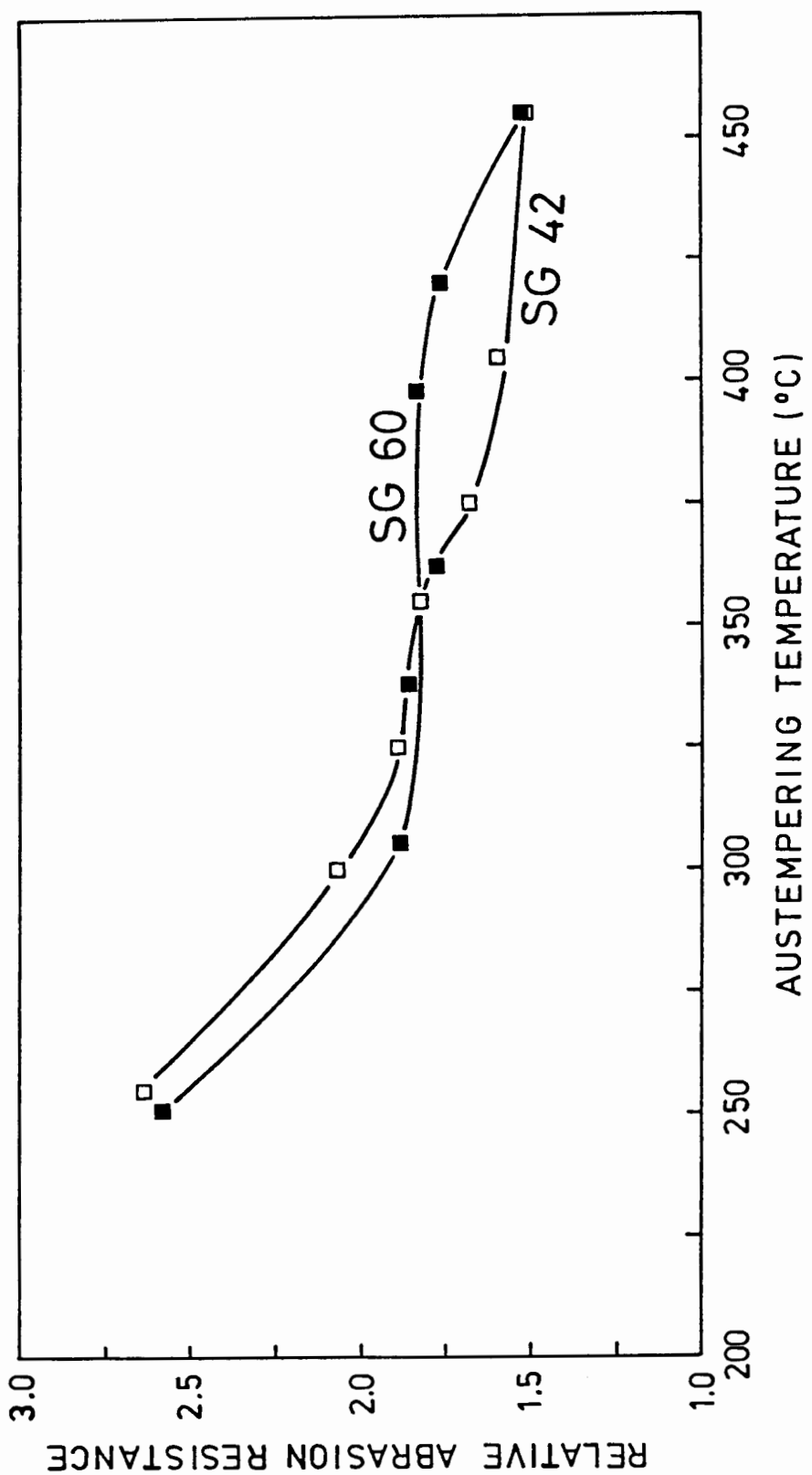

Figure 6.1 : Relative abrasion resistance as a function of austempering temperature for grades SG42 and SG60. Austempered for 30 minutes at temperature. Austenitised at 900° for 60 minutes

Figure 6.1 illustrates that the relative abrasion resistance of these austempered spheroidal irons falls from a value in excess of 2.5. to 1.5 as the temperature is increased from 250°C to 450°C. In the case of the grade SG60 iron, this fall in abrasion resistance with increasing austempering temperature is arrested between the temperature range 300°C to 400°C. A similar effect is noticed for the grade SG42 iron, over a smaller temperature range, 300°C to 350°C. It is also apparent that below 350°C grade SG42 has a superior wear resistance, whereas above this temperature grade SG60 has the better abrasion resistance.

The abrasion resistance of the austempered irons is additionally found to be dependent on the holding time at the austempering temperature (Figures 6.2 - 6.7).

As the holding time is increased from 2 minutes to between 30 and 60 minutes, depending on austempering temperatures, the abrasion resistance falls. Beyond a holding time of 30-60 minutes the abrasion resistance appears to remain constant.

It is interesting to note from Table 6.1 that all the austempered irons had better abrasion resistance than three of the proprietary abrasion resistant steels. Both grades of austempered iron at 250°C for 30 minutes had better abrasion resistance than all six of the abrasion resistant alloys tested, including Hadfields manganese steel.

It might be expected that the graphite phase would give rise to a lubrication effect and thus improve abrasion resistance. However, this does not appear to be the case. Abrasion alloy Alloy A, with a similar matrix microstructure and hardness to the grade SG60 (as received), had a higher abrasion resistance.

The reason for the apparent ineffectiveness of graphite as a lubricant is probably due to the conditions under which the dry abrasions occur. Relatively high loads, 0.3 MPa, and coarse 300 μm, virgin Al_2O_3 abrasive particles would probably prevent graphite film formation by destroying any film due to the adhesion and ploughing mechanisms.

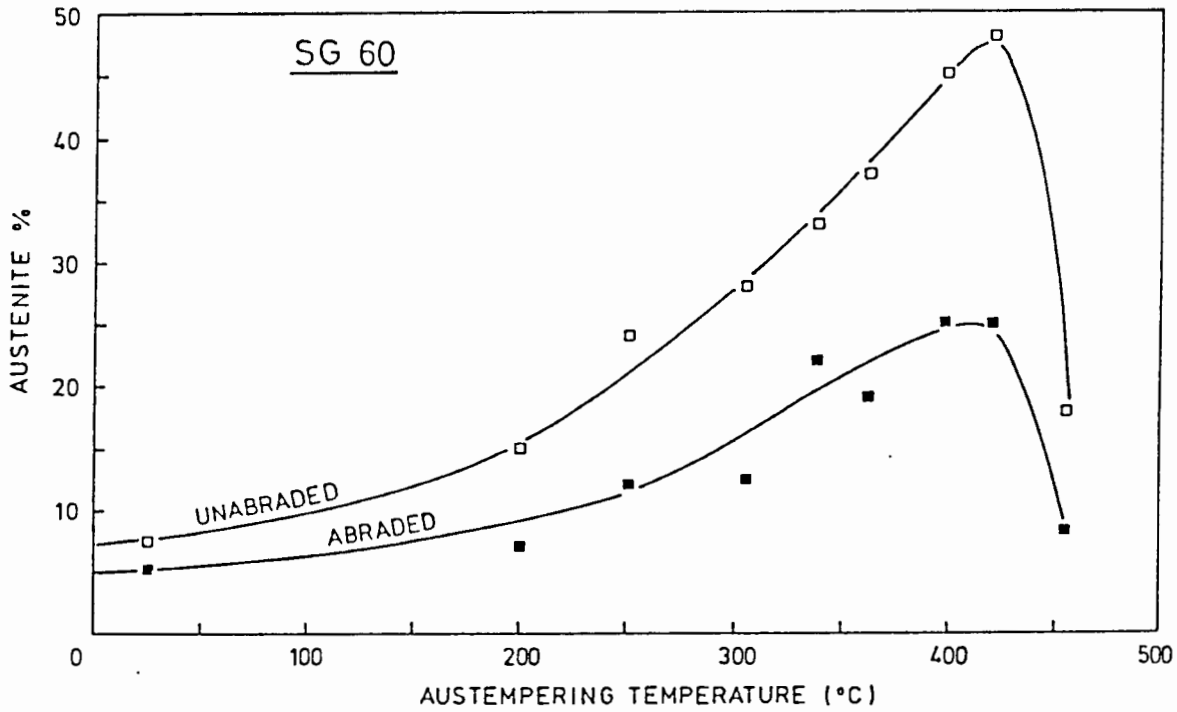

Figure 6.2 : Retained austenite quantities found in grade SG60 austempered for 30 minutes at various temperatures. Austenitised at 900°C for 60 minutes.

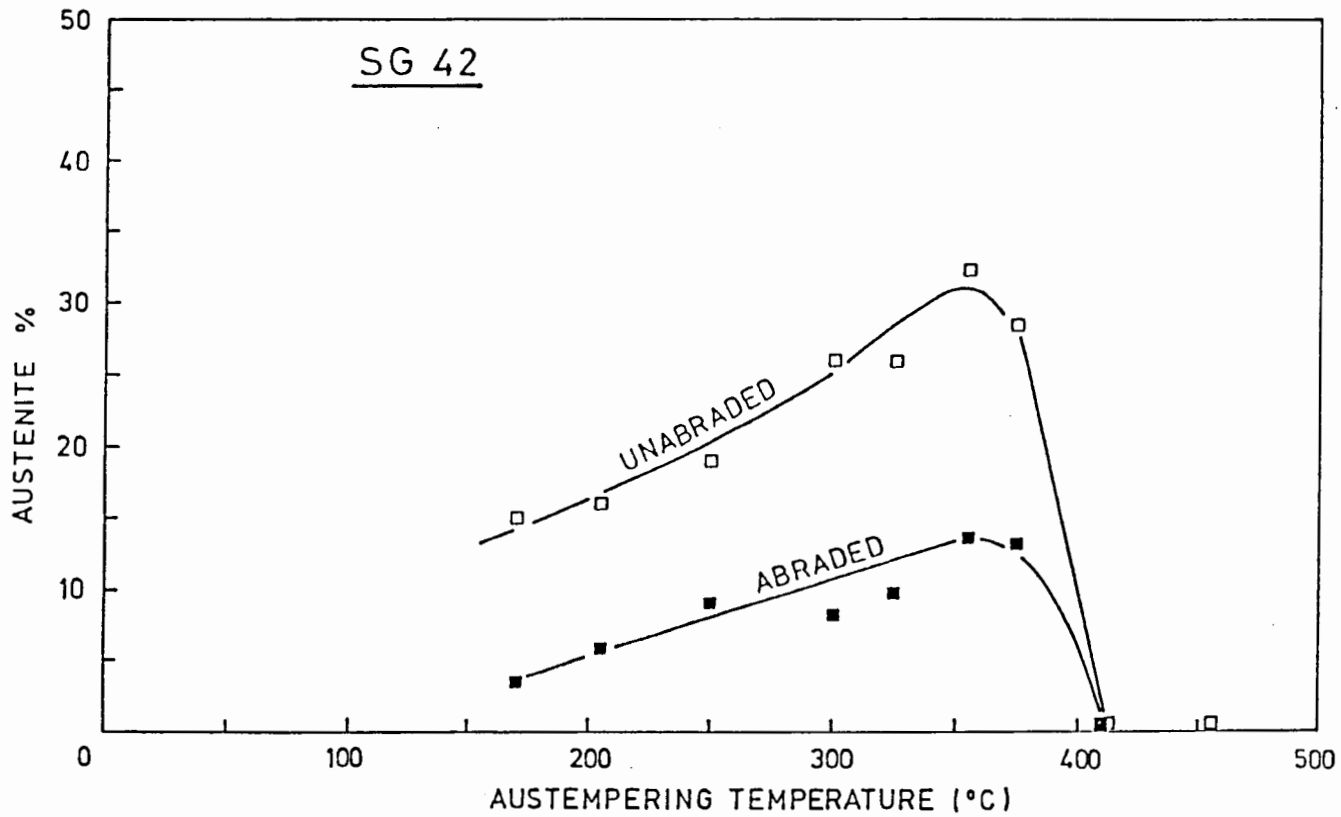

Figure 6.3 : Retained austenite quanitities found in grade SG42 austempered for 30 minutes at various temperatures. Austenitised at 900°C for 60 minutes.

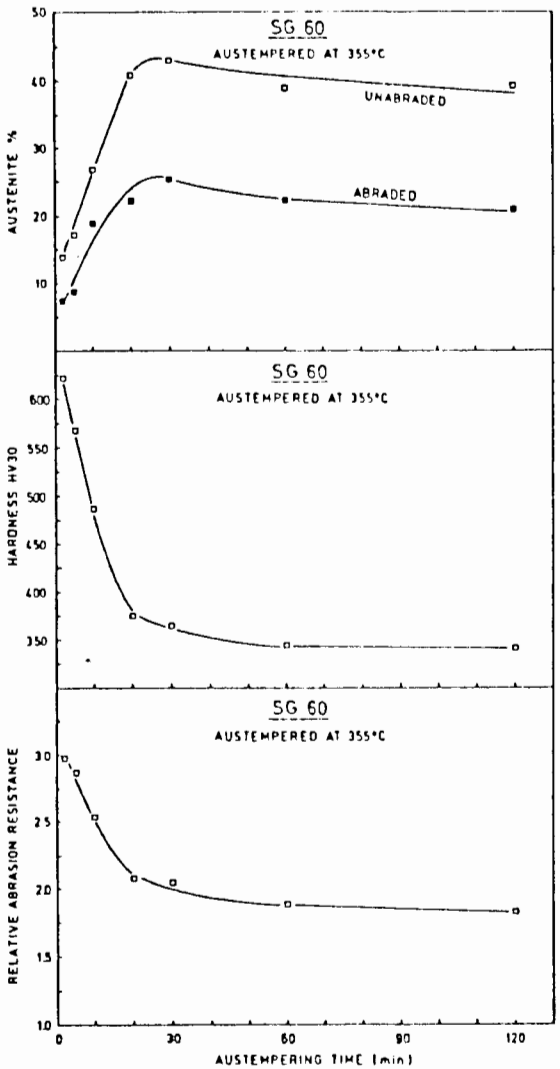

Figure 6.4 : Retained austenite, hardness and relative abrasion resistance of grade SG60 with austempering time. Austempered at 355°C and austenitised at 900°C for 60 minutes

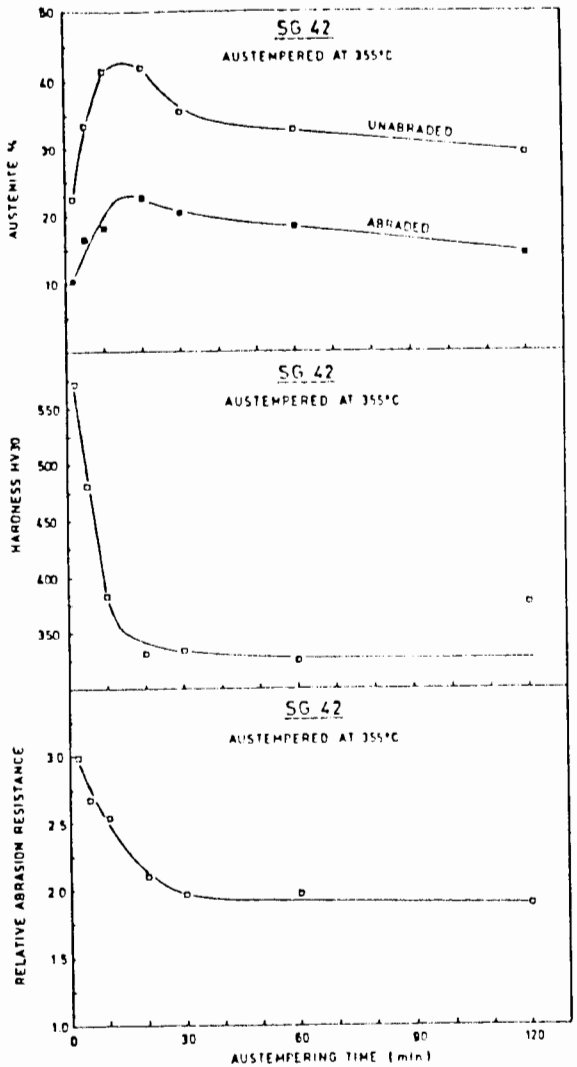

Figure 6.5 : Retained austenite, hardness and relative abrasion resistance of grade SG42 with austempering time. Austempered at 355°C and austenitised at 900°C for60 minutes

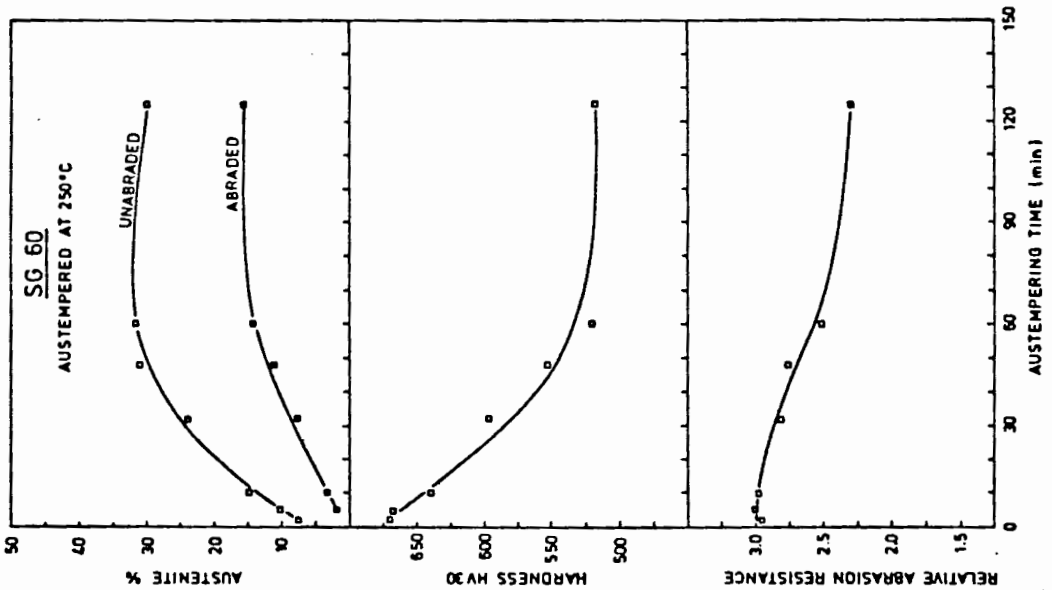

Figure 6.6 : Retained austenite, hardness and relative abrasion resistance of grade SG60 with austempering time. Austempered at 250°C and austenitised at 900°C for 60 minutes

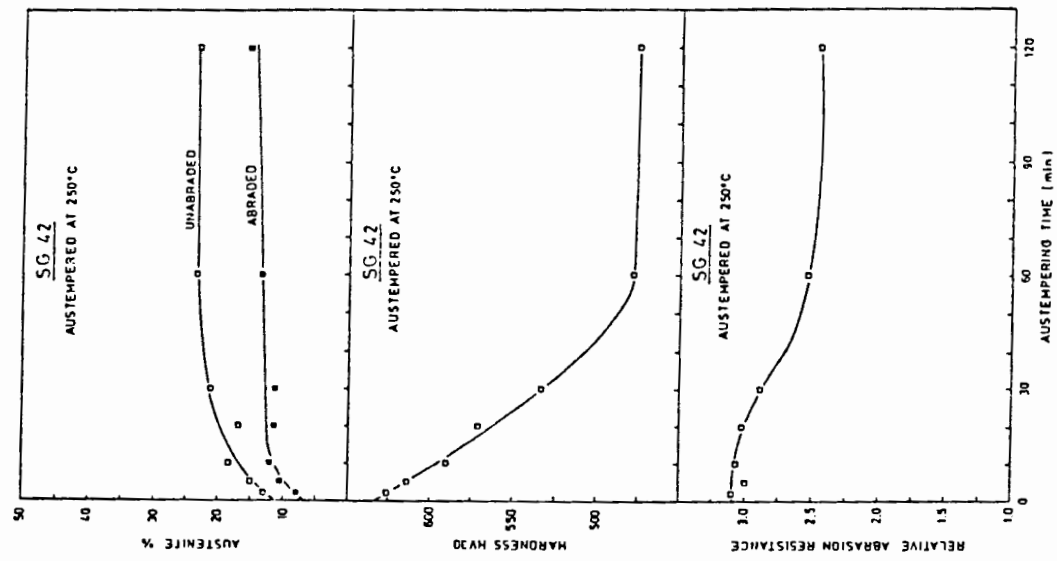

Figure 6.7 : Retained austenite, hardness and relative abrasion resistance of grade SG42 with austempering time. Austempered at 250°C and austenitised at 900°C for60 minutes

It was also noticeable that the hardness of the surface layers in the austempered irons increased significantly following abrasion to values approaching the as-quenched hardness of each iron, e.g. 663 HV30 for grade SG60. The change in hardness is illustrated in Figure 6.8 for grade SG60. The change in hardness was found to be greater for the higher austempering temperatures.

Single particle dry abrasion tracks across the polished surfaces were examined under the scanning electron microscope. Wear tracks appear to cut through the matrix. These wear tracks pass through the graphite spheroid without disturbing them or plucking them from the matrix. Very little or no wear debris was found on the polished surfaces. Evidence of plastic deformation can be seen alongside the wear tracks. (Figure 6.9 (a-c)).

Abrasion debris removed from the abrasion belt appears similar to normal machining chips, having shear steps on one side and fine wear grooves on the other (Figure 6.9 (d)). The curved nature of the chips indicate a certain degree of ductility.

6.2 X-RAY DIFFRACTION

The effect of dry abrasion on retained austenite was to decrease the quantity of retained austenite in all the austempered irons as illustrated in Figures 6.2 - 6.7.

The amount of austenite which transformed to martensite appeared to be closely related to the original amount of austenite in those specimens with a predominantly ferritic/austenitic matrix. In Figure 6.2 the percentage decrease in austenite in the abraded surface layers was found to be approximately 45% for grade SG60 while for grade SG42, in Figure 6.3, it was some 5-10% higher.

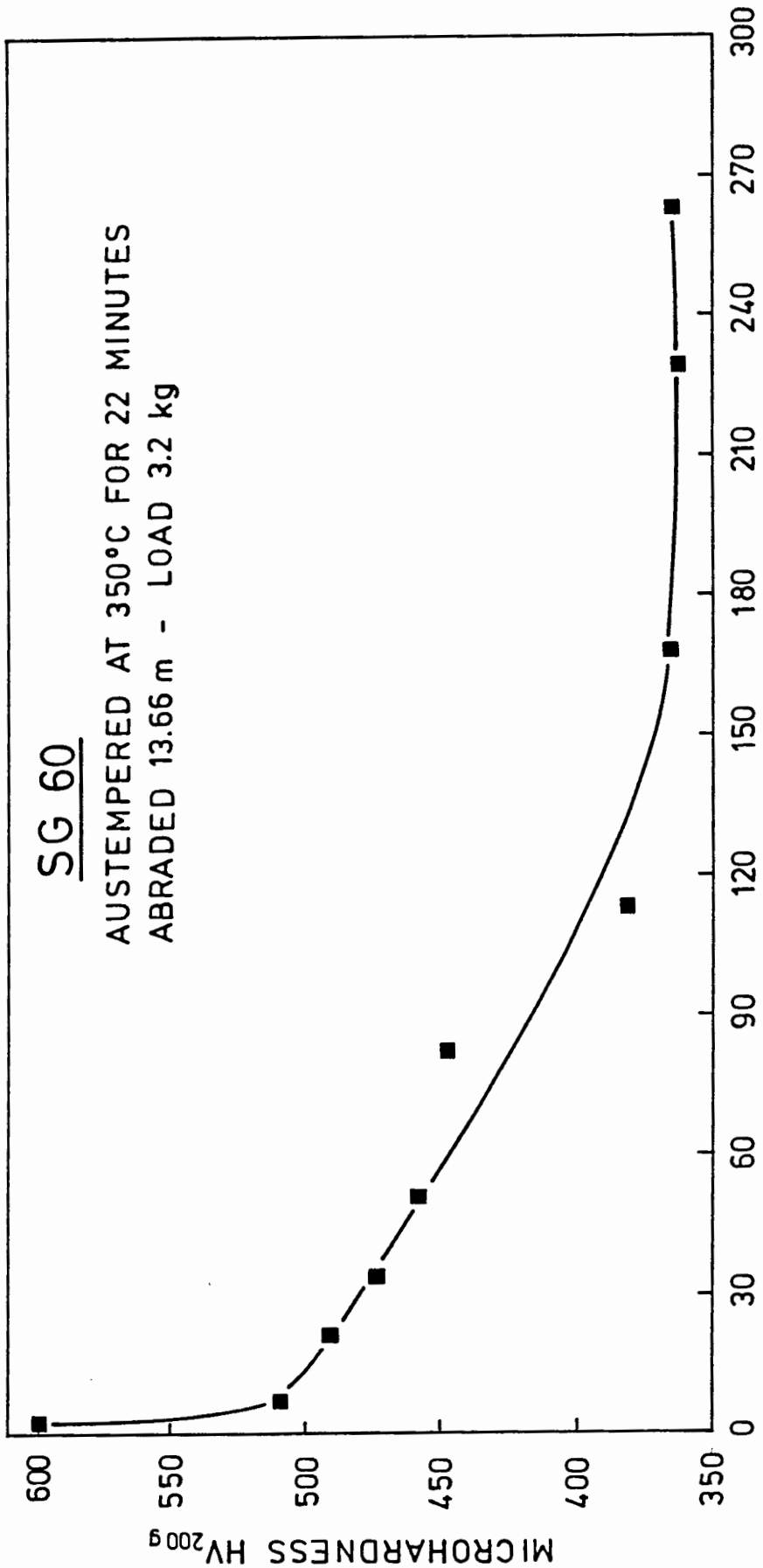

Figure 6.8 : Microhardness survey of abraded surface layers in grade SG60 iron. Austempered at 350°C for 22 minutes and austenitised at 900°C for 60 minutes

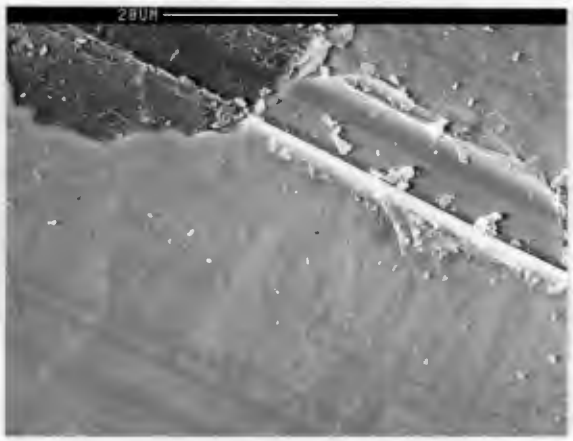

(a) Grade SG60 austempered at 355°C

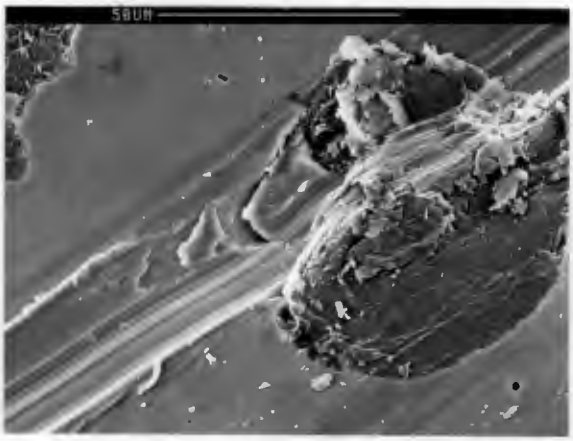

(b) Grade SG42 austempered at 245°C

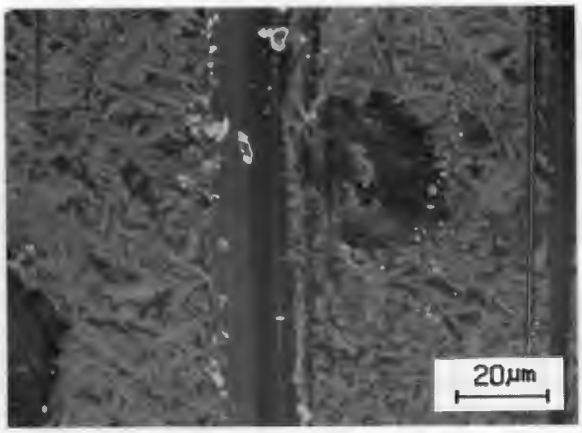

(c) Grade SG60 austempered at 300°C

(d) Abrasion wear debris

Figure 6.9 : Scanning electron micrographs of single particle abrasion wear tracks on austempered iron and abrasion wear debris. Etched in Nital

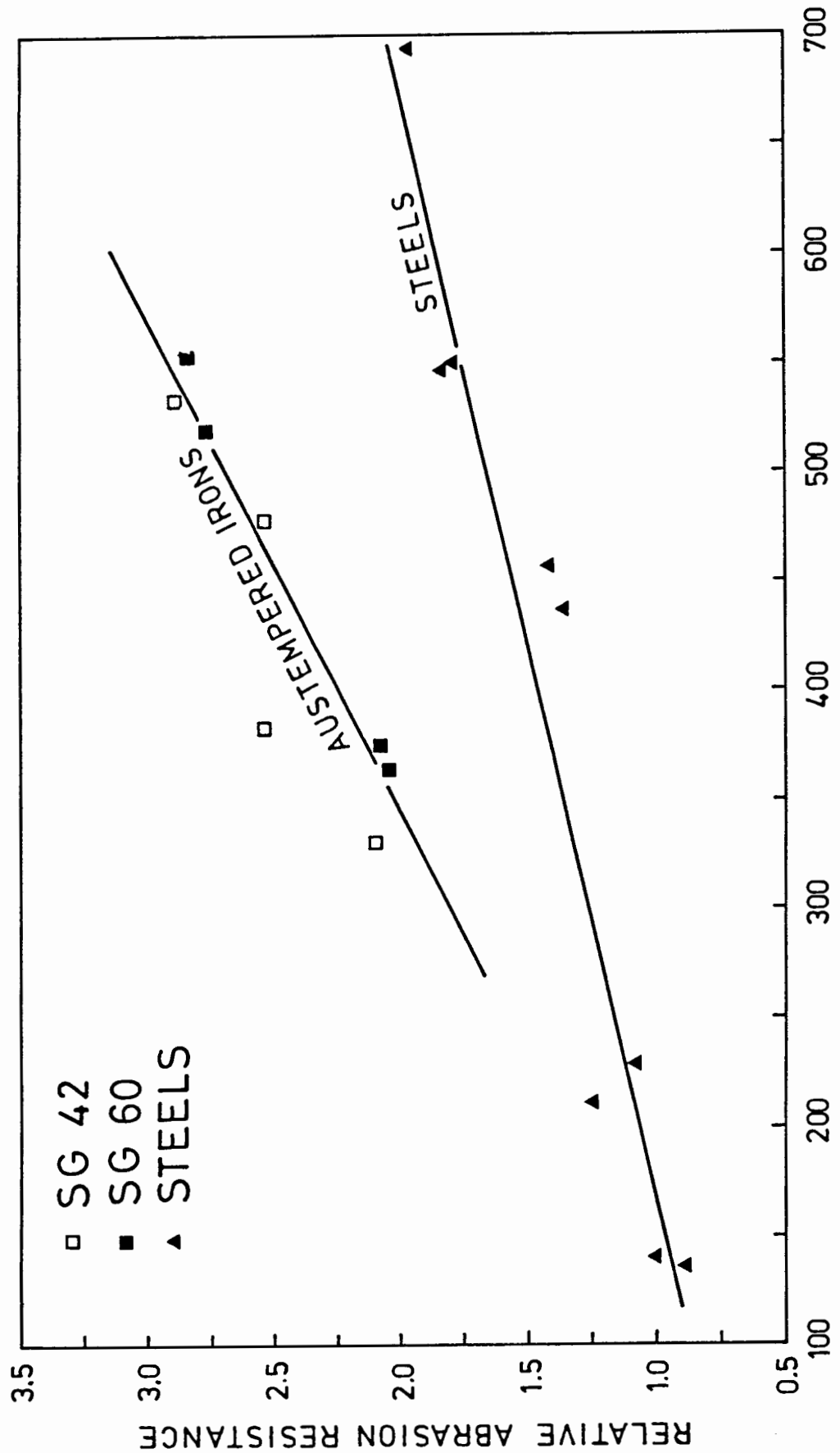

Figure 6.10 : Relative abrasion resistance as a function of hardness for austempered spheroidal cast irons and steels

6.3 DISCUSSION OF RESULTS

It is apparent from the results of the present laboratory investigation that the superior properties achieved by austempering spheroidal cast irons makes them very attractive materials for many situations involving abrasive wear. Examination of Table 6.1 demonstrates that these austempered irons out perform proprietary abrasion resistant steels. Furthermore Figure 6.10 illustrates quite clearly that these materials have a superior abrasion resistance to all the steels tested at similar hardness levels. Such a result emphasised yet again that no simple mechanical property such as initial bulk hardness appears to lend itself readily to predicting abrasive wear resistance. Obviously for the optimisation of these austempered irons it is necessary that the microstructural parameters which contribute to dry abrasion resistance are understood.

It is to be expected that such large changes in the morphology and constitution of the microstructures found in austempered irons will lead to significant changes in abrasive wear resistance. From the results and discussion in Chapter 6 it is apparent that the large variations that are attainable in the morphology and constitution of the microstructures can and will lead to significant changes in abrasive wear resistance. As the austempering temperature is lowered from around 400°C, the ferrite plates become finer and more acicular and the amount of retained austenite less, which results in an increase in hardness, strength and relative abrasion resistance. Obviously a number of factors contribute to the increase in abrasion resistance as the transformation temperature is lowered. These include the fineness of the duplex ferrite/austenite structure, the stress induced transformation of austenite to martensite and the precipitated epsilon carbide blocking dislocation movement. All these features are expected to lead to high work hardening rates and consequently better abrasion resistance. Nevertheless, it appears that the best wear resistance is provided by an essentially martensitic matrix. Figures 6.4 - 6.7 illustrate that the introduction of ferrite plates and increased quantities of retained austenite into the structure lowers both the hardness and the abrasive wear resistance. This effect is observed for both irons investigated. After 30 minutes at an austempering temperature of 355°C the absence of martensite due to austenite stabilization results in a levelling off of the hardness and relative abrasion resistance. The same is true for an austempering temperature of 250°C but only after 60 minutes.

Unfortunately, the introduction of martensite into the structure has been shown to have a markedly deleterious effect on the toughness and ductility of the resultant material. From an engineering viewpoint it would appear that such materials would have limited commercial value. Austempered irons which exhibit the best combination of strength and toughness are those which have considerable quantities of retained austenite in the structure.

It is of interest to note therefore that austempered irons containing large quantities of retained austenite of up to 40%, have better abrasion resistance than steels of equivalent bulk hardness. The reason for such significant wear resistance can be found when we examine Figures 6.2 - 6.7 which show that abrasion leads to the transformation of considerable quantities of the retained austenite to martensite with a consequent large increase in the hardness of the surface layers (Figure 6.8). Stress induced martensitic transformations have distinct advantages in improving wear resistance (45). These transformations lead to a high work hardening capacity in the resultant product and a high strain to fracture. Obviously the maximum advantage will be gained when an optimum amount of martensite forms during abrasion to give a high work hardening rate.

The maximum amount of transformation that can be achieved is dependent on the strain suffered by the material and the maximum temperature M_d at which the transformation of austenite to martensite can be mechanically induced. The M_d temperature is related to the M_s temperature which in turn is dependant on the composition of the austenite as indicated by the Nehrenburg (57) formula (wt %):

$$M_s(°C) = 500 - 300\ C - 33\ Mn - 22\ Cr - 17\ Ni - 11\ Si - 11\ Mo$$

The influence of the stress induced martensitic transformation on the abrasion resistance of the austempered irons can be observed in Figure 10. The abrasion resistance for the SG60 grade shows a gradual decline as the austempering temperature is raised form 250°C. However, from a temperature of around 300°C, the abrasion resistance remains constant up to a temperature of approximately 400°C when it declines again. This constancy of abrasion resistance over a 100°C temperature range occurs despite a continued fall in hardness and strength, due to the development of coarser ferritic plates and an increase in austenite content from 25% to 45%. Clearly the volume of austenite transforming to martensite during abrasion becomes greater as the austempering temperature is raised from 300 - 400°C leading to an increasing improvement in abrasion resistance which offsets the anticipated continued fall in RAR values based on declining mechanical properties.

These results indicate that the SG60 grade austempered at 400°C has a similar abrasion resistance as the same material austempered at 300°C but with a toughness at least 100% higher. A similar effect is also noted for the SG42 grade but over a shorter temperature range from 300 - 350°C.

In the present case it has also been shown that the abrasive wear resistance of the SG42 grade is superior to the SG60 grade despite its initial lower hardness and strength levels at each austempering temperature (Fig 6.1). This superior wear resistance can be attributed to the increased amount of austenite to martensite transformation shown in the SG42 grade compared to the SG60 grade following abrasion. The percentage of austenite transforming to martensite in the SG42 grade compared to the SG60 grade has been shown to be 5 to 10% higher for specimens austempered in the temperature range 250°C - 350°C and having similar quantities of retained austenite prior to abrasion. Such a result suggests that the austenite in the SG42 specimens is less stable because of a higher M_d temperature than that found in the SG60 grade.

Since the M_S temperature is raised by a decrease of carbon in the austenite, the maximum percentage of retained austenite expected at the lower austempering temperatures should be lower, since carbide is precipitated within the ferrite flakes below a temperature of 350°C. Such an effect can be observed in Figures 6.4 and 6.5 showing the maximum amount of retained austenite formed in grade SG42 at two different temperatures. Almost 45% retained austenite was found at 355°C compared to 25% at 250°C. It is, therefore, to be expected that if the percentage of austenite transforming to martensite remains constant during abrasion, then the influence on abrasion resistance will become less as the austempering temperature is lowered.

Thus two factors appear to be paramount in contributing to the abrasion resistance of austempered iron with duplex ferritic/austenitic matrices, namely the morphology of the structure and the amount of austenite that transforms during abrasion. Below a temperature of 300°C the fine ferrite/austenite matrix containing epsilon carbide appears to be dominant in providing abrasion resistance. However, above an austempering temperature of 300°C, large quantities of stress induced austenite to martensite transformations occur during abrasion which result in a product which is strongly abrasion resistant. In order to ensure that the maximum advantage is gained from the stress induced martensitic transformation, the heat treatment schedule should be carefully planned to provide the maximum quantity of retained austenite in the structure following austempering.

6.3.1 Mechanisms of Dry Abrasive Wear

There is little evidence to suggest that the mechanisms of abrasive wear operating in the present work are different from those observed in previous work utilising the same apparatus (30,50). The abrasive alumina grains appear to cause both ploughing and cutting of fine microchips from the surfaces of the austempered irons. These surface characteristics were found on all specimens austempered at all temperatures. This result indicates a similarity in the surface hardness, and therefore surface properties, of all specimens following abrasion. Alternatively, the hardness difference between the alumina (1800 HV) and the work hardened austempered iron surfaces (600 HV) was too great to differentiate between possible slight changes in surface properties and behaviour.

This result is expected from previous work (29,31,40) which showed that the surface hardness of the material must be in excess of 0.5 of the wearing material to have any significant effect on the mechanism of material removal.

The dominant mechanism would appear to be the removal of material through microcutting. This gives rise to straight sided clean wear tracks as shown in Figures 6.9 (a-c). The resulting debris shows evidence of extensive plastic deformation by shear. This is indicative of the high ductility of the austempered iron and the large amount of strain suffered by the removed material. At the head of the wear track, immediately in front of the abrading particle, high compressive stresses are generated which allow this high strain to occur. It is to be expected that the transformation of large quantities of retained austenite would also contribute to the strain experienced by these surface layers. This leads to microfracture of the deformed surface, resulting in the appearance of fine crushed chips or wear debris. These debris characteristics appear to be similar for all austempered irons although a softer matrix would tend to have longer chips.

There was no evidence to suggest the lubricating action of the graphite played any part in the abrasion mechanism.

The abrasive particles appear to cut through the graphite nodules without disturbing them. No significant graphite particles were observed to be present on the surface of the worn specimens. They would thus appear to be worn and dispersed in the same manner as the remainder of the material. It would therefore appear that graphite is detrimental to the abrasive wear of these irons. This is to be expected since the graphite does not stiffen the overall structure but rather the reverse. This is confirmed by the higher relative abrasive wear resistance of steel (1.00), which has a similar hardness and matrix structure to the as received SG42 iron (0.89).

CHAPTER 7

CONCLUSIONS

1. The variation of austenitising and austempering temperatures and times of the two commercial irons has been shown to significantly alter the morphology and constitution of the matrix.

   The matrix of these irons has been shown to have a dual phase structure of acicular ferrite needles and austenite.

   a) Below the austempering temperature of 850°C no acicular ferrite and retained austenite is present in the matrix. Increasing the length of austentitisation time increases the final amount of retained austenite in the matrix.

   b) Increasing the austempering temperature from 250°C to 450°C has been shown to coarsen the ferrite plates and to increase the amount of austenite in the structure.

   c) The maximum amount of austenite found in the structure is also dependent on austempering time. This ranges from 60 minutes at the lower temperatures to 30 minutes at the higher temperatures.

2. Mechanical properties of the two grades of iron have been shown to be dependent upon austempering temperature. The lower austempering temperatures result in higher tensile strengths, and lower toughness. The higher austempering temperatures produce lower tensile strengths but higher toughness values.

3. The dry abrasion resistance of two commercial irons austempered between 250°C and 400°C has been shown to be greatly superior to that of mild steel and proprietary abrasion resistant alloys at similar bulk hardness levels.

4. The lower austempering temperatures result in better abrasion resistance under slow rates of strain. However, austempering at higher temperatures provides better toughness, as measured by the Charpy impact test. Such combinations of abrasion resistance and toughness would clearly allow these alloys to compete successfully in many situations involving wear.

5. The origin of the high abrasion resistance can be rationalised in terms of the changing morphology of the duplex ferrite/austenite matrix with austempering temperature and the high strains that can be accommodated before material is lost from the surface. This capacity for accommodating strain is provided by the strain associated with the stress induced transformation of austenite to martensite and the high work hardening rate of the resulting product.

REFERENCES

1 ROLLASON F.C. (1973) : "Metallurgy for Engineers", 4th Edition, Edward Arnold Ltd.

2 GUNDLACH R.B. and JANOWAK J.F. (1984): 1st International Conference on Austempered Ductile Iron, AS,. Chicago.

3 KARSAY S.I. (1976) : "Ductile Iron I - Production", Quebec Iron and Titanium Corporation.

4 HIGGINS R.A. (1983) : "Engineering Metallurgy - Part I", p 377.

5 HARDING R.A.(1986) : "Heat Treatment Plant for Austempering Ductile (SG) Iron", BCIRA Report 1650.

6 FORREST R.D.(1985) : "Austempered Ductile Iron for Both Strength and Toughness", Machine Design, pp 95-99.

7 FULLER A.G. (1985) : "Austempered Ductile Irons - Present Application", Materials and Design, Vol. 6, No. 3, June/July 1985.

8 HARRIS D.A. and MAITLAND R.J. (1970) : "The Effect of Austenitizing of Lower Bainite in a Spheroidal Cast Iron", Iron and Steel, October 1970, pp 325 - 328.

9 RUNDMAN K.B. and KLUG R.C. (1982) : "An X-Ray and Metallurgical Study of an Austempered Ductile Cast Iron", AFS Transactions, pp 499-508

10 JANOWAK J.F. and GUNLACH R.B. (1983) : "Development of a Ductile Iron for Commercial Austempering", AFS Transactions, pp 377-388.

11 DORAZIL F. and KRAUS E. (1970) : "The Effect of Austenitizing Temperature on the Isothermal Decomposition of Austenite in Unalloyed Ductile Iron", Slevarenstri, 18, pp 503-506.

12 JOHANSSON M. (1977) : "Austenitic-Bainitic Ductile Iron", AFS Transactions 85, pp 117-122.

13 HEHEMAN R. (1968) : "The Bainitic Transformation", Phase Transformations, American Society for Metals.

14 VIGNERON B., SCHISSLER J.M. and FAIVRE R. (1977) : "La Transformation Bainitique des Alliages Fe-C-Si", Hommes et Fonderie, pp 17-34.

15 DORAZIL E. (1979) : "Zwischenstufenumwandeln von Gusseisen mit Kugelgraphit", Giesserei-Praxis, 18, pp 355-366.

16 MORTON P.A., unpublished research, Climax Molybdenum Co.

17 HARDING R.A. (1986) : "Effects of Metallurgical Process Variables on Austempered Ductile Irons", Metal and Materials, February 1986, pp 65-71.

18 SANDVIK B.P.J. (1982) : "The Bainitic Reaction in Fe-Si-C Alloys: the Secondary Stage", Metal Transactions, Vol 13A, pp 789-800.

19 FRANETOVIC V., SACHDEV A.K. and RYNTZ E.F. (1987) : "A Transmission Electron Microscopy Study of Austempered Lower Bainitic Nodular Cast Iron", Metallography 20, pp 15-36.

20 HWANG, D.H. and THOMAS G. (1977) : "Metallography of Bainitic Transformations in Silicon Containing Steels", Metal Transactions, 8A, pp 1661-1674.

21 BHADESHIA H.K.D.H. and EDMONDS D.V. (1979) : "The Bainitic Transformations in a Silicon Steel", Metal Transactions, 10A, pp 895-907.

22 SHEPPERSON S.V. (1985) : Materials Engineering Project, University of Cape Town.

23 MOORE D.J., RUNDMAN K.B. and RAINS T.M. (1984) : "The Effect of Thermomechanical Processing on Bainite Formation in Several Austempered Ductile Cast Irons", 1st International Conference on Austempered Ductile Iron, ASM, Chicago pp 13-31.

24 DORAZIL E., BARTA B. and MUMSTEROVA E. (1973) : "Mechanical Properties of Austempered, Unalloyed S.G. Cast Iron", Giessereitechnik, 19, No. 3, pp 79-83.

25 DORAZIL E. (1979) : "Zwischenstufenumwandeln von Gusseisen mit Kugelgraphit", Giesserei-Praxis, 18, pp 355-366.

26 SHIOKAWA T. (1978) : "On the Austempering of Ductile Cast Irons", 59th Japanese Ductile Cast Iron Association Licensee Conference.

27 JANOWAK J.F. and MORTON P.A. (1984) : "A Guide to Mechanical Properties Possible by Austempering 1.5%Ni-0.3%Mo Ductile Iron", AFS Transactions, 87, pp 515.

28 ARCHARD J.F. and HIRST W. (1957) : "The Wear of Metals Under Unlubricated Conditions", Proceedings, Royal Society (London), A238, p 515.

29 MOORE M.A. (1980) : "Abrasive Wear", Fundamentals of Friction and Wear of Materials, American Society of Metals, Materials Science Seminar.

30 NOEL R.E.J. (1981) : "The Abrasive-Corrosive Wear Behaviour of Metals", M.Sc Thesis, Department of Materials Engineering, University of Cape Town.

31 MOORE M.A (1978) : "Abrasive Wear", Metals in Engineering Applications, Vol. 1, pp 97-109.

32 KRUSCHOV M.M. (1957) : "Resistance of Metals to wear by Abrasion as Related to Hardness", Proceedings of Conference on Lubrication and Wear, Institute of Mechanical Engineers, London, pp 655-659.

33 VINGSBO O. (1979) : "Wear and Wear Mechanisms", Wear of Materials, ASME, pp 620-635.

34 KRUSHOV M.M. and BABICHEV M.A. (1958) : "Resistance to Abrasive Wear of Structurally Heterogeneous Materials", Friction and Wear in Machinery, 12, pp 27-35.

35 SIN H., SAKA N. and SUH N.P. (1979) : "Abrasive Wear Mechanisms and the Grit Size Effect", Wear, 55(1), pp 163-190.

36 MURRAY M.J., MUTTON P.J. and WATSON J.D. (1979) : "Abrasive Wear Mechanisms in Steels", Wear of Materials, ASME, pp 257-265.

37 RICHARDSON R.C.D. (1967) : "The Wear of Metals by Hard Abrasives", Wear, 10, pp 219-230.

38 KRUSCHOV M.M. (1957) : "Resistance of Metals to Wear by Abrasion as Related to Hardness", Proceeding of Conference on Lubrication and Wear, Institute of Mechanical Engineers, London, pp 655-659.

39 ZUM-GAHR K.H. (1979) : "How Microstructure Affects Abrasive Wear Resistance", Metal Progress, pp 46-69.

40 MOORE M.A. (1974) : "The Relationship Betwen the Abrasive Wear Resistance, Hardness and Microstructure of Ferritic Materials", Wear, 28, pp 59-68.

41 KAR M.J. (1981) : "Investigation of the Role of Microstructure on the Two Body Abrasive Wear of Steels", Wear of Materials, pp 415-425.

42 SALESKY W.J. (1980) : "Sliding Wear, Toughness and Microstructural Relationships in High Strength Fe/Cr/C Experimental Steels", M.Sc Thesis, University of Berkely, California.

43 KWOK M.J. and THOMAS G. (1983) : "Microstructural Influence on Abrasive Wear Resistance of High Strength/High Toughness Medium Carbon Steels", Wear of Materials, pp 140-147.

44 BHAT M.S., ZACKAY V.P. and PARKER E.R. (1979) : Proceedings of the Conference on Wear of Materials, Dearborn, Michigan.

45 ALLEN C., PROTHEROE B. and BALL A. (1981) : "The Abrasive-Corrosive Wear of Stainless Steels", Wear, 74, pp 287-305.

46 LARSEN-BADSE J. and MATHEW K.G. (1969) : "Influence of Structure on the Abrasion Resistance A1040 Steel", Wear, 14, pp 199-206.

47 ZUM-GAHR K.H. (1979) : "Relation Between Abrasive Wear Rate and the Microstructure of Metals", Wear of Materials, ASME, pp 266-276.

48 SARE I.R. (1979) : "Abrasion Resistance and Fracture Toughness of White Cast Iron", Metal Technology, 6 (11), pp 412-418.

49 UETZ H., SOMMER K. and KHOSROWI M. (1981) : "Correlation Betwen Model and Workshop Tests Using Abrasive Wear Operation Procedures", Wear, 69 (1), pp 25-41.

50 McQUEER J.I. (1985) : "Abrasion Resistance of a Series of Vanadium White Cast Irons", M.Sc. Thesis, Department of Materials Engineering, University of Cape Town.

51 LARSEN-BADSE J. (1968) : "Influence of Grit Diameter and Specimen Size on Wear During Sliding Abrasion", Wear, 12, pp 35-53.

52 RICHARDSON R.C.D. (1968) : "The Wear of Metals by Relatively Soft Abrasive", Wear, 11, pp 245-275.

53 MISRA A. and FINNIE I. (1980) : "A Classification of Three Body Abrasive Wear and the Design of a New Tester', Wear, 60, pp 111-121.

54 MISRA A. and FINNIE I. (1981) : "An Experimental Study of Three Body Abrasive Wear", Wear of Materials, pp 426-431.

55 MISRA A. and FINNIE I. (1981) : "Correlations Between Two-Body and Three-Body Abrasion and Erosion of Metals", Wear, 68, pp 33-39.

56 AVERBACH B.L. and COHEN M. (1948) : "X-ray Determination of Retained Austenite by Integrated Intensities", Metals Tech, pp 401-415.

57 ANGUS H.T. (1976) : "Cast Iron", Butterworth & Co. (Publishers) Ltd., London, U.K.

APPENDIX

DETERMINATION OF RETAINED AUSTENITE IN A MARTENSITE MATRIX USING X RAY DIFFRACTION

The Problem

Austenite is a solid solution of iron with a cubic structure. When cooled rapidly there is a metastable shear transformation which yields martensite. Depending on the composition and applied cooling rate, austenite may be retained in the composition. Since the mechanical properties of a steel depend on the ratio of martensite (α -body centred tetragonal phase) and austenite (γ -FCC phase) determination of the amount of retained austenite is essential.

Methods of Determining Retained Austenite

Both austenite and martensite have the same chemical composition and their solubility in any known solvent is identical. Hence a determination of their quantities by chemical means is not possible.

Optically the microstructure of retained austenite and martensite are indistiguishable. However, the physical properties of austenite and martensite are different e.g. the magnetic behaviour and the coefficient of expansion differ. These properties can be used in estimates of the retained austenite content.

More commonly used methods are those that are able to distinguish between the two crystal structures of austenite and martensite. Two such successful methods are Mössbauer spectrography and X-ray diffraction. By far the simplest method is X-ray diffraction and was used in this study.

Theory

Quantitative X-ray diffraction analysis for determination of the relative amounts of two phases in a mixture requires the comparison of the intensities of two suitable reflections (hkl) of both phases. These reflections must not coincide with any other Kα reflection. They should also be fairly close to each other to avoid systematic errors. For the austenite/martensite mixture the diffraction lines best meeting these requirements are the (200) reflection of the martensite, and the (220) reflection of the austenite.

Integrated intensities are used to compare the two peaks i.e. the area under the diffraction peaks. The integrated intensity of a reflection (hkl) can be expressed as follows:

$$I\ (hkl) = K.FF.LP.\ m.\ e^{-2m}.A(\theta)\frac{(V)}{v^2} \qquad (1)$$

where

- K = Proportionality constant, depending on the intensity of the radiation used and the crystal size of the sample
- FF = The product of the structure factor and its complex conjugate for the reflection (hkl).
- LP = Lorentz-polarisation factor, for sample without texture, this factor can be simply tabulated as a function of the Bragg angle.
- m = Multiplicity factor for the (hkl) plane
- e^{-2m} = Debye-Waller temperature factor
- $A(\theta)$ = Absorption factor, the irradiated volume and hence the absorption factor are constant for every angle (θ) if the specimen surface is plane
- V = The relative volume of the phase to be analysed
- v = The volume of the elementary cell of the component which gives the reflection (hkl)

The proportionality constant and the absorption factor have the same value for the intensities I (220) and I (200). For the ratio P of these intensities the formula becomes

$$P = \frac{I_\gamma(222)}{I_\alpha(200)} = \frac{FF.\ LP.\ e^{-2m}\ \frac{V_\gamma}{v_\gamma^2}\ m_\gamma(220)}{FF.\ LP.\ e^{-2m}\ \frac{V_\alpha}{v_\alpha^2}\ m_\alpha(200)} \qquad (2)$$

The numerical values using Mo radiation for these factors are as follows:

	Austenite	Martensite
FF	$(536)^2$	$(288)^2$
LP	23	30
e^{-2m}	0.80	0.84
m	12	6
v	$(3.58)^3$	$(2.86)^3$

Substituting these values yields

$$P = 1.31\frac{V_\gamma}{V_\alpha} \qquad (3)$$

This method is reliable where only the 2 phases, martensite and austenite exist. If a third phase such as ferrite is present it cannot be used. For the partial volumes V and V the following equation applies

$$V_\alpha + V_\gamma = 1 \qquad (4)$$

Combining (3) and (4) yields the following expression for the partial volumes of the austenite phase

$$V_\gamma = \frac{P}{P + 1.31} \qquad (5)$$

If carbides are present their quantity may be estimated from metallographic investigations. Equations (4) and (5) will then be slightly different As X-rays only penetrate a thin layer beneath the surface of a specimen (2 µm for Mo radiation) and the volume examined is comparativeley small, the physical condition of the surface layer is of great importance. Care must be taken to prevent undue heating of the austenite. To prepare the surface for X-ray diffraction the specimen is mechanically polished down 0.25 µm and then lightly etched with 2.5% nital to remove any strained material.

Diffractometer conditions

For this study, the conditions used for the determination of retained austenite are listed. These conditions were based on information taken from a Philips Scientific report and experience on the diffractometer.

Radiation	Mo Kα
Voltage	45 Kv
Current	30 MA
Range	10^3
Window	40
Time constant	1 sec
Bragg angle (200)	28.6°
Bragg angle (220)	32.5°
Filter	Zr
Divergence slit	1°
Receiving slit	0.2 mm
Scatter slit	1°
Scanning speed	2°/minute
Chart speed	4cm/minute

Calculation

A trace (fig. A) consists of two peaks, the (220) and the (200) peaks. To find the integrated intensity ratio, it is necessary to divide the total integrated intensity of the (200) peak by that of the (220) peak. In order to do this, the integrated intensity for each peak separately must be known i.e. the total intensity above the background intensity. Thus the average counts of the background taken over the same angular spread as the peak is subtracted from the total counts under the peak. Having calculated this for each peak, the integrated intensity ratio can be calculated, i.e.

$$P = \frac{(220)\gamma \text{ total counts - background counts}}{(200)_{\alpha} \text{ total counts - background counts}}$$

$$P = \frac{\text{Austenite peak counts}}{\text{Martensite peak counts}}$$

$$\text{then } V_{\gamma} = \frac{P}{P + 1.31} \qquad \text{where } V_{\gamma} = \text{volume fraction of retained austenite}$$

Example

Background 1	Martensite	Background 2	Austenite	Background 3
26.85-27.65	28.10-29.70	30.20-31.00	31.00-32.66	32.60-33.40
= 0.80°	= 1.6°	= 0.80°	= 1.6°	= 0.8°
27067	75573	22902	49338	24437

Martensite Peak = 75573 - (27067 + 22902) = 25604

Austenite Peak = 49338 - (22902 + 24437) = 1999

$$P = \frac{1999}{25604} = 0.078$$

$$V_\gamma = \frac{0.078}{1.31 + 0.078} = 0.562$$

= 5.62% retained austenite.

The sensitivity, reproducability and accuracy of X-ray diffraction measurements are discussed by Averbach and Cohen. Sensitivity depends largely upon the radiation used and monochromatic radiation is necessary for maximum sensitivity. Reproducability is high with standard deviation as good as 0.2%. Supposedly the lower limit of determination of retained austenite by XRD. The standard deviation for the reproduceability for this investigation was ± 0.8%. Accuracy however is more difficult to measure due to the problem of obtaining reliable standards, but Averbach and Cohen (56) indicate that it is adequate above 1% retained austenite.

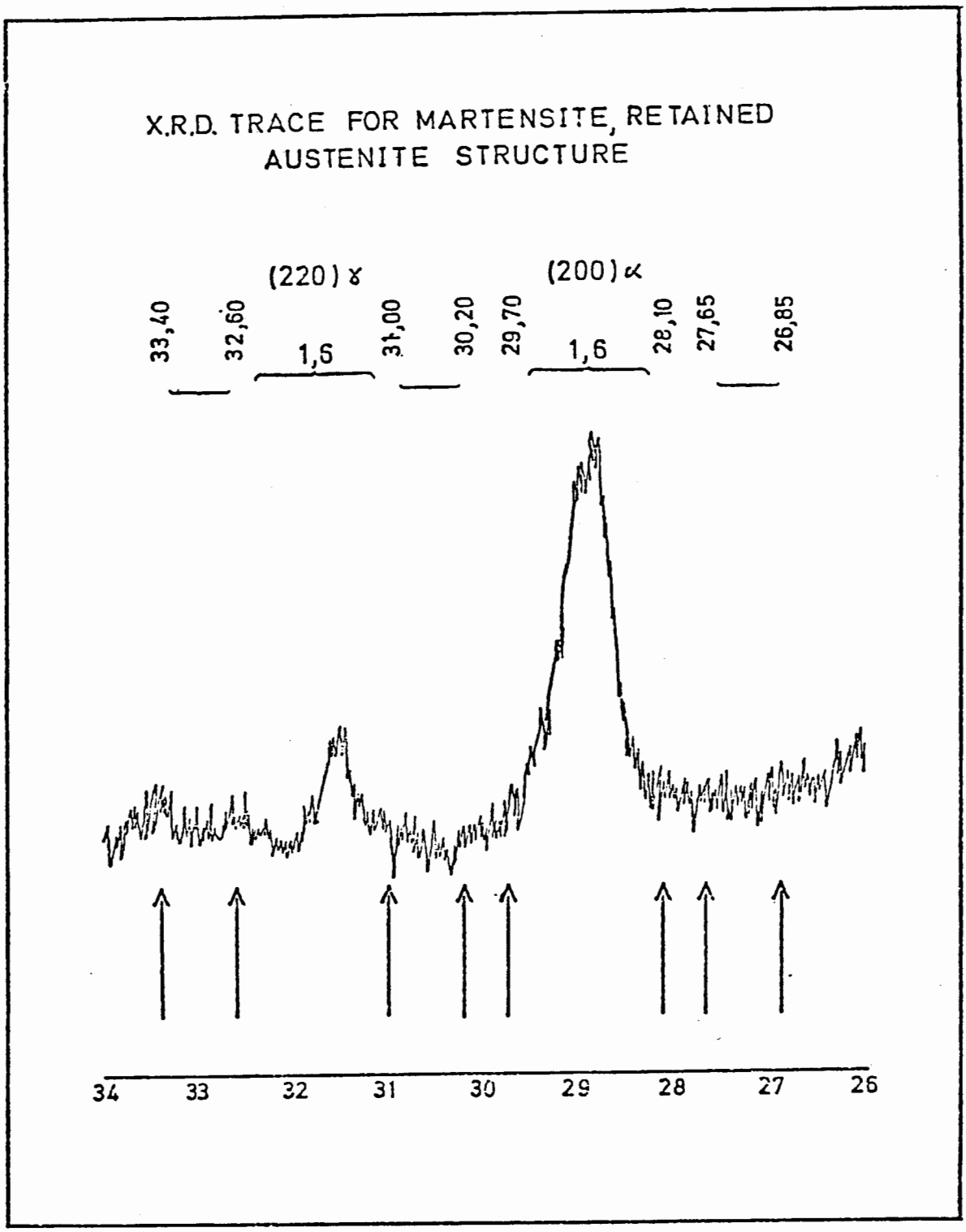

Fig. A